8-2013

Control Studies of DFIG based Wind Power Systems

Zhiqiang Jin
zjin@utk.edu

To the Graduate Council:

I am submitting herewith a dissertation written by Zhiqiang Jin entitled "Control Studies of DFIG based Wind Power Systems." I have examined the final electronic copy of this dissertation for form and content and recommend that it be accepted in partial fulfillment of the requirements for the degree of Doctor of Philosophy, with a major in Electrical Engineering.

Fangxing Li, Major Professor

We have read this dissertation and recommend its acceptance:

Yilu Liu, Leon M. Tolbert, Jim Ostrowski

Accepted for the Council:

Carolyn R. Hodges

Vice Provost and Dean of the Graduate School

(Original signatures are on file with official student records.)

Control Studies of DFIG based Wind Power Systems

A Dissertation Presented for the
Doctor of Philosophy
Degree
The University of Tennessee, Knoxville

Zhiqiang Jin
August 2013

DEDICATION

I dedicate my work to my beloved parents, my dear wife Ying Guo, and my so loved daughter Emma Jin.

ACKNOWLEDGEMENTS

First and the foremost, I would like to express my gratitude to my academic advisor, Dr. Fangxing “Fran” Li for his continuous guidance and support for this and all other research and course works during my PhD study at the University of Tennessee.

I am very thankful to Dr. Leon M. Tolbert, Dr. Yilu Liu, and Dr. Jim Ostrowski for their time and effort in serving as the members of my dissertation committee.

I would also like to thank all the professors and friends of the CURENT research center for their encouragement in my research.

Last but not the least, I am greatly indebted to my parents and my wife, for their unconditional love and support which made it possible for me to finish this work.

ABSTRACT

Wind energy as an outstanding and competitive form of renewable energy, has been growing fast worldwide in recent years because of its importance to reduce the pollutant emission generated by conventional thermal power plants and the rising prices and the unstable supplies of fossil-fuel. However, in the development of wind energy, there are still many ongoing challenges.

An important challenge is the need of voltage control to maintain the terminal voltage of a wind plant to make it a PV bus like conventional generator with excitation control. In the literature with PI controllers, the parameters of PI controllers need to be tuned as a tradeoff or compromise among various operating conditions. In this work, a new voltage control approach is presented such that PI control gains are dynamically adjusted based on the dynamic, continuous sensitivity which essentially indicates the dynamic relationship between the change of control gains and the desired output voltage. Hence, this control approach does not require estimation or tuning of fixed control gains because it has the self-learning mechanism via the dynamic sensitivity. This also gives the plug-and-play feature of DFIG controllers to make it promising in utility practices.

Another key challenge in power regulation of wind energy is the control design in wind energy conversion system (WECS) to realize the tradeoff between the energy cost and control performance subject to stochastic wind speeds. In this work, the chance constraints are considered to address the control inputs and system outputs, as opposed to deterministic constraints in the literature, where the chance constraints include the stochastic behavior of the wind speed fluctuation. Two different control problems are considered here: The first one assumes the wind speed disturbance's distribution is

Gaussian; and the second one assumes the disturbance is norm bounded, and the problem is formulated as a min-max optimization problem which has not been considered in the literature. Both problems are formulated as semi-definite program (SDP) optimization that can be solved efficiently with existing software tools. Also, simulation results are provided to demonstrate the validity of the proposed method.

TABLE OF CONTENTS

CHAPTER 1 Introduction And General Information 1
1.1 Power System Stability 1
1.1.1 Definitions and Classification of Power System Stability 1
1.2 Renewable Energy 4
1.2.1 Solar Energy 5
1.2.2 Wind Energy 5
1.3 Wind Turbine based Power System 6
1.3.1 Wind Energy Conversion System 7
1.3.2 Wind Turbines Topologies [9] 8
1.4 Contribution of this Work 11
1.5 Organization of the Dissertation 13
CHAPTER 2 Literature Review 14
2.1 Chapter Introduction 14
2.2 Voltage Regulation for Wind Turbine based Power System 14
2.3 Power Regulation for Wind Energy Conversion System 17
2.4 Scope of this Work 20
CHAPTER 3 Voltage Regulation For Wind Turbine Based Power System 22
3.1 Chapter Introduction 22
3.2 Modeling of the Wind-Turbine Doubly-Fed Induction Generator 22
3.2.1 Turbine Model 22
3.2.2 Rotor Side Control System 23
3.2.3 Grid Side Control System 25
3.2.4 Pitch Angle Control System 26
3.3 Adaptive Control Strategy 26
3.3.1 Voltage Control System Configuration 28
3.3.2 Sensitivity φ 29
3.3.3 Initial Values of Control Parameters 30
3.3.4 Dynamic Update of $k_p^{(t)}$ and $k_i^{(t)}$ 32
3.3.5 Limit for $k_p^{(t)}$ 34
3.3.6 Flow Chart 35
3.4 Simulations and Results 36
3.4.1 Demonstration of Instability with Inappropriate PI Gains 36
3.4.2 Case One: Set Final Voltage to 1.01 p.u. 38
3.4.3 Case Two: Set Final Voltage to 1.04 p.u. 41
3.4.4 Case Three, Four, and Five: Load=200, 800, and 1100kW, respectively 43
3.5 Discussion and Conclusion 47
CHAPTER 4 Power Regulation For Wind Energy Conversion System I 48
4.1 Chapter Introduction 48
4.2 Modeling of Variable Speed Variable Pitch WECS 48
4.2.1 Wind Speed Model 49
4.2.2 Pitch Actuator Model 49
4.2.3 Aerodynamic System 49
4.2.4 Drive Train Model 50

4.2.5 Generator Model 51
4.2.6 WECS Linearization 51
4.3 Problem Formulation 53
4.3.1 Discrete-Time Model 53
4.3.2 Cost Function 54
4.3.3 Problem Formulation 55
4.4 Proposed Control Strategy 57
4.4.1 SDP 57
4.4.2 Approximating Chance Constraints to Linear Constrains 58
4.4.3 SDP Approach for Problem 1 61
4.4.4 SDP Approach for Problem 2 63
4.5 Results and Discussion 64
4.5.1 Case One: Step Change to the Wind Speed 64
4.5.2 Case Two: The Disturbance Distribution is Gaussian 67
4.5.3 Case Three: The Disturbance is Norm-Bounded 71
4.6 Discussion and Conclusion 73
CHAPTER 5 Power Regulation For Wind Energy Conversion System II 75
5.1 Chapter Induction 75
5.2 Modeling of Variable Speed Variable Pitch WECS [30, 42] 75
5.2.1 Wind Speed Model 76
5.2.2 Pitch Actuator Model 76
5.2.3 Aerodynamic System 76
5.2.4 Drive Train Model 77
5.2.5 Generator Model 77
5.2.6 WECS Linearization 78
5.3 Proposed Control Strategy 79
5.4 Problem Formulation 80
5.4.1 Discrete-Time Model 80
5.4.2 Cost Function 81
5.4.3 Problem Formulation 82
5.5 Results and Discussion 83
5.5.1 Case 1: The Disturbance Distribution is Gaussian 84
5.5.2 Case 2: The Disturbance is Norm-Bounded 85
5.6 Discussion and Conclusion 86
CHAPTER 6 Conclusion And Future Work 88
6.1 Conclusion and Contribution 88
6.2 Future Work 90
LIST OF REFERENCES 91
APPENDIX 96
Vita 99

LIST OF FIGURES

Fig. 1.1 Classification of power system stability [1] 2
Fig. 1.2 Distribution map of wind power capacity 6
Fig. 1.3 Typical configuration of a Type 1 WTG [9] 9
Fig. 1.4 Typical configuration of a Type 2 WTG [9] 9
Fig. 1.5 Typical configuration of a Type 3 WTG [9] 10
Fig. 1.6 Typical configuration of a Type 4 WTG [9] 11
Fig. 1.7 Typical configuration of a Type 5 WTG [9] 11
Fig. 3.1 Wind turbine DFIG system..... 22
Fig. 3.2 Wind turbine power characteristics [29] 23
Fig. 3.3 Rotor side control system. 24
Fig. 3.4 Grid side control system 25
Fig. 3.5 Reference voltage curve for the proposed control approach 27
Fig. 3.6 Terminal voltage control loop 28
Fig. 3.7 Expected result case..... 32
Fig. 3.8 Flow chart showing the control process 35
Fig. 3.9 Sample power system with DFIG for simulation study 36
Fig. 3.10 Demonstration of instability with inappropriate PI gains..... 38
Fig. 3.11 Results for case one: set final voltage to 1.01 p.u. 41
Fig. 3.12 Results for case two: set final voltage to 1.04 p.u. 43
Fig. 3.13 Results for case three: Load = 200 kW 44
Fig. 3.14 Results for case four: Load = 800 kW..... 45
Fig. 3.15 Results for case five: Load = 1100 kW 46
Fig. 4.1 Wind energy conversion system..... 48
Fig. 4.2 Results when wind speeds change from 20 m/s to 21m/s (Group one left side; group two right side)..... 65
Fig. 4.3 Results when wind speeds change from 20 m/s to 19m/s (Group one left side; group two right side)..... 66
Fig. 4.4 Results for disturbance distribution is Gaussian..... 69
Fig. 4.5 Comparison of Probability of Pg within bounds under two models: with constraints and without constraints, where the x-coordinate represents 10 different tries, and the y-coordinate represents the probabilities in the range..... 70
Fig. 4.6 Comparison of Probability of w_g within bounds under two models: with constraints and without constraints, where the x-coordinate represents 10 different tries, and the y-coordinate represents the probabilities in the range..... 70
Fig. 4.7 Results for disturbance is Norm-bounded 73
Fig. 5.1 Wind energy conversion system..... 75
Fig. 5.2 Wind turbine characteristic for maximum power point tracking 79
Fig. 5.3 Results in the partial load region as disturbance is Gaussian..... 84
Fig. 5.4 Results in the partial load region as disturbance is Norm-bounded 86

CHAPTER 1 INTRODUCTION AND GENERAL INFORMATION

1.1 Power System Stability

Power systems play a critical role in human being's daily life. Some large power system failures with enormous social and economic impacts motivated power engineers to seek the reason of such failures. According to historical data, many major blackouts have been caused by power system instability problems since the 1920s, which have made the power community realize that the power system stability is a key problem to address [1-3].

Power systems have changed drastically in recent years. Today's power system in the U.S. is a large-scale, interconnected system with increasing complexity via new technologies such as renewable generations. All these lead to the occurrence of different forms of power system instability, which may lead to power system blackouts, such as voltage instability, frequency instability and inter-area oscillations.

1.1.1 Definitions and Classification of Power System Stability

Power system stability, as one case of dynamic system stability with definition found in both of math and control literatures, e.g. Lyapunov stability theory, has been defined in many power and control literatures. According to IEEE's definition considering the interconnection trends of today's power system in [1], power system stability is defined as follows:

"Power System Stability is the ability of an electric power system, for a given initial operating condition, to regain a state of operating equilibrium after being subjected to a physical disturbance, with most system variables bounded so that practically the entire system remains intact."

Power system stability is essentially a single problem. However, a power system may undergo different types of instabilities. So, it is evidently very important to analyze the characteristics of instabilities and maybe even the factors that contribute to instabilities so as to devise methods of improving the stability. The IEEE classification of power system stabilities is justified theoretically by the concept of partial stability [4-6], considering the followings [7]:

- The physical nature of the resulting mode of instability as indicated by the main system variable in which instability can be observed.
- The size of the disturbance considered, which influences the method of calculation and prediction of stability.
- The devices, processes, and the time span that must be taken into consideration in order to assess stability.

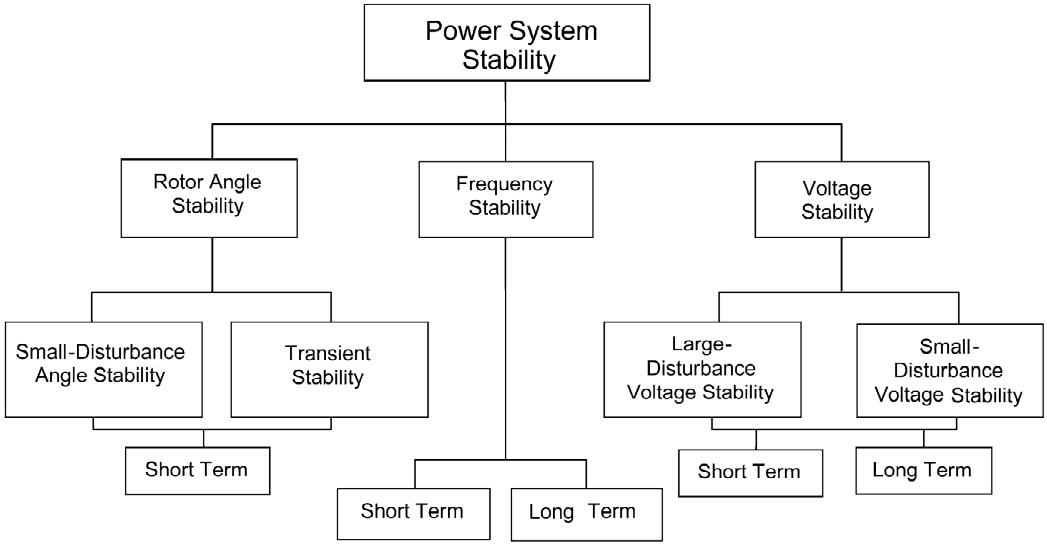

Fig. 1.1 Classification of power system stability [1]

The overall classification of power system stability is given in Fig. 1 above, identifying its categories and subcategories.

Rotor Angle Stability

Rotor angle stability refers to the ability of synchronous machines of an interconnected power system to remain in synchronism after being subjected to a disturbance. It depends on the ability to maintain/restore equilibrium between electromagnetic torque and mechanical torque of each synchronous machine in the system. It can further be classified as:

1. Small-disturbance (or small signal) rotor angle stability, which is concerned with the ability of the power system to maintain synchronism under small disturbances.
2. Large-disturbance rotor angle stability or transient stability, which is concerned with the ability of the power system to maintain synchronism when subjected to a severe disturbance.

Frequency Stability

Frequency stability refers to the ability of a power system to maintain steady frequency following a severe system upset resulting in a significant imbalance generation and load. It depends on the ability to maintain/restore equilibrium between system generation and load, with minimum unintentional loss of load.

Voltage Stability

Voltage stability refers to the ability of a power system to maintain steady voltages at all buses in the system after being subjected to a disturbance form a given initial operating condition. It depends on the ability to maintain/restore equilibrium between load demand and load supply from the power system. It can further be categorized as:

1. Small-disturbance voltage stability, which refers to the system's ability to maintain steady voltages when subjected to small perturbations such as incremental changes in system load.
2. Large-disturbance voltage stability, which refers to the system's ability to maintain steady voltages following large disturbances such as system faults, loss of generation, or circuit contingencies.

1.2 Renewable Energy

Renewable energy, also known as alternative energy, is coming from natural resources such as sunlight, wind, rain, tides, and geothermal heart, which are renewable (naturally replenished), instead of from our primary energy supply such as fossil fuels, coal, oil and natural gas. Renewable energy has received growing interests recently because of the two huge challenges nowadays: oil dependency and global warming. Since the prices of fossil-fuel are rising and their supplies are increasingly unstable, people have to discover new energy to make their life less dependent on oil. Also, the global warming problem has received increasing concerns due to pollutant emission. All these lead to the development of renewable energy. Presently, about 16% of global final energy consumption comes from renewable energies, with 10% coming from traditional biomass, which is mainly used for heating, and 3.4% from hydroelectricity. New renewable energies accounted for another 3% and are growing very rapidly.

In the U.S., most of the states have Renewable Portfolios Standard, which is an individual state-wide policy aiming at achieving a certain date, typically targets a range from 10% to 20% of total capacity by 2020. Apparently, renewable energy will still

develop quickly in the future. Next, solar energy and wind energy, two cases of renewable energy are introduced.

1.2.1 Solar Energy

Solar energy, radiant light and heat from the sun, has been harnessed by humans since ancient times using a range of ever-evolving technologies. These solar energy technologies include solar heating, solar photovoltaic, solar thermal electricity and solar architecture. Solar technologies are broadly characterized as either passive solar or active solar depending on the way they capture, convert, and distribute solar energy. Obviously, solar energy is the most easily available source of renewable energy. The development of solar technologies will have long-term benefits.

1.2.2 Wind Energy

Wind Power is derived from uneven heating of the Earth's surface from the Sun and the warm core. Most modern wind power is generated in the form of electricity by converting the intrinsic energy of the wind into mechanic power through the rotation of wind turbine blades, and then transformed to electric power by electrical generators. As an outstanding and competitive form of renewable energy, wind energy was the fastest growing energy technology in the 1990s, in terms of percentage of yearly growth of installed capacity per technology source. The growth of wind energy, however, has not been evenly distributed around the world [8].

Figure 1.2 shows U.S. installed wind capacity in 2011 [46]. As we can see from the figure, most of the wind power concentrates in west coast, central south and northeast of

USA. Texas is the state with most wind power installed, followed by Iowa, California, Minnesota, Illinois, Washington and Oregon.

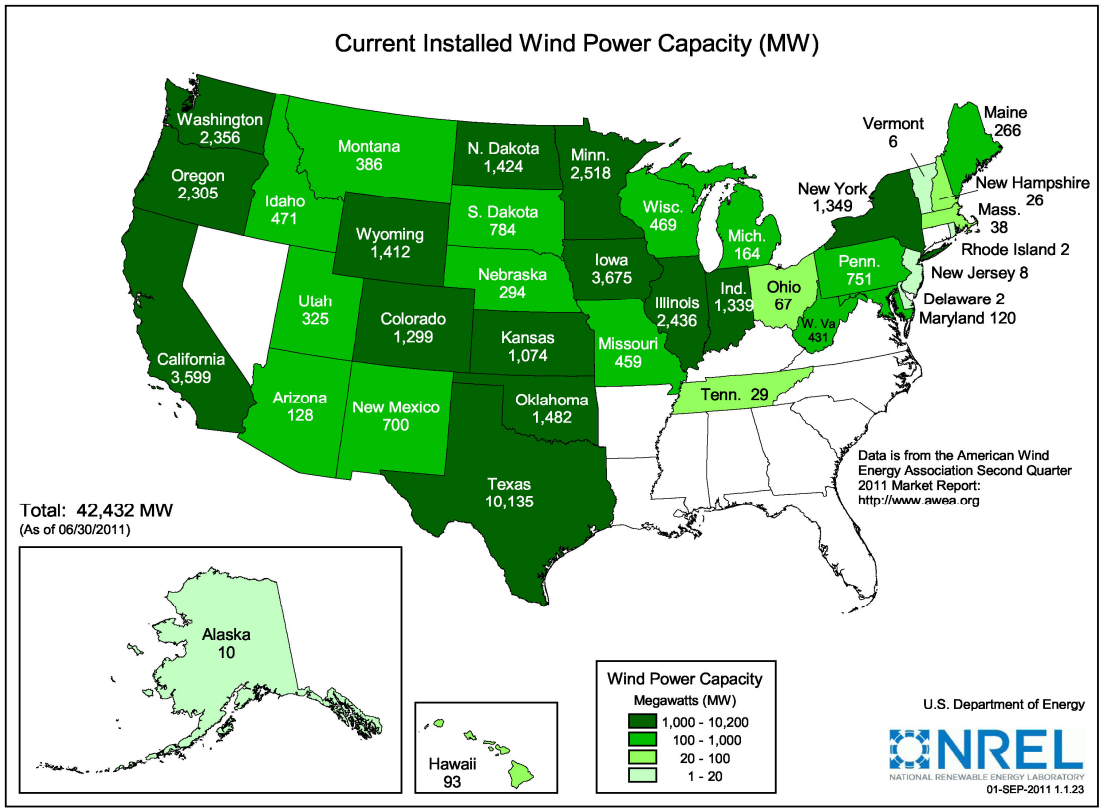

Fig. 1.2 Distribution map of wind power capacity [46]

1.3 Wind Turbine based Power System

Wind energy is basically used to produce electrical power. Globally, the long-term technical potential of wind energy is believed to be five times of the total global energy production of today. The development of the wind turbine plant could require better design for the wind turbine based power system. The discussion below presents an introduction to the wind turbines based power system.

1.3.1 Wind Energy Conversion System

Wind energy conversion system (WECS) can be divided into those that depend on aerodynamic drag and those that depend on aerodynamic lift. Modern wind turbines are based predominately on aerodynamic lift. Lift devices use airfoils (blades) that interact with the incoming wind. The force resulting from the airfoil body intercepting the airflow consists not only of a drag force component in the direction of the flow but also of a force component that is perpendicular to the drag: the lift forces. The lift force is a multiple of the drag force and therefore the relevant driving power of the rotor [8].

Wind turbines using aerodynamic lift can be further divided according to the orientation of the spin axis into horizontal axis and vertical axis turbines. The horizontal axis, or propeller-type, approach currently dominates wind turbine applications. A horizontal axis wind turbine consists of a tower and a nacelle that is mounted on the top of the tower. The nacelle contains the generator, gearbox and the rotor. Horizontal axis wind turbines typically use a different number of blades, depending on the purpose of the wind turbine. Two-bladed or three-bladed turbines are usually used for electricity power generation.

Vertical axis turbines use vertical, often slightly curved, symmetrical airfoils. They have the advantage that they operate independently of the wind direction and that the gearbox and generating machinery can be placed at ground level. Compared to horizontal axis, the research and development of vertical axis turbines has almost stopped worldwide.

1.3.2 Wind Turbines Topologies [9]

Wind turbines can be classified by their mechanical power control, and further divided by their speed control. At the top level, turbines can be classified as either stall regulated (with active stall as an improvement) or pitch regulated. Stall regulation is achieved by shaping the turbine blades such that that airfoil generates less aerodynamic force at high wind speed, eventually stalling, thus reducing the turbine's torque. Pitch regulation, on the other hand, is achieved through the use of pitching devices in the turbine hub, which twist the blades around their own axes. As the wind speed changes, the blade quickly pitches to the optimum angle to control torque in order to capture the maximum energy or self-protect, as needed.

Wind turbines can be divided further into four different types. Type one is fixed speed; type two is limited variable speed; type three is variable speed with either partial power electronic conversion and type four is variable speed with full power electronic conversion.

The fixed speed wind turbine generator is implemented with an asynchronous squirrel-cage induction generator (SCIG), and then connected to the grid via a step-up transformer. The speed of the wind turbine is fixed to the electrical grid's frequency. The wind turbine will produce active power when the turbine shaft rotates faster than the electrical grid frequency creating a negative slip. The main drawback of the fixed speed wind turbine is that the reactive power consumed by the induction generator for its excitation field and the large currents the machine can draw when started "across-the-line". So, a soft starter and discrete steps of capacitor banks are employed by the turbine.

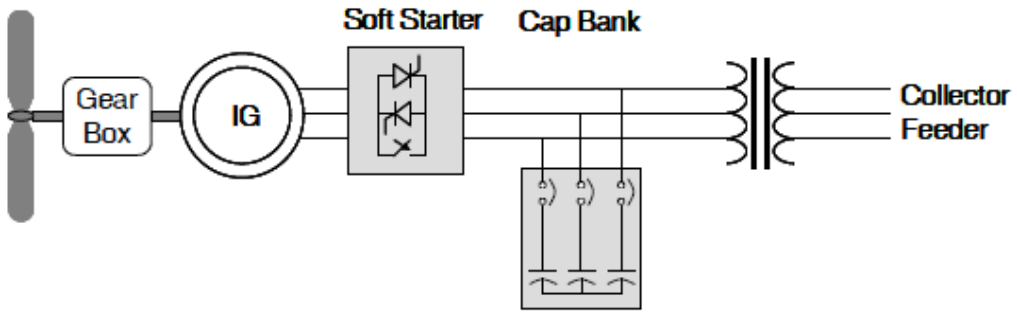

Fig. 1.3 Typical configuration of a Type 1 WTG [9]

The limited variable speed wind turbine uses wound rotor induction generator and the generator is connected to the grid directly. A capacitor bank performs the reactive power compensation. A smoother grid connection is achieved by using a soft-starter. Because the type of wind turbine has a variable addition rotor resistance, which can be changed by an optically controlled converter mounted on the rotor shaft. So, the total resistance is controllable. This optical coupling eliminates the need for costly slip rings that need brushes and maintenance. The rotor resistance can be changed and thus controls the slip. So the power output in the system is controlled.

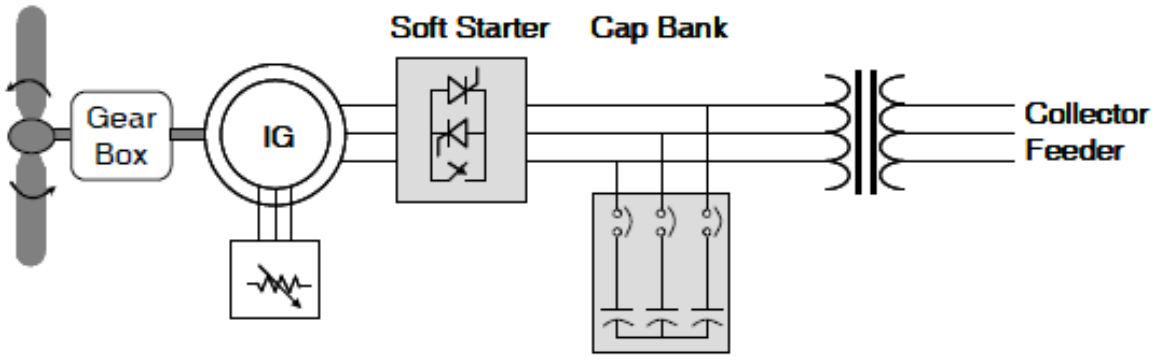

Fig. 1.4 Typical configuration of a Type 2 WTG [9]

The variable speed with partial power electronic conversion is known as the doubly fed induction generator (DFIG). It uses a wound rotor induction generator and partial scale frequency converter on the rotor circuit. The partial scale frequency converter performs the reactive power compensation and the smoother grid connection. It has a wider range of dynamic speed control. The main drawbacks are the use of slip rings and protection in the case of grid faults.

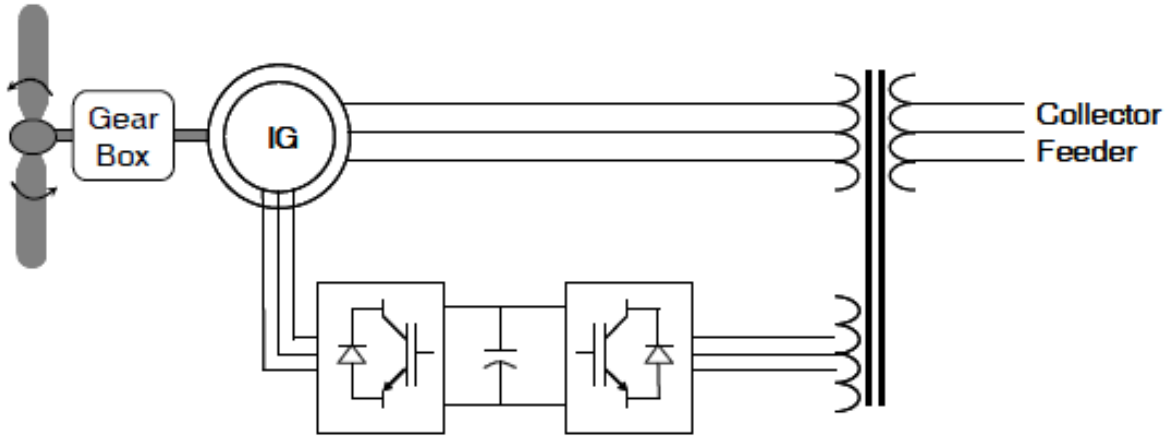

Fig. 1.5 Typical configuration of a Type 3 WTG [9]

The variable speed with full scale frequency converter wind turbine corresponds to the full variable speed wind turbine, with the generator connected to the grid through a full-scale frequency converter. The frequency converter performs the reactive power compensation and the smoother grid connection. The generator can be excited electrically.

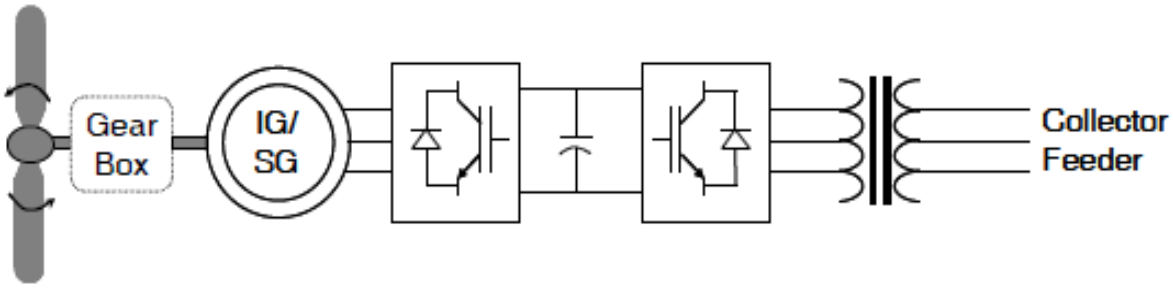

Fig. 1.6 Typical configuration of a Type 4 WTG [9]

There is one other machine type (type 5), in which a mechanical torque converter between the rotor's low-speed shaft and the generator's high-speed shaft controls the generator speed to the electrical synchronous speed. A synchronous machine is used directly connected to the medium voltage grid.

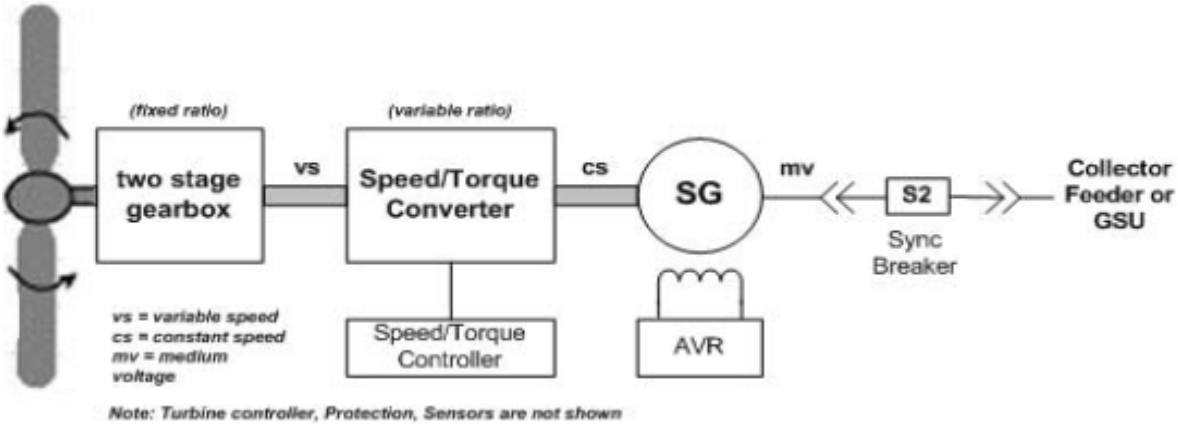

Fig. 1.7 Typical configuration of a Type 5 WTG [9]

1.4 Contribution of this Work

An important challenge for voltage regulation of DFIG based wind power system is the need of voltage control to maintain the terminal voltage of a wind plant to make it a PV bus such as conventional generators with excitation control. In this work, a new

voltage control approach based on a different philosophy is presented. In the proposed approach, the PI control gains for the DFIG system are dynamically adjusted based on the dynamic, continuous sensitivity which essentially indicates the dynamic relationship between the change of control gains and the desired output voltage. This control approach does not require any good estimation of fixed control gains because it has the self-learning mechanism via the dynamic sensitivity.

Another key challenge in power regulation of wind energy is the control design in wind energy conversion system (WECS) to realize the tradeoff between the energy cost and control performance subject to stochastic wind speeds. In this work, we consider chance constraints on control inputs and system outputs other than deterministic constraints in the literature, where the former ones include the stochastic behavior of the wind speed fluctuation. Here, two different control problems are considered: The first one assumes the wind speed disturbance distribution is Gaussian, where chance constraints can be reduced to deterministic constraints with Gaussian statistics; and the second one assumes the disturbance is norm bounded, and the problem is formulated as a min-max optimization problem which has not been considered in the literature. Then, both problems are formulated as semi-definite program (SDP) optimization problems that can be solved efficiently through existing software tools. Last, simulation results are provided to demonstrate the validity of the proposed method.

1.5 Organization of the Dissertation

Chapter 2 presents a review of relevant literatures.

Chapter 3 addresses the challenge of voltage control to maintain the terminal voltage of a wind plant to make it a PV bus, like conventional generators with excitation control. Also, a new voltage control approach based on a different philosophy is presented.

Chapter 4 focuses on the power control of the wind energy conversion system above the rated value considering the energy cost and control performance subject to stochastic wind speeds. A semi-definite programming (SDP) method is proposed with chance constraints on control inputs and system outputs. The wind speed fluctuation is modeled as Gaussian distribution or bounded with distribution unknown. The simulation results are also given at the end of the chapter.

Chapter 5 focuses on the power control of the wind energy conversion system in partial load region considering the energy cost and control performance subject to stochastic wind speeds. The semi-definite programming (SDP) method proposed in Chapter 4 is employed to perform power control in partial load region. The wind speed fluctuation is modeled as Gaussian distribution or norm bounded with distribution unknown. The simulation results are also given at the end of the chapter.

In Chapter 6, the conclusion regarding the whole work is given and the future work is also discussed.

CHAPTER 2 LITERATURE REVIEW

2.1 Chapter Introduction

This chapter briefly presents the review of the past and on-going research findings relevant to this work.

2.2 Voltage Regulation for Wind Turbine based Power System

For wind turbine based power system, an important challenge is the need of voltage control to maintain the terminal voltage of a wind plant to make it a PV bus like conventional generators with excitation control.

For wind plant, a doubly fed induction generator (DFIG) gives better wind energy transfer efficiency as opposed to other wind generators. They can also offer significant enhancement for transmission support regarding voltage control, transient performance, and damping [11].

DFIG employs a series of voltage-source converters consisting of a rotor-side converter (RSC) and a grid-side converter (GSC) to feed the wound rotor. This makes it different from the conventional induction generator. DFIG also has an additional advantage of flexible control and stability over other induction generators due to its control capacity of these converters [10].

[12] and [13] describe the modeling of a grid connected doubly-fed induction generator (DFIG) from the basic flux linkage, voltage and torque equations. For the small-signal analysis, different models are formulated and compared with each other for different assumptions, such as one or two-mass drive train, with or without stator

transients. Eigen-values and participation factor analysis of the linearized models are carried out to relate the DFIG electromechanical modes to its relevant state variables. In [14], a simple DFIG wind turbine model in which the power converter is simulated as a controlled voltage source, regulating the rotor current to meet the command of real and reactive power production is developed. The model described has the form of traditional generator model and is easy to integrate using PSS/E. For this DFIG model, the back-to-back converters somehow can be replaced by a matrix converter, which is operated with close-to-unity power factor at the grid side [16].

The decoupled control of DFIG has been popular in recent research. It has four controllers, named $P_{ref,}$ $V_{sref,}$ V_{dcref} and Q_{cref}, which are required to maintain the maximum power tracking, stator terminal voltage, dc voltage level, and GSC reactive power level, respectively. The proportional-integral (PI) controllers are popularly employed. As for the gains tuning of PI controllers, the trial-and-error method somehow can be really difficult. Therefore, different optimization methods are used to optimizing parameters of controllers. As in [15, 18], the particle swarm optimization (PSO) is proposed to control the doubly fed induction generator based wind turbine. The PSO algorithm is employed to search for the optimal parameters of controllers and achieve the optimal coordinated control of multiple controllers in the proposed tuning method. The system stability under both small and large disturbances is also analyzed based on the presented generic dynamic model of WT and its associated controllers. [17] also proposes the particle swarm optimization algorithm to design the optimal PI controllers for rotor-side converter of the DFIG. Other optimization algorithms may also work pretty well for gain

tuning of PI controllers. As in [14], an algorithm based on the foraging behavior of E. coli bacteria in our intestine is proposed to do the harmonic estimation for a signal distorted with additive noise. The author also proposes this bacteria foraging technique to tune the damping controller employed to enhance the damping of the oscillatory modes.

Decoupled P-Q control is also popular in control of doubly fed induction generator. [19, 20]

Oscillation issue is one important issue to solve in power system. The control of inter-area oscillation in power systems with high wind power penetration is achieved via doubly fed induction generator, which is modeled by MATLAB/Simulink [21, 22].

Wind energy is often installed in rural, remote areas characterized by weak, unbalanced power transmission grids. In induction wind generators, unbalanced three-phase stator voltages cause a lot of problems, such as over-current, unbalanced currents, reactive power pulsations and stress on the mechanical components from torque pulsations. So, more attentions are given to unbalanced conditions problems. In DFIGs, control of the rotor currents allows for adjustable speed operation and reactive power control [25-27].

As discussed above, many previous works in gain tuning for DFIG are based on some optimization approaches to reach a tradeoff or compromise such that the wind system can achieve good, though not always the most desired, performance under various operating conditions and avoid worst-case performance under some extreme conditions. These works may remind us whether there is any approach that the gain parameters of PI controllers used in DFIG or even other power systems for control problems can be tuned

automatically or adaptively according to different conditions? A novel philosophy has been successfully applied in [28] for the voltage control of three-phase distributed energy resources. Here, the proposed dynamic tuning is carried out during the process for stability control, such as regulating output voltage of DFIG. When the system operating condition varies in real time, the proposed approach autonomously learn the voltage response change w.r.t. the control gain change such that it can dynamically change the control gains in real time to achieve the ideal performance. Hence, the desired performance can be maintained with the proposed control using dynamic gain tuning.

2.3 Power Regulation for Wind Energy Conversion System

Wind energy as an outstanding and competitive form of renewable energy, has been growing fast in many countries recently not only because it is an important solution to reduce the pollutant emission generated by conventional thermal power plants, but also because the prices of fossil-fuel are rising and their supplies are increasingly unstable. Different wind energy conversion system (WECS) configurations have been used during the last 20 years. Induction and synchronous generators have both been tried in WECSs. According to power electronic converters' development, WECSs of variable-speed variable pitch type allow a better performance, as the generator torque and the pitch angle of the turbine blades can be controlled independently and simultaneously, which make them widely used.

Even so, there are still a lot of challenges to the wind power industry in present. These challenges include wind speed's randomness which may bring fluctuations to output power, as well as undesirable dynamic loading of the drive train during high

turbulence. Therefore, sophisticated control strategy plays an important role in wind energy conversion systems. A well-defined WECS can generate more efficient electrical energy, provide a better power quality, and lower the cost by alleviating aerodynamic and mechanical loads.

A variable speed variable pitch WECS has two operating regions, which can be divided into the partial load regime and full load regime based on the wind speed. The partial load regime is defined as the wind speed is larger than the cut-in speed (at which speed, the WECS starts to produce power) and lower than the rated speed (at which speed, the output power gets rated value). In this region, the WECS is supposed to extract maximum power and the pitch angle is kept constant. The full load regime is defined as wind speed is above the rated speed and below the cut-out speed (at which speed, the WECS stops to produce power). In this region, the WECS is supposed to extract whatever the rated value the wind speed is through adjusting the pitch angle.

Several control methods and techniques have been used in the partial load regime. As discussed in [31], a classic controller that has slow dynamics relative to the mechanical dynamics of the drive train is implemented in commercial wind turbines. [31] evaluates the implementation, on a test bench, of a controller whose dynamics can be adjusted to be faster and compares in particular its aerodynamic efficiency with the conventional controller. [32] reviews the design of algorithms for wind turbine pitch control and also for generator torque control in the case of variable speed turbines. It also discusses some recent and possible future developments. It then focuses on the torque control using additional sensors in variable speed turbines, which are used primarily to maximize energy capture below rated wind speed and to limit the torque above rated. In [33], the

small signal stability problem is also analyzed. However, for PI controllers being used, the parameters usually need to be tuned to obtain control gains as a tradeoff or compromise so that they can work in different operating conditions. Moreover, a gain-scheduling control method to control variable speed WECS in the context of LPV (linear parameter-varying) systems has been proposed in [34]. A Linear Quadratic Gaussian (LQG) approach is used in [35].

Even more research has been done and more papers have been published focusing in the full load regime. Linear Quadratic Gaussian controllers have been designed for WECS control in order to reach a trade-off between the maximization of the energy harvested from the wind and the minimization of the damage caused by mechanical fatigue [36-39].

Also, papers focusing on both regimes have been published [30, 41 and 42]. In [41], the authors propose a universal tracking control of Wind Energy Conversion System to obtain the maximum power. In [31, 42], model predictive control techniques are proposed to perform the wind power control. In both papers, the authors propose a multivariable control strategy based on MPC for the control of Wind Energy Conversion System. The WECS is modeled as a linear system and the wind speed is modeled as a stochastic process. However, MPC needs to predict disturbances in a finite horizon based on the past estimates during the computation of the control input, as both [31] and [42] use a state-space model for the disturbance while parameters of the model are assumed known. This is somehow limited in practice even for Gaussian disturbances as they are very hard to predict. This issue leads to exploration of novel control methods to perform power control in WECS.

2.4 Scope of this Work

As discussed in 2.2, many previous works in gain tuning for DFIG control are based on some optimization approaches to reach a tradeoff or compromise such that the wind system can achieve good, though not always the most desired, performance under various operating conditions and avoid the worst-case performance under some extreme conditions. In this work, the author presents a new voltage control approach based on different philosophy. In the proposed approach, the PI control gains for the DFIG system are dynamically adjusted based on the dynamic, continuous sensitivity which essentially indicates the dynamic relationship between the change of control gains and the desired output voltage. Hence, this control approach does not require any good estimation because the dynamic sensitivity is applied in the control approach.

For power control in WECS, as discussed above in 2.3, in order to tackle the difficulties of using MPC method, the problem of the variable speed variable pitch WECS power control is solved with a constrained stochastic linear quadratic control method. The disturbance (i.e., the wind speed measurement error) is modeled as the random noise, and is not predicted using any assumed model. Thus, the measured output will be stochastic due to the random disturbance of wind speed measurement, which causes that the constraints on the output can only be enforced in a probabilistic sense, e.g. chance constraints. In the first case, it is assumed that the disturbance is Gaussian and considers a stochastic problem by minimizing the expectation of the cost function. Moreover, unlike [42], where a state-space model is employed to predict the disturbance, the problem will be solved through its Gaussian statistics. In the second case, no assumption is made to the distribution on the disturbance (wind speed measurement

error), which is more realistic, but a bound on its amplitude is assumed instead. More specifically, the problem is formulated as a min-max problem to compute the optimal control that minimizes the largest cost generated in the disturbance space. Both problems are converted to SDP optimization problems which can be solved through existing software tools.

CHAPTER 3 VOLTAGE REGULATION FOR WIND TURBINE BASED POWER SYSTEM

3.1 Chapter Introduction

This chapter presents an adaptive control strategy, which is proposed to maintain the terminal voltage of a wind plant to make it a PV bus such as a conventional generator bus with excitation control.

3.2 Modeling of the Wind-Turbine Doubly-Fed Induction Generator

3.2.1 Turbine Model

The wind turbine doubly fed induction generator (DFIG) system is shown in Fig. 3.1.

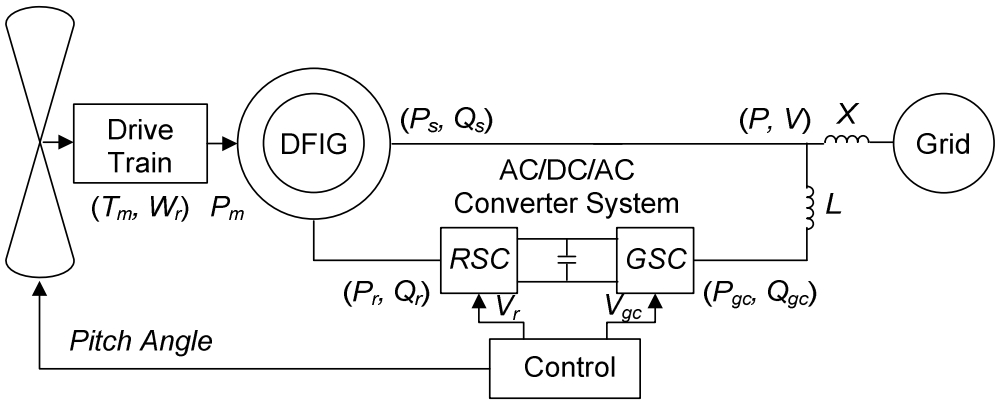

Fig. 3.1 Wind turbine DFIG system

The wind power captured by the wind turbine is converted into mechanical power by the wind turbine, and then transmitted to the grid by a doubly fed induction generator. The stator side of the DFIG is connected to the grid directly. The rotor side of the DFIG is connected to the grid through a back-to-back converter system. This converter system

can be divided to two components: rotor side converter (C_{rotor}) and grid side converter (C_{grid}). A capacitor is connected between these two converters as the DC voltage source.

The control system generates voltage signals to control the power output, terminal voltage, and DC voltage. There are three control parts: Rotor Side Control, Grid Side Control, and Pitch Angle Control.

3.2.2 Rotor Side Control System

The rotor-side converter is used to control the wind turbine power output and the voltage measured at the grid terminal. The wind power output is controlled to follow a pre-defined curve, see Fig. 3.2. The terminal voltage controller is designed to control the terminal voltage to maintain a constant value such that the terminal of this wind turbine DFIG system can be modeled as a PV bus according to a particular wind speed.

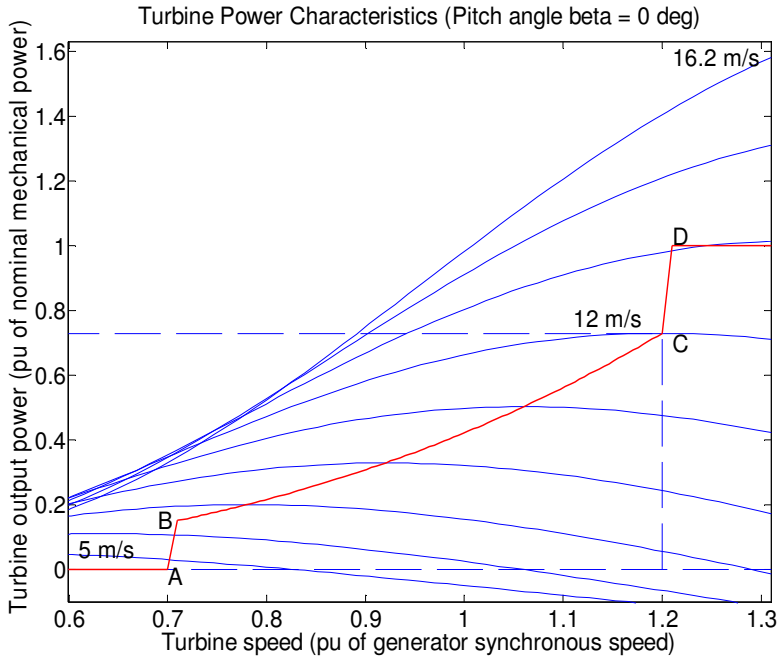

Fig. 3.2 Wind turbine power characteristics [29]

The rotor side control loop is illustrated in Fig. 3.3. For the rotor-side controller the d-axis of the rotating reference frame used for d-q transformation is aligned with the air-gap flux.

As shown in Fig. 3.3 (a), the terminal voltage is compared to the reference voltage, then, the error will be reduced to zero by the AC Voltage Regulator, with I_{dr_ref} as the output. Next, I_{dr} will be compared to I_{dr_ref} and the error will be reduced to zero by another PI controller in the Process part, with V_{dr} as the output.

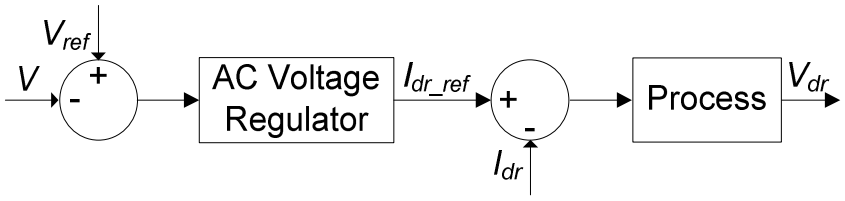

(a)

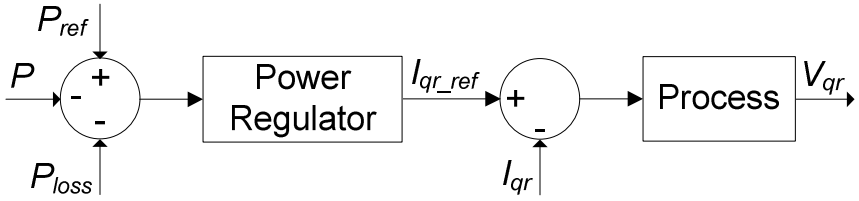

(b)

Fig. 3.3 Rotor side control system

As shown in Fig. 3.3 (b), P_{loss}, the power losses, is added to the output power. The sum is compared with the reference power. A power regulator is used to reduce the error to zero and output I_{qr_ref}. Then, another PI controller is used to reduce the error to zero in the Process part and output V_{dr}. These voltage signals will be fed back to the system as

voltage control signals.

3.2.3 Grid Side Control System

The grid side control system is illustrated in Fig. 3.4. The C_{grid} converter is used to regulate the voltage of the DC bus capacitor. For the grid-side controller the d-axis of the rotating reference frame used for d-q transformation is aligned with the positive sequence of the grid voltage.

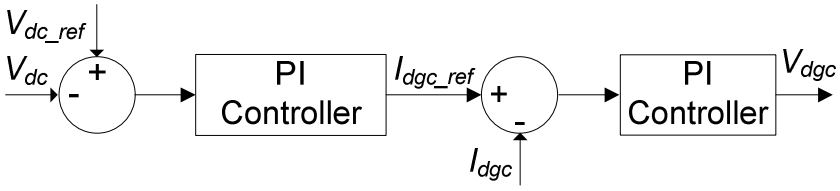

(a)

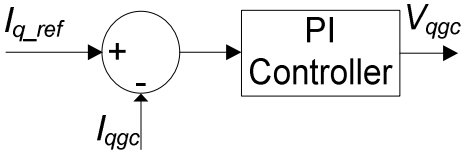

(b)

Fig. 3.4 Grid side control system

A proportional-integral (PI) controller is used to reduce the error between V_{dc} and V_{dc_ref}, and the output is I_{dgc_ref} for the current regulator. Here I_{dgc} is the current in phase with grid voltage which controls active power flow. Then, an inner current regulation loop consisting of a current regulator controls the magnitude and phase angle of the voltage generated by the converter C_{grid}, i.e., V_{gc}. Here, V_{gc} has two parts, V_{qgc} and V_{dgc},

where V_{qgc} depends on the difference between I_{qgc} and the specified reference I_{q_ref}, and V_{dgc} depends on the difference between I_{dgc} and I_{dgc_ref} which is produced by the DC voltage regulator and. The current regulator is assisted by feed forward terms which predict the C_{grid} output voltage.

3.2.4 Pitch Angle Control System

The pitch angle is kept constant at zero degree until the wind speed reaches a specified value (see Fig. 3.2.). Then, beyond this value, the pitch angle is proportional to the speed deviation from this specified speed. However, the rotational speed is usually chosen less than the point-D speed because it is of less interest for electromagnetic transients [29].

3.3 Adaptive Control Strategy

When there is a drop of the terminal voltage of the DFIG due to wind speed change or load change, it needs to quickly recover to its scheduled value pre-defined by operators. In the proposed approach, we first define an exponential curve, as illustrated in Fig. 3.5, as the desired response based on the value immediately after the voltage drop as the initial value (V_0) and the final steady-state value (V_{final}, usually the desired voltage schedule). The transition from V_0 to V_{final} follows an exponential increase defined with the shape of $1 - e^{-\frac{t}{\tau}}$, where τ is a user-defined time constant. In other words, the voltage deviation from V_{final} is $\Delta V(t) = \Delta V_{t0} e^{-\frac{t}{\tau}}$, which is an exponential decay. Hence, as long as we can keep the voltage response following the desired curve as shown in Fig. 3.5, the stability will be maintained without instability or overshoot problems.

Here, a period of 5τ (i.e., 5 times of the time constant) is chosen as the desired response time because the voltage after 5τ is almost the same as V_{final} (e^{-5} =0.007≈0 and $V(t=5\tau)$ = 0.993 V_{final} ≈ V_{final}. Hence, if the operators prefer the voltage rise time is t_r seconds, then the time constant τ is $0.2t_r$ seconds.

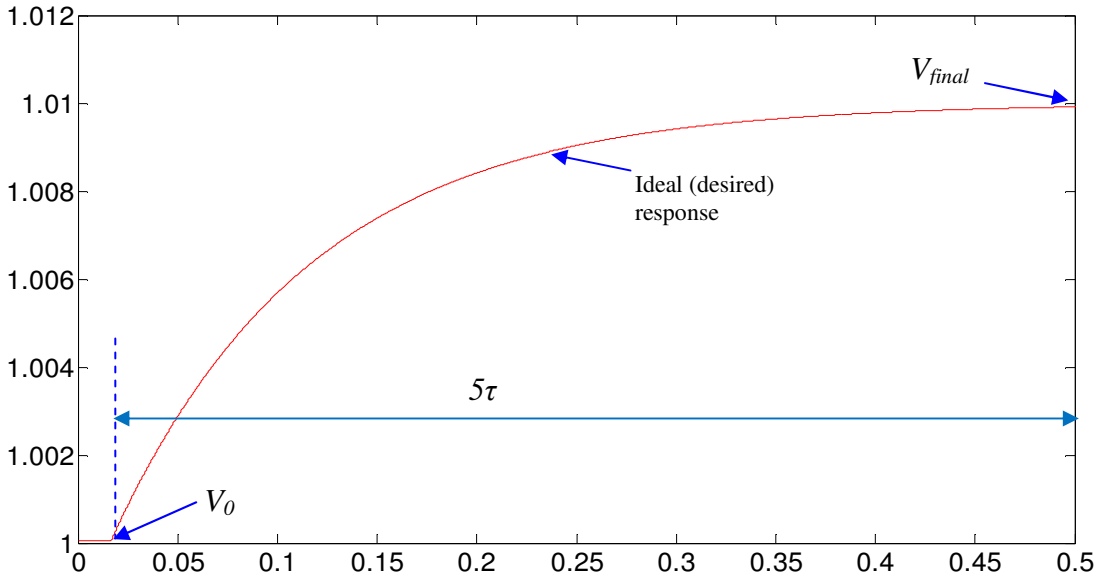

Fig. 3.5 Reference voltage curve for the proposed control approach

Next, the PI controllers with dynamical adjustment are applied to reduce the error between the actual voltage response and the ideal (desired) response to zero. Initially, very small values of the PI controller gains are applied, which lead to a large error. However, the control gains may be gradually increased to speed up the reduction of the error such that the actual voltage may catch up the desired voltage regulation curve. The increasing pattern may be stopped when the actual voltage curve is aligned with the desired curve. The above process is somewhat similar to accelerate a moving object to

catching another moving target at the desired velocity. Once the object reaches the desired velocity, the acceleration may be stopped (to avoid overshoot).

Hence, the above control process differs from conventional PI control and/or gain tuning because of the dynamic adjustment of the PI control gains during the voltage regulation process, while conventional PI control uses fixed control gains during the process or different control gains under different scenarios. Since the proposed control process starts with a small value of control gains, it will not have the overshoot problem at the very beginning. Then, the gains will be gradually increased such that the actual voltage response can "speed up" to eventually catch up the desired response curve.

Next, more technical details are elaborated.

3.3.1 Voltage Control System Configuration

Fig. 3.6 shows the actual control part of the rotor side control.

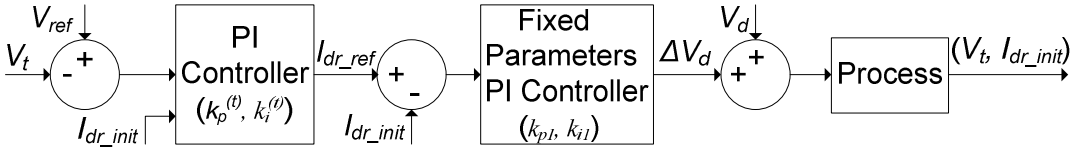

Fig. 3.6 Terminal voltage control loop

First, the error between the reference voltage and the actual voltage goes into the first PI controller, which has flexible PI control gains (i.e., $k_p^{(t)}$ and $k_i^{(t)}$) and gives updated value of I_{dr_ref}. The difference between the I_{dr_ref} and I_{dr_init} is the initial value for the second fixed-gain controller. Hence, we can obtain the equation to calculate the output of the first PI controller as follows:

$$I_{dr\_ref}^{(t)} = I_{dr\_init}^{(t)} + k_p^{(t)}(V_{ref}^{(t)} - V_t^{(t)}) + k_i^{(t)} \int_t^{t+1} (V_{ref}^{(t)} - V_t^{(t)}) d\tau \tag{3.1}$$

The second fixed-gain (i.e., k_{p1} and k_{i1} in Fig. 3.6) PI controller is used to control I_{dr_init} to reach its reference value I_{dr_ref}. The equation to calculate the output of the second PI controller is given by:

$$\begin{aligned} \Delta V_d^{(t)} &= k_{p1}[k_p^{(t)}(V_{ref}^{(t)} - V_t^{(t)}) + k_i^{(t)} \int_t^{t+1} (V_{ref}^{(t)} - V_t^{(t)}) d\tau] \\ &+ k_{i1} \int_t^{t+1} [k_p^{(t)}(V_{ref}^{(t)} - V_t^{(t)}) + k_i^{(t)} \int_t^{t+1} (V_{ref}^{(t)} - V_t^{(t)}) d\tau] d\tau \end{aligned} \tag{3.2}$$

The sampling frequency is usually very high (at the level of multiple kHz), so $d\tau$ is very small. Then, we can linearize the above equation based on the sampling frequency as follows:

$$\Delta V_d^{(t)} = (V_{ref}^{(t)} - V_t^{(t)}) \cdot (k_p^{(t)} k_{p1} + k_i^{(t)} k_{p1} d\tau + k_p^{(t)} k_{i1} d\tau + k_i^{(t)} k_{i1} d\tau d\tau) \tag{3.3}$$

3.3.2 Sensitivity φ

We may define a sensitivity φ as follows:

$$\varphi = \frac{\Delta V_t^{(t)}}{\Delta V_d^{(t)}} = \frac{V_t^{(t)} - V_t^{(t-1)}}{V_d^{(t)} - V_d^{(t-1)}} \tag{3.4}$$

This sensitivity φ shows the amount of $V_t^{(t)}$ change when there is a small change of $V_d^{(t)}$. It represents the intrinsic relationship among control variables affecting the voltage control process. This sensitivity φ is related to the entire DFIG system, or the "plant" model. With a small change to $V_d^{(t)}$ applied at each step in a very small interval, this φ should be almost constant within several sampling periods.

In this DFIG design, $V_d^{(t)}$ is an intermediate parameter. It can be expressed as follows:

$$V_d = R_r \cdot i_{dr} - (\omega - \omega_r) \cdot (L_{lr} + L_m) \cdot i_{qr} - (\omega - \omega_r) \tag{3.5}$$

Since $V_t^{(t)}$ is the terminal voltage of stator, it can be written as:

$$V_t = \sqrt{V_{qs}^{\ 2} + V_{ds}^{\ 2}} \tag{3.6}$$

In DFIG, the positive sequence phasor model for the asynchronous machine can be written as:

$$V_{qs} = R_s \cdot i_{qs} + \omega \cdot \left[(L_{ls} + L_m) \cdot i_{ds} + L_m \cdot i_{dr} \right] \tag{3.7}$$

$$V_{ds} = R_s \cdot i_{ds} - \omega \cdot \left[(L_{ls} + L_m) \cdot i_{qs} + L_m \cdot i_{qr} \right] \tag{3.8}$$

Hence, we have

$$\varphi = \frac{\Delta V_t}{\Delta V_d} = \frac{\partial \left(\sqrt{V_{qs}^{\ 2} + V_{ds}^{\ 2}} \right)}{\partial V_d} = \frac{\frac{\partial \left(\sqrt{V_{qs}^{\ 2} + V_{ds}^{\ 2}} \right)}{\partial i_{qs}}}{\frac{\partial V_d}{\partial i_{qs}}} = \frac{V_{qs} R_s - V_{ds} (L_{ls} + L_m) \omega}{-\left(\sqrt{V_{qs}^{\ 2} + V_{ds}^{\ 2}} \right) (\omega - \omega_r) L_m} \tag{3.9}$$

with $R_s \ll L_m$ and $L_{ls} \ll L_m$, we have

$$\varphi \cong \frac{V_{ds}}{\left(\sqrt{V_{qs}^{\ 2} + V_{ds}^{\ 2}} \right) (\omega - \omega_r)} \leq \frac{1}{(\omega - \omega_r)_{init}} \tag{3.10}$$

where, V_{qs} and i_{qs} are the q-axis stator voltage and current, respectively; V_{ds} and i_{ds} are d axis stator voltage and current; R_s and L_{ls} are stator resistance and leakage inductance; R_r and L_{lr} are rotor resistance and leakage inductance; L_m is magnetizing inductance; ω and ω_r are synchronous speed and electrical angular velocity. All the values are in per unit [29].

3.3.3 Initial Values of Control Parameters

Here, $k_p^{(0)}$ and $k_i^{(0)}$ can start from very small values. This subsection gives a systematic approach to identify the upper bound of such "small values". To simplify our control approach, we may update these two parameters each step with a constant proportional relationship given by

$$k_i^{(t)} = \alpha \cdot k_p^{(t)} \; k_i^{(t)} = \alpha \cdot k_p^{(t)} \tag{3.11}$$

where, α is a constant number. The choice of this α value is elaborated in the next subsection.

Then, we have:

$$\begin{aligned} V_d^{(t)} &= (V_{ref}^{(t)} - V_t^{(t)}) \cdot (k_p^{(t)} k_{p1} + k_i^{(t)} k_{p1} d\tau + k_p^{(t)} k_{i1} d\tau + k_i^{(t)} k_{i1} d\tau d\tau) \\ &= (V_{ref}^{(t)} - V_t^{(t)}) \cdot k_p^{(t)} (k_{p1} + \alpha k_{p1} d\tau + k_{i1} d\tau + \alpha k_{i1} d\tau d\tau) \end{aligned} \tag{3.12}$$

Since V_t is less than V_{ref}, we have

$$\varphi = \frac{\left(V_t^{(1)} - V_t^{(0)}\right)}{\Delta V_d^{\,0}} \le \frac{\left(V_{ref}^{\;(0)} - V_t^{(0)}\right)}{\Delta V_d^{\,0}} = \frac{1}{k_p^{(0)} \cdot (k_{p1} + \alpha k_{p1} d\tau + k_{i1} d\tau + \alpha k_{i1} d\tau d\tau)} \tag{3.13}$$

Therefore, we have

$$k_p^{(0)} \le \frac{1}{(k_{p1} + \alpha k_{p1} d\tau + k_{i1} d\tau + \alpha k_{i1} d\tau d\tau) \cdot \varphi} \tag{3.14}$$

To ensure $k_p^{(0)}$ is less than the right-hand side (RHS) of (3.14), we may set $k_p^{(0)}$ less than the minimum value of the RHS of (3.14). Hence, as long as we have (3.15), Eq. (3.14) will be always satisfied.

$$k_p^{(0)} \le \frac{\left(\omega - \omega_r\right)_{init}}{(k_{p1} + \alpha k_{p1} d\tau + k_{i1} d\tau + \alpha k_{i1} d\tau d\tau)} \tag{3.15}$$

Eq. (3.15) gives the upper bound of the initial value of the control gains. It can

guarantee that $k_p^{(0)}$ and $k_i^{(0)}$ are small enough such that overshoot does not occur from the beginning. Since the above derivation always takes the conservative side, this should give relatively slow start w.r.t. the desired response curve. This is preferred because it is always desired to start with conservative values, and the initially slow response can be accelerated at a later time while aggressive initial values may immediately lead to undesired overshoot.

3.3.4 Dynamic Update of $k_p^{(t)}$ and $k_i^{(t)}$

The key of the proposed control is to dynamically adjust the control gains, k_p and k_i. Here as previously mentioned in (3.11) in III(C), k_i and k_p are assumed to keep a constant ratio given by, i.e., $k_i^{(t)} = \alpha \cdot k_p^{(t)}$ $k_i^{(t)} = \alpha \cdot k_p^{(t)}$.

The value of α represents the ratio of the effect caused by the proportional part and the integral part of the PI controller. Essentially, the result is expected to be like the curve in Fig. 3.7.

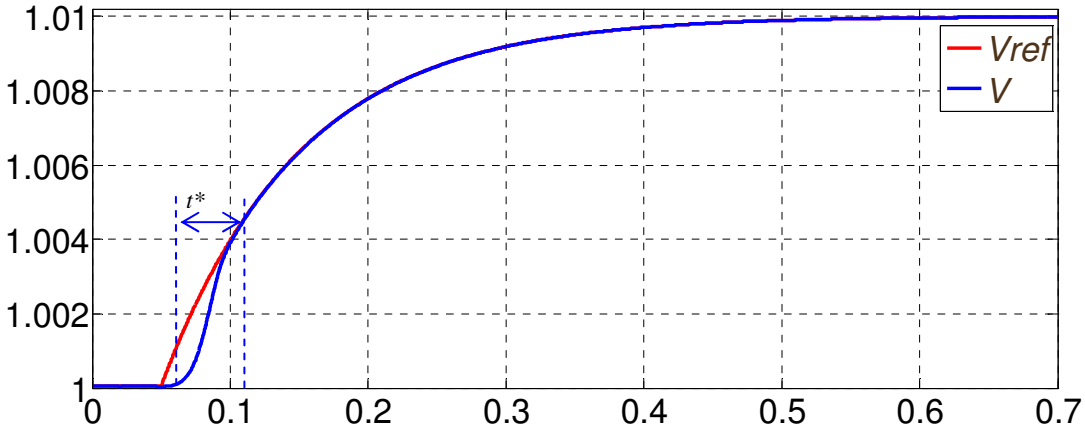

Fig. 3.7 Expected result case for terminal voltage recovery

The effect of the integral part is set roughly equal to the effect of the proportional part when the difference between the reference and the terminal voltage reaches the maximum. If the time needed for the process is t^*, it is assumed that the time needed for the difference to reach the maximum at $0.5\times t^*$. So α can be roughly calculated as follows:

$$\alpha = \frac{k_i^{(t)}}{k_p^{(t)}} = \frac{\left(V_{ref} - V_t\right)_{\max}}{\int_t^{t+t^*}\left(V_{ref} - V_t\right)dt} \cong \frac{\left(V_{ref} - V_t\right)_{\max}}{0.5\cdot\left(V_{ref} - V_t\right)_{\max}\cdot t^*} = \frac{2}{t^*} \tag{3.16}$$

Also, we consider the control gains are changed by a co-efficient β from the time t to time t+1. This is given by.

$$k_p^{(t+1)} = \beta \cdot k_p^{(t)} \tag{3.17}$$

Assuming the "catching-up" process ends after t^*, then we have:

$$k_p^0 \beta^{t^*\cdot f_s} \le k_p^{\max} \tag{3.18}$$

where f_s is the sampling frequency and $t^*\times f_s$ is the number of updates for k_p. The limit of k_p, or k_p^{max}, is given by (3.19), which is elaborated in detail in the next subsection.

$$k_p^{\max} \le \frac{1}{\varphi^{\max}(k_{p1} + \alpha k_{p1} d\tau + k_{i1} d\tau + \alpha k_{i1} d\tau d\tau)}\, k_p^{max} \le \frac{1}{\varphi^{max}\cdot(k_{p1}+\alpha k_{p1} d\tau + k_{i1} d\tau + \alpha k_{i1} d\tau d\tau)} \tag{3.19}$$

where $\varphi^{\max}$ is the largest value of φ which is dynamically updated during the control process.

Therefore, we have

$$k_p^0 \beta^{t^*\cdot f_s} \le k_p^{\max} \le \frac{1}{\varphi^{\max}(k_{p1} + \alpha k_{p1} d\tau + k_{i1} d\tau + \alpha k_{i1} d\tau d\tau)} \tag{3.20}$$

Hence, the value of β can be chosen as:

$$\beta = \left[k_p^0 \varphi^{\max}(k_{p1} + \alpha k_{p1} d\tau + k_{i1} d\tau + \alpha k_{i1} d\tau d\tau)\right]^{\frac{-1}{t^*\cdot f_s}} \tag{3.21}$$

3.3.5 Limit for $k_p^{(t)}$

The goal of the proposed method is to control the terminal voltage such that it can reach the final value smoothly following the ideal response curve as much as possible. At the beginning of this voltage control process, the error between the reference and the voltage increases and essentially reaches the peak value. Then, it starts to decrease. As previously described, here the dynamically adjusted control gains play as the "acceleration factor" or "de-acceleration factor" during this control process. By doing so, the voltage error may go to zero without going to negative (i.e., overshoot). Thus, there should be a maximal value of $k_p^{(t)}$. From (3.4), we know

$$\left(V_t^{(t+1)} - V_t^{(t)}\right) = \Delta V_d^{(t)} \varphi \left(V_t^{(t+1)} - V_t^{(t)}\right) = \Delta V_d^{(t)} \varphi \tag{3.22}$$

With (3.12), we can obtain

$$\left(V_t^{(t+1)} - V_t^{(t)}\right) = (V_{ref}^{(t)} - V_t^{(t)}) \cdot k_p^{(t)} (k_{p1} + \alpha k_{p1} d\tau + k_{i1} d\tau + \alpha k_{i1} d\tau d\tau) \varphi \tag{3.23}$$

It is necessary to ensure the following equation such that there will not be any overshoot

$$\left(V_t^{(t+1)} - V_t^{(t)}\right) < \left(V_{ref}^{(t)} - V_t^{(t)}\right) \tag{3.24}$$

Hence, we have

$$(V_{ref}^{(t)} - V_t^{(t)}) \cdot k_p^{(t)} (k_{p1} + \alpha k_{p1} d\tau + k_{i1} d\tau + \alpha k_{i1} d\tau d\tau) \cdot \varphi < (V_{ref}^{(t)} - V_t^{(t)}) \tag{3.25}$$

Therefore, we have

$$k_p^{(t)} (k_{p1} + \alpha k_{p1} d\tau + k_{i1} d\tau + \alpha k_{i1} d\tau d\tau) \cdot \varphi < 1 \tag{3.26}$$

$$k_p^{(t)} < \frac{1}{(k_{p1} + \alpha k_{p1} d\tau + k_{i1} d\tau + \alpha k_{i1} d\tau d\tau) \cdot \varphi} \tag{3.27}$$

To ensure that $k_p^{(t)}$ is less than the right-hand side (RHS) of (3.27), we may set $k_p^{(t)}$ less than the minimum value of the RHS of (3.27), which occurs at $\varphi=\varphi^{max}$. Hence, as long as we have (3.28), Eq. (3.27) is always ensured.

$$k_p^{\max} < \frac{1}{\varphi^{\max} \cdot (k_{p1} + \alpha k_{p1} d\tau + k_{i1} d\tau + \alpha k_{i1} d\tau d\tau)} \tag{3.28}$$

3.3.6 Flow Chart

The whole control process is briefly presented in the flowchart shown in Fig. 3.8.

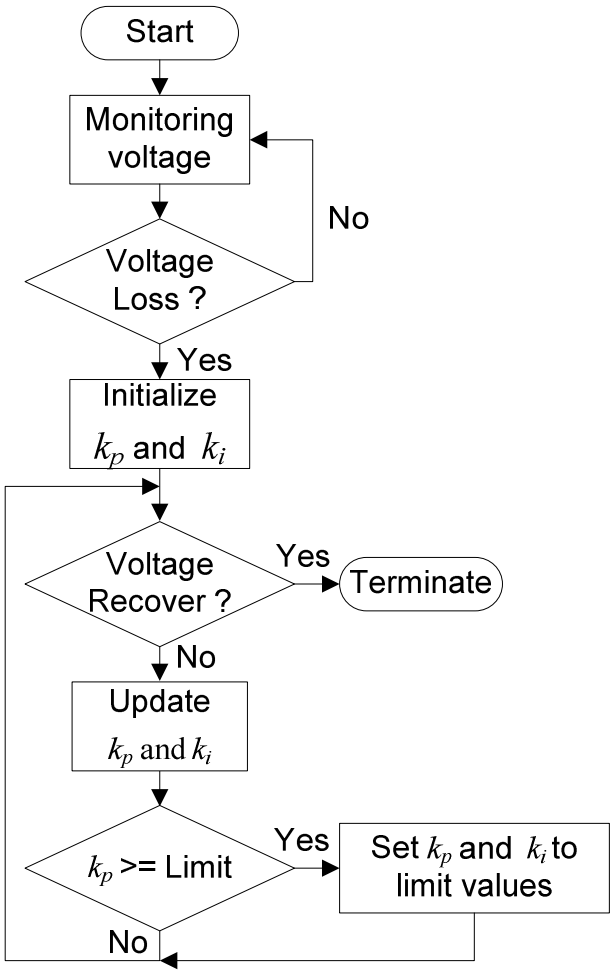

Fig. 3.8 Flow chart showing the control process for terminal voltage recovery

3.4 Simulations and Results

The power system under study is shown in Fig. 3.9. The wind farm, which consists of six 1.5 MW wind turbines, is connected to a 25 kV distribution system. This farm exports power to a 120 kV grid through a 30 km 25 kV feeder. A 2 MVA plant consisting of a motor load and of a 200 kW resistive load is connected on the same feeder at bus B25. A 500 kW load is connected to the DFIG system [29].

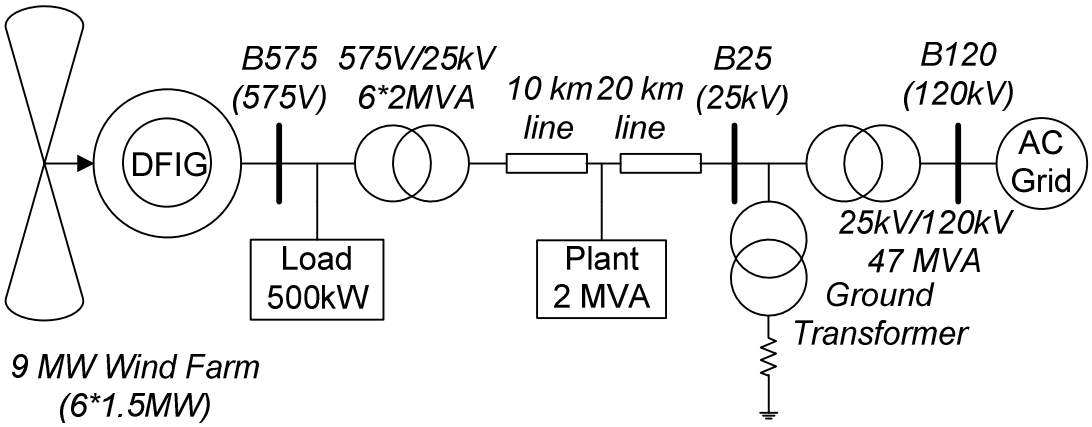

Fig. 3.9 Sample power system with DFIG for simulation study

In this section, first, a demonstration of inappropriate fixed PI gains is shown to verify the importance of PI gains. Then, several case studies are carried out to illustrate that the proposed approach of dynamically adjusted PI gains can achieve desired performance under various operating conditions.

3.4.1 Demonstration of Instability with Inappropriate PI Gains

As previously mentioned in Sections 3.1 and 3.2, the motivation of this work is to present an approach to avoid the potential instability raised by fixed control gains. With

inappropriate k_p and k_i values, different responses like unstable response, stable but oscillating response, or sluggish response may happen. The results from an example are shown in Fig. 3.10 (a) (b) (c) (d) for the case that the reference voltage changes from a stable state value 1.0 p.u. to 1.01 p.u. to mimic a small disturbance. Control gains of k_p=4.5 and k_i=1080 are chosen. The results include active power, reactive power, terminal voltage, and DC voltage.

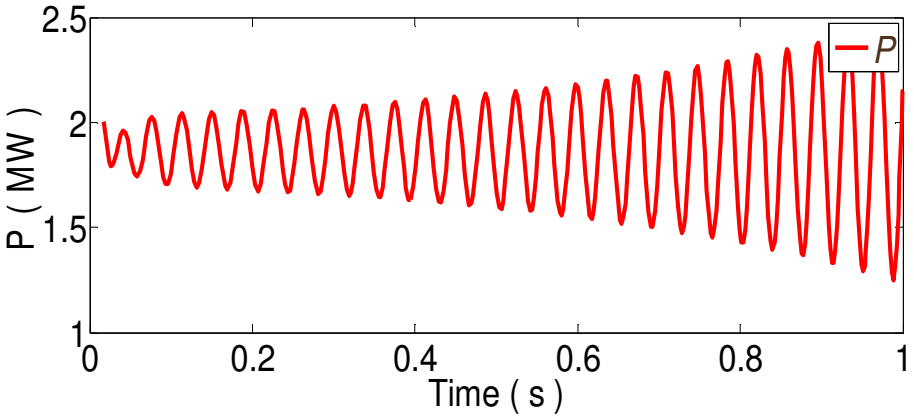

Fig. 3.10 (a) Real power output voltage

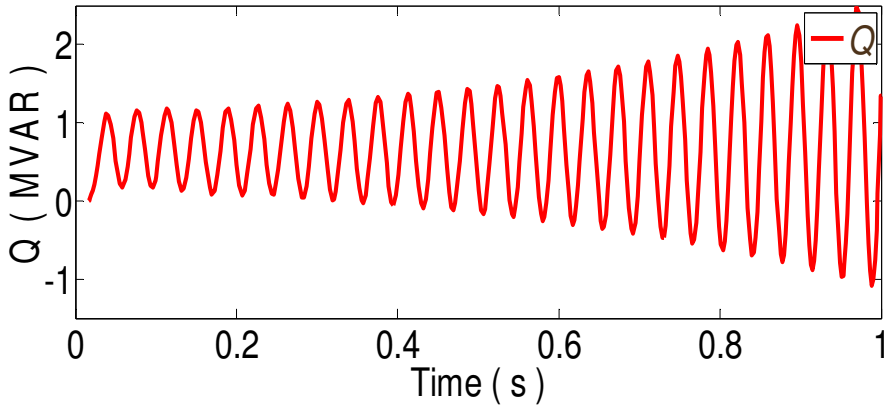

Fig. 3.10 (b) Reactive power output

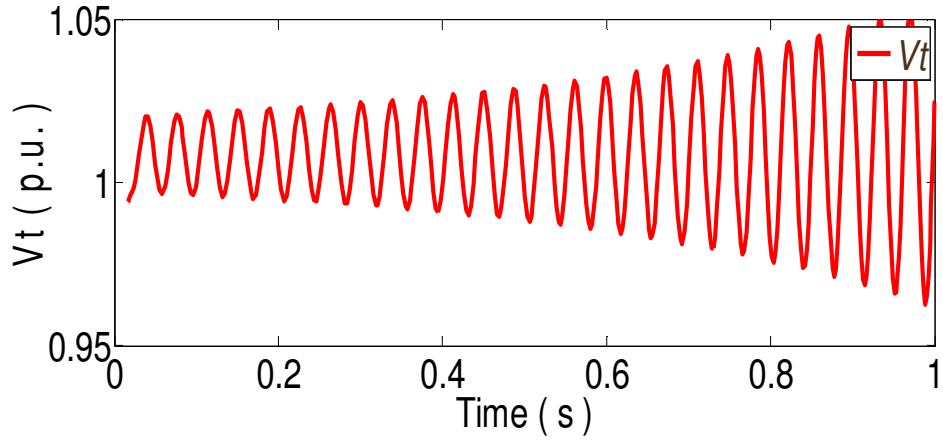

Fig. 3.10 (c) Terminal voltage

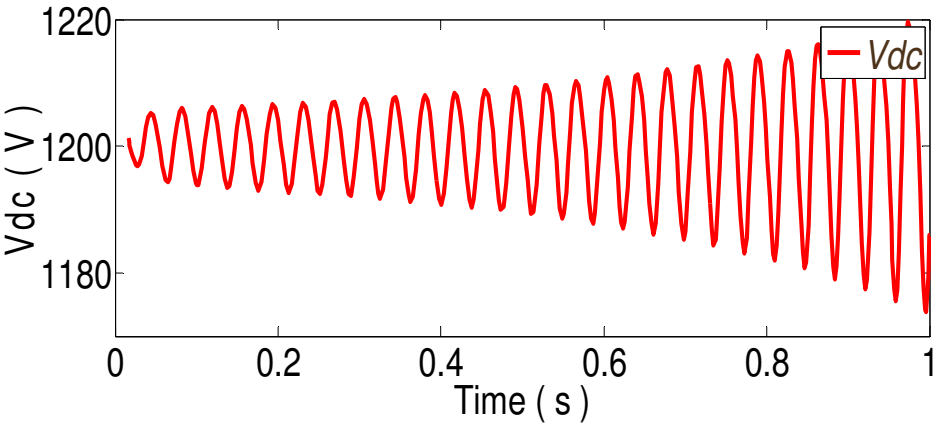

Fig. 3.10 (d) DC voltage

Fig. 3.10 Demonstration of instability with inappropriate PI gains

3.4.2 Case One: Set Final Voltage to 1.01 p.u.

As mentioned in the opening part in section 3, users may define the desired time to regulate the terminal voltage from the time of disturbance to the final steady-state value. Here the transient time for voltage is set to 0.5 seconds since this is fast enough before other conventional (usually much slower) voltage controls take effect or are activated.

Since an exponential decay of the voltage difference, i.e., $\Delta V(t) = (V_{final} - V_{t0})e^{-\frac{t}{\tau}}$, is preferred with 5τ as the desired transition time, τ is 0.1 sec in this and the next a few studies.

In this case study, a step change of voltage reference is made from 1.0 to 1.01 per unit. The dynamically adjusted control gains are employed. As shown in Fig. 3.11 (a), a smooth transition can be achieved. Note that the control gain such as k_p changes dynamically. As shown in Fig. 3.11(b), initially, the terminal voltage lags the desired voltage. Then, it gradually catches up the desired voltage growth curve. Once it reaches the desired curve, the control gain k_p stops increasing and the actual curve matches the desired curve very well. Fig. 3.11(c) shows the dynamic values of k_p. The above process is similar to accelerate a moving object to reach the desired velocity. Once the desired velocity is reached, the accelerating factor (i.e., k_p) may stop increasing and remain the value at that point.

Fig. 3.11 (d) shows the value of φ and Fig. 11(e) shows the value of V_{dc}.

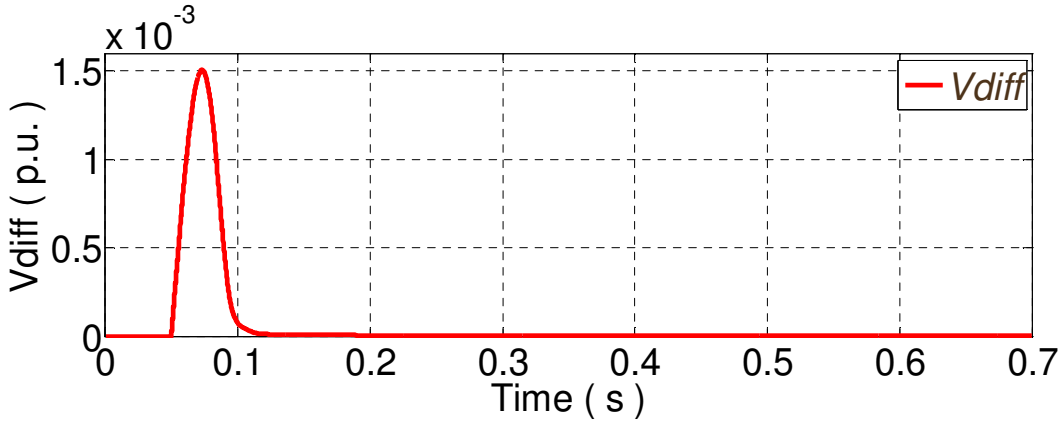

Fig. 3.11 (a) Voltage error (or difference) between the voltage reference and the actual voltage in per unit

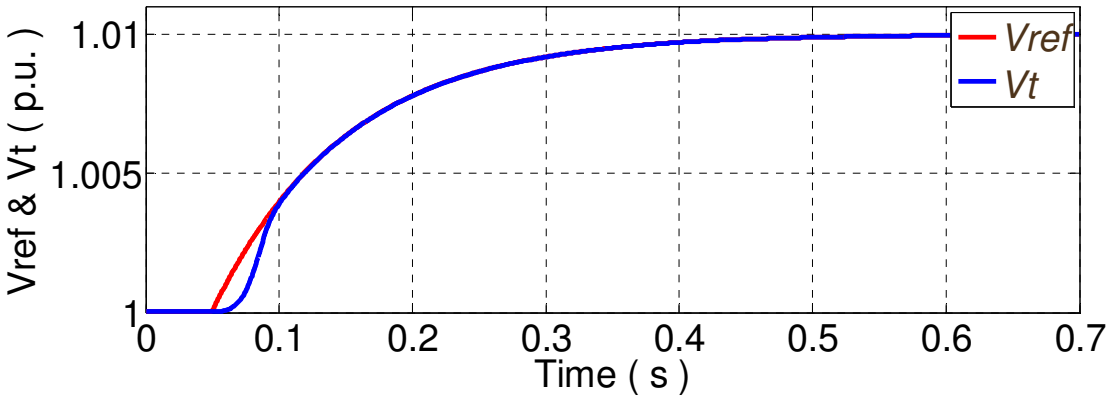

Fig. 3.11 (b) Actual (blue) and the desired voltage response curve (red) in per unit

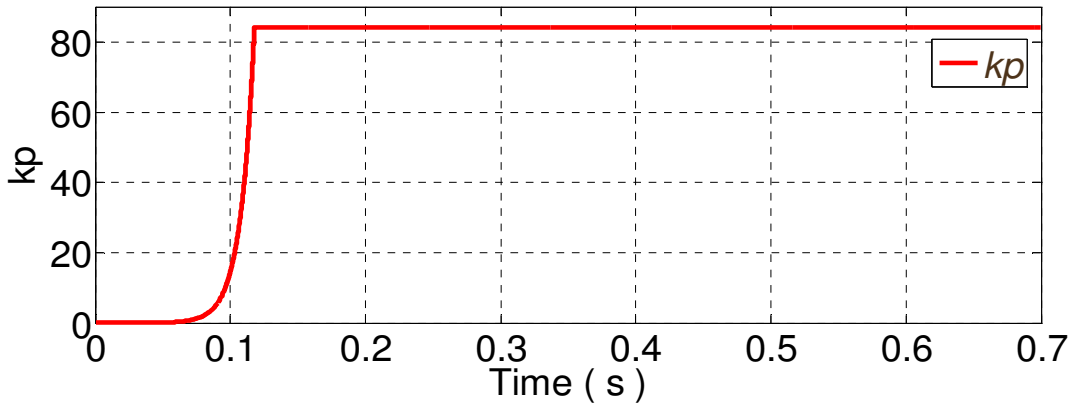

Fig. 3.11 (c) Control gain kp

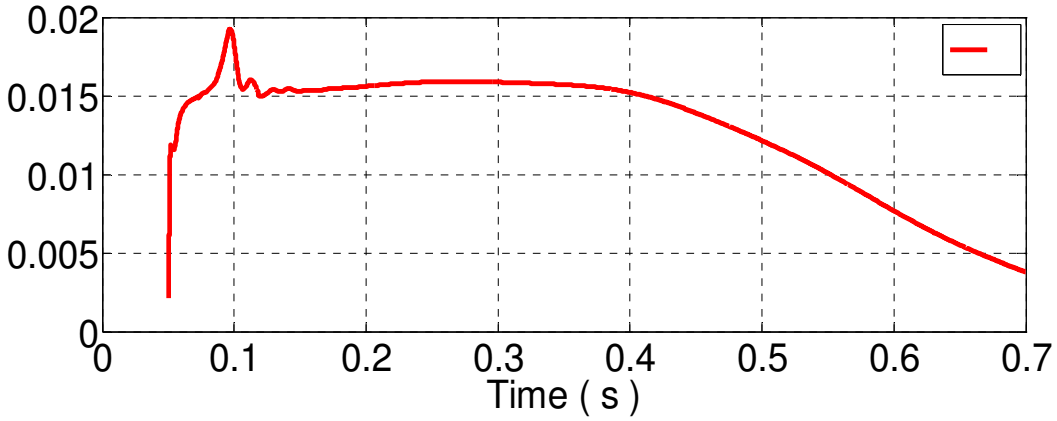

Fig. 3.11 (d) Sensitivity φ ($\varphi^{max} = 0.02$)

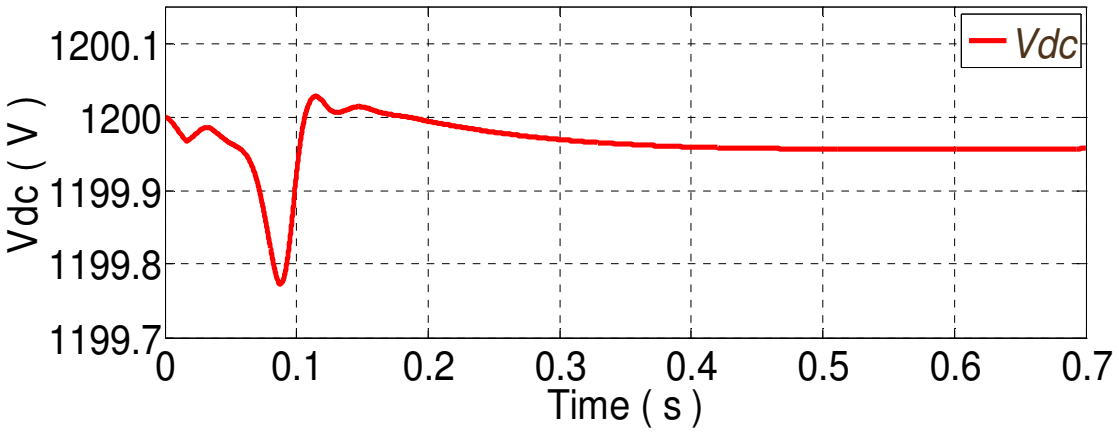

Fig. 3.11 (e) DC voltage

Fig. 3.11 Results for case one: set final voltage to 1.01 p.u.

3.4.3 Case Two: Set Final Voltage to 1.04 p.u.

Fig. 3.12 (a) (b) (c) (d) (e) show the results of Case Two, in which the voltage reference is changed from 1.0 to 1.04 p.u. to mimic a larger disturbance. The results are very similar to the previous case study, and similar observations can be made.

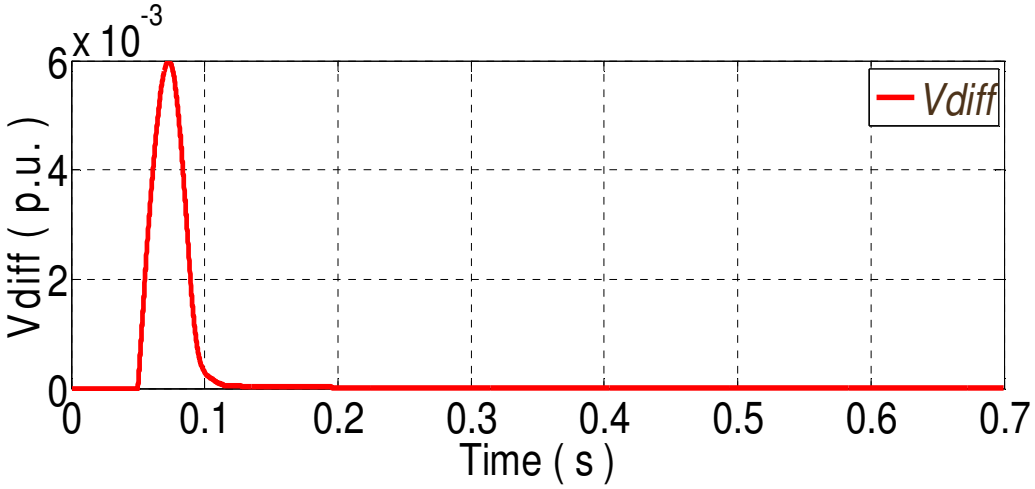

Fig. 3.12 (a) Voltage error (or difference) in per unit

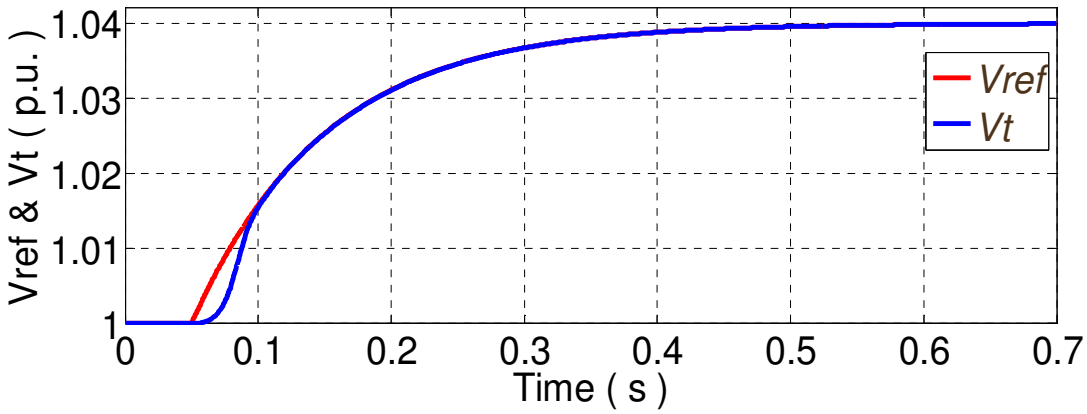

Fig. 3.12 (b) Actual (blue) and the desired voltage response curve (red) in per unit

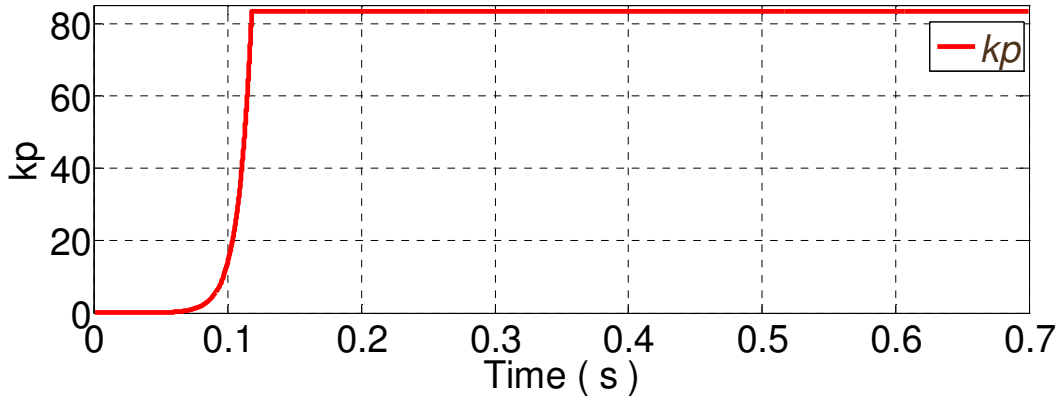

Fig. 3.12 (c) Control gain kp

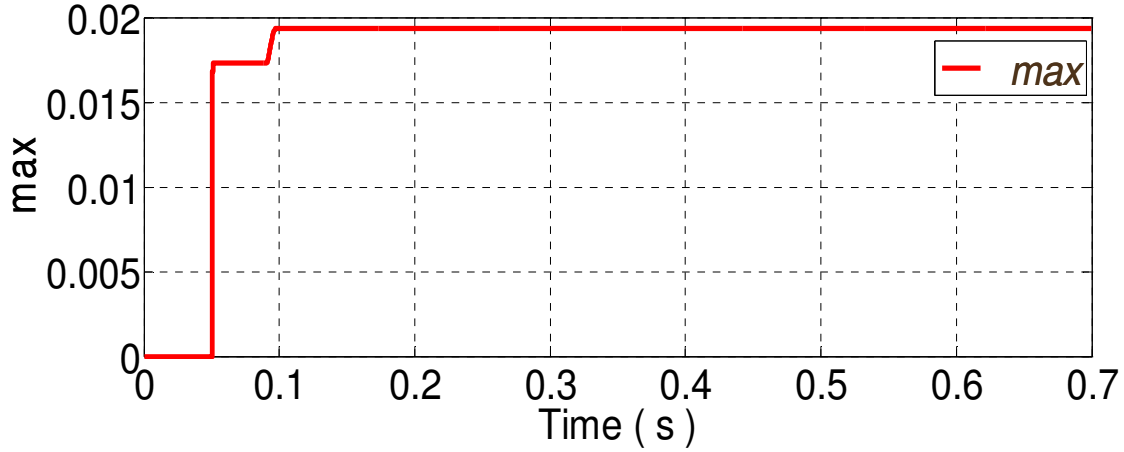

Fig. 3.12 (d) Sensitivity φ (φ^{max} =0.02)

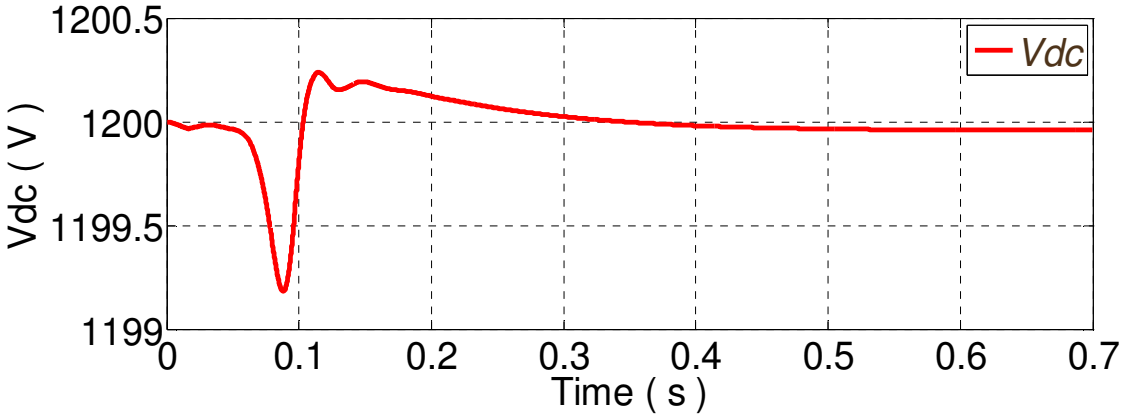

Fig. 3.12 (e) DC voltage

Fig. 3.12 Results for case two: set final voltage to 1.04 p.u.

3.4.4 Case Three, Four, and Five: Load=200, 800, and 1100kW, respectively

Different loads may have different effects on the terminals voltage of the wind turbine DFIG system. Hence, three additional case studies are performed. These cases are similar to Case One, but differ in the amount of load. Considering the load in Case One is 500 kW, the load levels in Cases Three, Four, and Five are changed to 200 kW, 800 kW, and 1100 kW, respectively. The results of the three most important variables, voltage error in p.u., voltage in p.u., and V_{dc} in volts are shown in Figures 3.13 (a) (b) (c), 3.14 (a) (b) (c), and 3.15 (a) (b) (c), respectively.

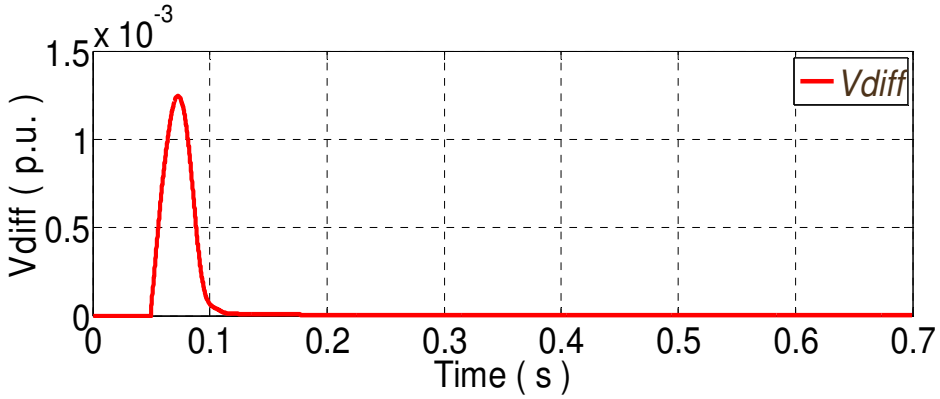

Fig. 3.13 (a) Voltage error (or difference) in per unit

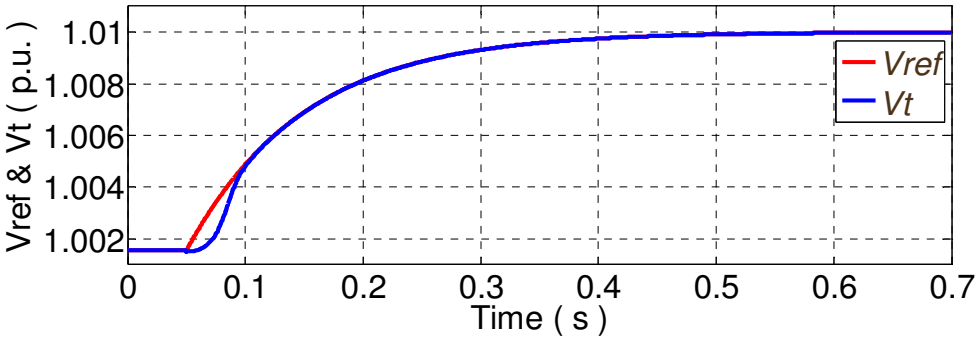

Fig. 3.13 (b) Actual (blue) and the desired voltage response curve (red) in per unit

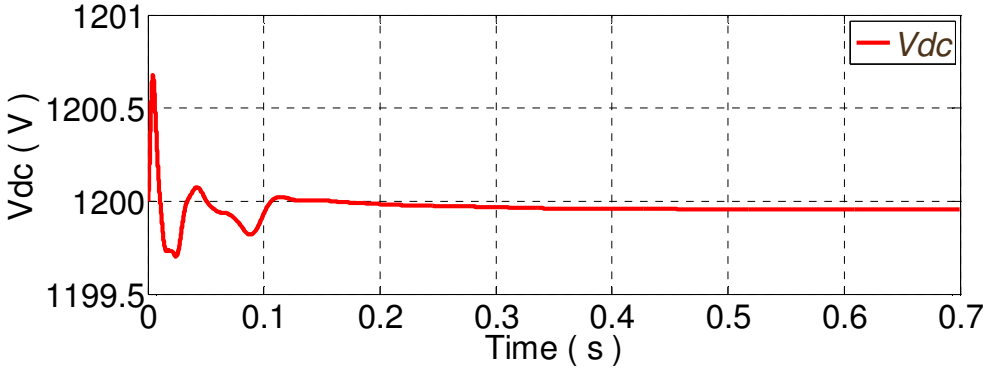

Fig. 3.13 (c) DC voltage

Fig. 3.13 Results for case three: Load = 200 kW

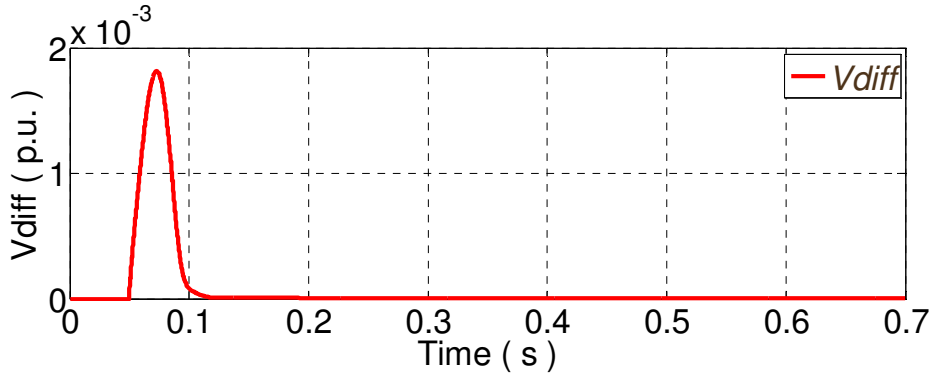

Fig. 3.14 (a) Voltage error (or difference) in per unit

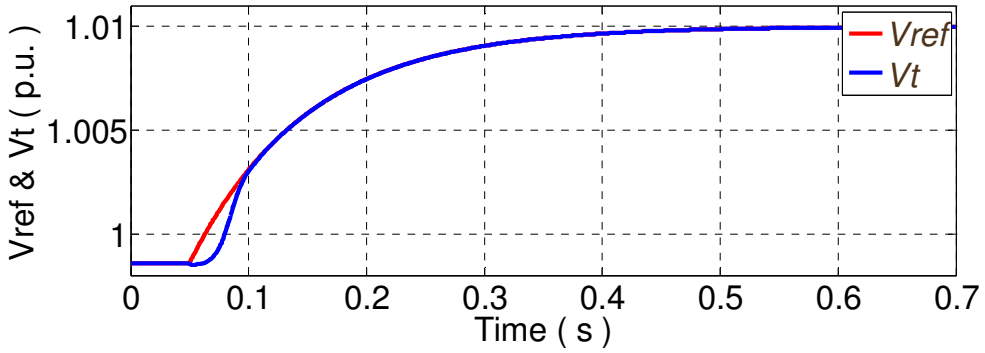

Fig. 3.14 (b) Actual (blue) and the desired voltage response curve (red) in per unit

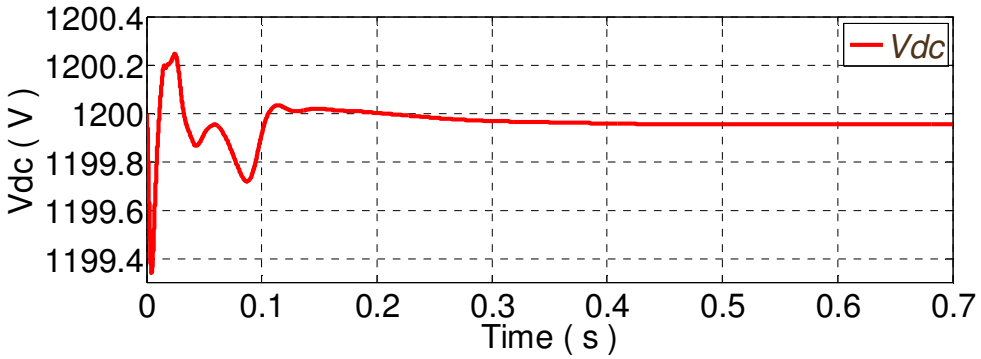

Fig. 3.14 (c) DC voltage

Fig. 3.14 Results for case four: Load = 800 kW

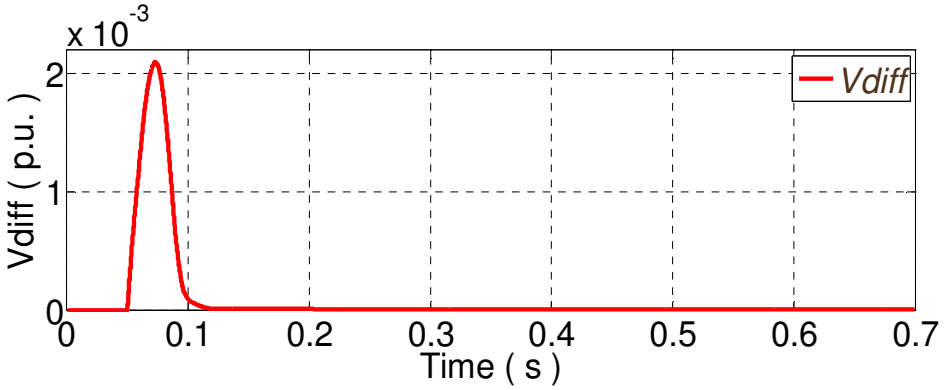

Fig. 3.15 (a) Voltage error (or difference) in per unit

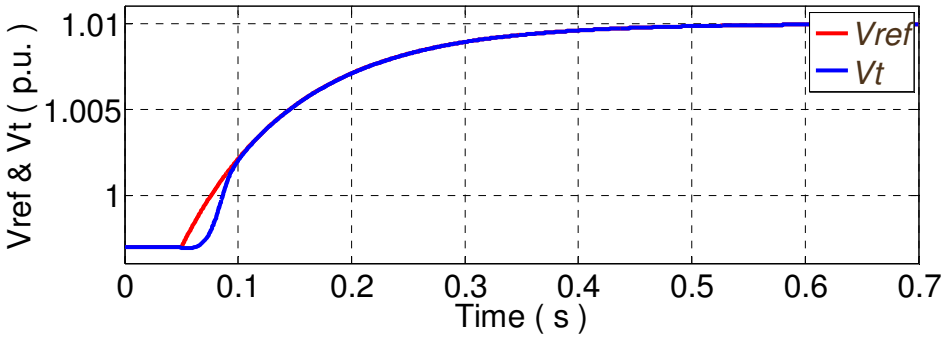

Fig. 3.15 (b) Actual (blue) and the desired voltage response curve (red) in per unit

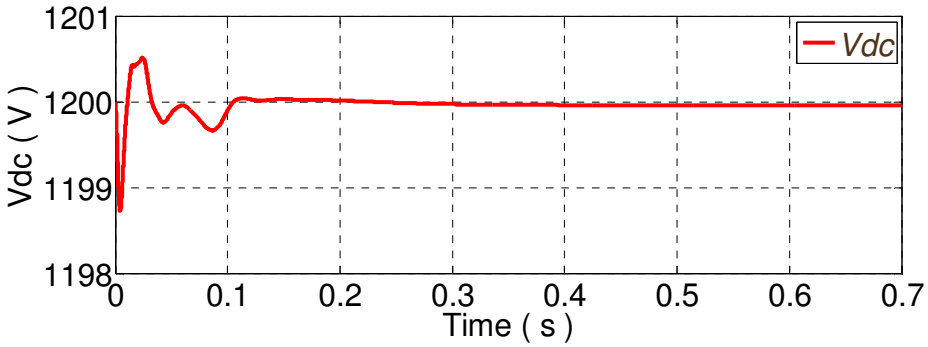

Fig. 3.15 (c) DC voltage

Fig. 3.15 Results for case five: Load = 1100 kW

As observed in these figures, the proposed control approach gives dynamically adjusted control gain k_p to catch up and then follow the desired performance very well.

3.5 Discussion and Conclusion

In this research work, a new DFIG voltage control approach based on a philosophy different from the previous works is presented. In the proposed approach, the PI control gains for the DFIG system are dynamically adjusted based on the dynamic, continuous sensitivity which essentially indicates the dynamic relationship between the change of control gains and the desired output voltage. Hence, this control approach does not require any good estimation of fixed control gains because it has the self-learning mechanism via the dynamic sensitivity. This also gives the plug-and-play feature of the proposed DFIG controller to make it promising in utility practices. Simulation results verify that the proposed approach performs as expected under various operating conditions.

CHAPTER 4 POWER REGULATION FOR WIND ENERGY CONVERSION SYSTEM I

4.1 Chapter Introduction

In this chapter, a semi-definite programming (SDP) control method is proposed to regulate the power output of Wind Energy Conversion System (WECS) in full load regime (above rated wind speed) considering the energy cost and control performance subject to stochastic wind speeds.

4.2 Modeling of Variable Speed Variable Pitch WECS

The Wind Energy Conversion System is shown in Fig. 4.1. The wind power captured by the wind turbine is converted into mechanical torque, then goes through the drive train, and finally transformed to electrical power and delivered to the grid by a doubly fed induction generator.

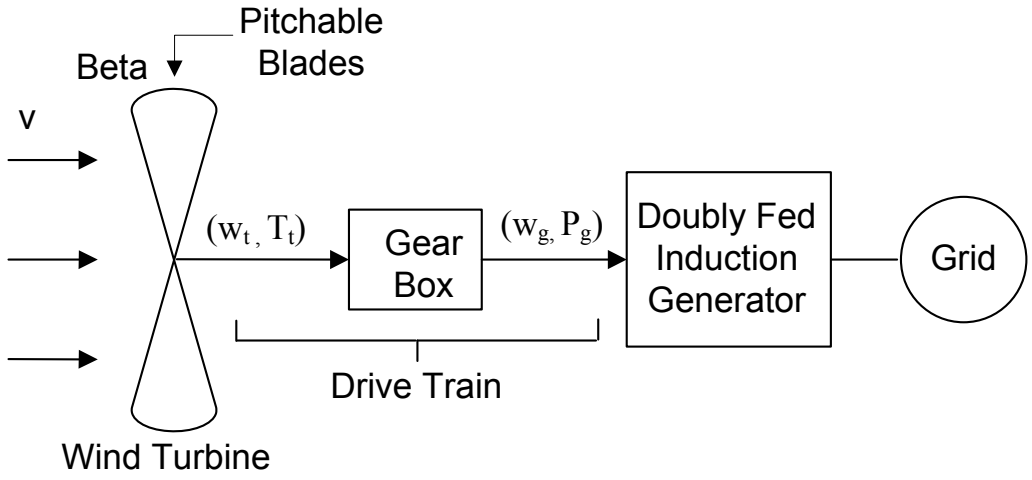

Fig. 4.1 Wind energy conversion system

The detailed parts of Wind Energy Conversion System will be introduced in the following sections.

4.2.1 Wind Speed Model

Wind speed is modeled as two components to mimic a real-time wind speed as shown in equation (4.1): v_m is describing the long-term, low-frequency variable component, and v_t is the turbulence, which describes the high-frequency variable component [30, 42].

$$v(t) = v_m(t) + v_t(t) \tag{4.1}$$

4.2.2 Pitch Actuator Model

A first-order dynamic system is used to model the pitch actuator system as in [30, 42]:

$$\dot{\beta} = -\frac{1}{\tau}\beta + \frac{1}{\tau}\beta_d \tag{4.2}$$

where, τ is the time constant of the pitch system, and β is the blade pitch angle.

The constraints of β and its derivative are given by:

$$\beta_{\min} \le \beta \le \beta_{\min} \tag{4.3}$$

$$\dot{\beta}_{\min} \le \dot{\beta} \le \dot{\beta}_{\min} \tag{4.4}$$

4.2.3 Aerodynamic System

The output of the aerodynamic system can be expressed as equation (4.5):

$$P_t = C_p(\lambda, \beta)\frac{\rho\pi R^2}{2}v^3 \tag{4.5}$$

where, P_t is the mechanical output power of the wind turbine; C_p is the performance coefficient of the wind turbine; ρ is the air density; R is the radius of wind turbine blades;

v is the wind speed; λ is the tip speed ratio of the rotor blade tip speed to wind speed, $\lambda = \omega_t R / v$ and ω_t is the speed of the low-speed shaft; β is the blade pitch angle.

The turbine torque Γ_t at the low-speed shaft is calculated as follows:

$$\Gamma_t = \frac{P_t}{\omega_t} = \frac{C_p(\lambda,\beta)}{\lambda}\frac{\rho\pi R^3}{2}v^2 \tag{4.6}$$

A generic equation is used to model $C_p(\lambda,\beta)$:

$$C_p(\lambda,\beta) = 0.5176\left(\frac{116}{\lambda_i} - 0.4\beta - 5\right)e^{-21/\lambda_i} + 0.0068\lambda \tag{4.7}$$

with

$$\frac{1}{\lambda_i} = \frac{1}{\lambda + 0.08\beta} - \frac{0.035}{\beta^3 + 1} \tag{4.8}$$

4.2.4 Drive Train Model

A two mass drive train model with flexible shaft is used with equations as follows: [30, 42]

$$\frac{d\omega_t}{dt} = -\frac{i}{J_t}\Gamma_{tw} + \frac{1}{J_t}\Gamma_t \tag{4.9}$$

$$\frac{d\omega_g}{dt} = \frac{i}{J_g}\Gamma_{tw} - \frac{1}{J_g}\Gamma_g \tag{4.10}$$

$$\frac{d\Gamma_{tw}}{dt} = k_s i\omega_t - k_s\omega_g - \left(\frac{i^2 B_s}{J_t} + \frac{B_s}{J_g}\right)\Gamma_{tw} + \frac{iB_s}{J_t}\Gamma_t + \frac{B_s}{J_g}\Gamma_g \tag{4.11}$$

$$\Gamma_{tw} = k_s\theta_{tw} + B_s\left(i\omega_t - \omega_g\right) \tag{4.12}$$

where, i is the gear ratio; Γ_{tw} and Γ_g are the flexible shaft torque and generator torque; ω_g is the generator angular velocity; k_s and B_s are the shaft stiffness and damping coefficients respectively; θ_{tw} is the shaft twist angle.

4.2.5 Generator Model

Generally speaking, electrical dynamic of the generator is much faster than the mechanical dynamic of the turbine system [44, 45]. In order to achieve the goal of designing better wind turbine controller, a simple model for the generator and converter system is employed:

$$\dot{\Gamma}_g = -\frac{1}{\tau_g}\Gamma_g + \Gamma_g^* \tag{4.13}$$

where τ_g is the time constant, and Γ_g^* is the generator torque set point.

4.2.6 WECS Linearization

The Wind Energy Conversion System is described by previous equations form (4.1) to (4.13). The nonlinearity of the whole system is the part describing the performance coefficient. In order to analyze the system using small signal method, the first step is to linearize the system at a specified operating point (OP). This OP can be obtained at long-term low-frequency wind speed v_m. Then we have

$$\begin{aligned}\Gamma_t &= f(\omega_t, v, \beta) \\ &= f(\omega_{t,op}, v_{op}, \beta_{op}) \\ &+ \left[\frac{\partial f}{\partial \omega_t}\Big|_{op} \Delta\omega_t + \frac{\partial f}{\partial v}\Big|_{op} \Delta v + \frac{\partial f}{\partial v}\Big|_{op} \Delta\beta\right] \\ &+ \cdots\end{aligned} \tag{4.14}$$

where Δ is used for representing variable's deviation from its OP. With linearization of a small deviation at OP, we have

$$\begin{aligned}\Delta\Gamma_t &= \frac{\partial f}{\partial \omega_t}\Big|_{op}\Delta\omega_t + \frac{\partial f}{\partial \nu}\Big|_{op}\Delta\nu + \frac{\partial f}{\partial \beta}\Big|_{op}\Delta\beta \\ &= L_\omega\Delta\omega_t + L_\nu\Delta\nu + L_\beta\Delta\beta\end{aligned} \tag{4.15}$$

where

$$L_\omega = \frac{\partial f}{\partial \omega_t}\Big|_{op} = \frac{\rho\pi R^2\nu^2}{2\omega_t}\left(-C_p(\lambda,\beta)\frac{\nu}{\omega_t} + R\frac{\partial C_p(\lambda,\beta)}{\partial\lambda}\right) \tag{4.16}$$

$$L_\nu = \frac{\partial f}{\partial \nu}\Big|_{op} = \frac{\rho\pi R^2\nu}{2}\left(3C_p(\lambda,\beta)\frac{\nu}{\omega_t} - R\frac{\partial C_p(\lambda,\beta)}{\partial\lambda}\right) \tag{4.17}$$

$$L_\beta = \frac{\partial f}{\partial \beta}\Big|_{op} = \frac{\rho\pi R^2\nu^3}{2\omega_t}\frac{\partial C_p(\lambda,\beta)}{\partial\beta} \tag{4.18}$$

The state vector, the control input and the measure output can be defined as

$$x = \left[\Delta\omega_t\ \Delta\omega_g\ \Delta\Gamma_{tw}\ \Delta\Gamma_g\ \Delta\beta\right]$$

$$u = \left[\Delta\Gamma_g^*\ \Delta\beta_d\right]$$

$$y = \left[\Delta\omega_g\ \Delta P_g\right]$$

Thus, the linearized WECS can be written as

$$\dot{x}(t) = \tilde{A}x(t) + \tilde{B}_u u(t) + \tilde{B}_\nu\Delta\nu(t) \tag{4.19}$$

$$y(t) = \tilde{C}x(t) \tag{4.20}$$

with

$$\tilde{A}=\begin{bmatrix} \frac{L_\omega}{J_t} & 0 & -\frac{1}{J_t} & 0 & \frac{L_\beta}{J_t} \\ 0 & 0 & \frac{1}{J_g} & -\frac{1}{J_g} & 0 \\ k_s+\frac{iB_s}{J_t} & -k_s & -\left(\frac{i^2B_s}{J_t}+\frac{B_s}{J_g}\right) & 0 & \frac{iB_s}{J_t}L_\beta \\ 0 & 0 & 0 & -\frac{1}{\tau_\beta} & 0 \\ 0 & 0 & 0 & 0 & -\frac{1}{\tau} \end{bmatrix}$$

$$\tilde{B}_u=\begin{bmatrix} 0 & 0 \\ 0 & 0 \\ 0 & 0 \\ \frac{1}{\tau_g} & 0 \\ 0 & \frac{1}{\tau} \end{bmatrix} \qquad \tilde{B}_v=\begin{bmatrix} \frac{L_v}{J_t} \\ 0 \\ \frac{iB_s}{J_t}L_v \\ 0 \\ 0 \end{bmatrix}$$

$$\tilde{C}=\begin{bmatrix} 0 & 1 & 0 & 0 & 0 \\ 0 & T_{g,rat} & 0 & \omega_{g,rat} & 0 \end{bmatrix}$$

4.3 Problem Formulation

In this section, the above linearized WECS model is converted into discrete-time format and then the problem is formulated in a general setting such that the SDP approach can be applied.

4.3.1 Discrete-Time Model

The discrete version of the linearized WECS can be written as follows

$$x(k+1)=A_d x(k)+B_u u(k)+B_d d(k) \tag{4.21}$$

$$y(k)=C_d x(k) \tag{4.22}$$

where

$A_d = e^{\tilde{A}T}$, $d(k)$ is the discrete version of $\Delta v(t)$, and $[B_u, B_d] = \left[\int_0^T e^{\tilde{A}T} dt\right]\left[\tilde{B}_u, \tilde{B}_d\right]$.

To simplify the notation in this paper, we set

$\mathbf{x} := [x(1)^T, ..., x(N)^T]^T$

$\mathbf{u} := [u(0)^T, ..., u(N-1)^T]^T$

$\mathbf{d} := [d(0)^T, ..., d(N-1)^T]^T$

4.3.2 Cost Function

Since this paper focuses on the power control of WECS in the full load region, which means the objective function is to control the outputs (ω_g and P_g) of the drive train part at rated values. Therefore, the cost function is to minimize the deviations of generator angular velocity (ω_g) and electric power (P_g) from the rated values. Meanwhile, also included is the change of control vector ($\partial\Gamma_g^*$ *and* $\partial\beta_d$, where ∂ represents the difference between the value at the current time and the previous time) at each time step. Thus, the cost function can be written as follows:

$$\min V_N(x_0, \mathbf{u}, \mathbf{d}) = \frac{1}{2}\left[\begin{array}{l}\sum_{k=1}^{N}\left(q_1\left(\omega_{g,rat} - \omega_g\right)_k^2 + q_2\left(P_{g,rat} - P_g\right)_k^2\right) \\ +\sum_{k=0}^{N-1}\left(r_1\left(\Delta T_g^*\right)_k^2 + r_2\left(\Delta\beta_d\right)_k^2\right)\end{array}\right] \tag{4.23}$$

subject to

$$\Delta\beta_{\min} \le \Delta\beta_d(k) \le \Delta\beta_{\max} \tag{4.24}$$

$$\beta_{\min} \le \beta_d(k) \le \beta_{\max} \tag{4.25}$$

$$P_{g,\min} \le P_g(k) \le P_{g,\max} \tag{4.26}$$

$$\omega_{g,\min} \le \omega_g(k) \le \omega_{g,\max} \tag{4.27}$$

For $k = 1,...,N$ in (4.26) and (4.27), and $k = 0,...,N-1$ in (4.24) and (4.25), where x_0 is the initial condition at each time step, and N is the finite prediction horizon.

Since

$$\Delta P_g = P_g - P_{g,rat} = \Delta\omega_g T_{g,rat} + \Delta T_g \omega_{g,rat}$$

$$\Delta\omega_g = \omega_g - \omega_{g,rat}$$

and

$$y(k) = \begin{bmatrix} \Delta\omega_g & \Delta P_g \end{bmatrix}^T = C_d x(k)$$

then, after some mathematical manipulations, we can rewrite equation (4.23) in the form below:

$$V_N\left(x(0), \mathbf{u}, \mathbf{d}\right) = \left[\sum_{k=1}^{N} x(k)^T Q x(k) + \sum_{k=0}^{N-1} \left(u(k) - u(k-1)\right)^T R \left(u(k) - u(k-1)\right) \right] \tag{4.28}$$

with

$$Q = \begin{bmatrix} 0 & 0 & 0 & 0 & 0 \\ 0 & \dfrac{q_1 + q_2}{\omega_{g,rat}^2} & 0 & \dfrac{q_2}{\omega_{g,rat} T_{g,rat}} & 0 \\ 0 & 0 & 0 & 0 & 0 \\ 0 & \dfrac{q_2}{\omega_{g,rat} T_{g,rat}} & 0 & \dfrac{q_2}{T_{g,rat}^2} & 0 \\ 0 & 0 & 0 & 0 & 0 \end{bmatrix}, R = \begin{bmatrix} r_1 & 0 \\ 0 & r_2 \end{bmatrix}$$

where $Q \geq 0$ (i.e., semi-definite positive matrices) and $R > 0$ (i.e., positive definite matrix).

4.3.3 Problem Formulation

In this work, two different sets of control inputs regarding the disturbance of wind speed are considered.

The first one assumes that the noise $d(k)$ is Gaussian with known statistics. Note that with Gaussian noises, the cost function in (4.28) is random depending on the noise. Unlike the works in the literature, where the noise terms in the cost function are evaluated by known model through Kalman Filter, in this work we keep them random, but consider the expectation of the cost function. Moreover, due to these unknown noises, the measurements $y(k)=\left[\Delta\omega_g \;\; \Delta P_g\right]^T$ are also stochastic which means they are not exactly known. In this sense, constraints (4.26) and (4.27) can only be enforced in a probabilistic form. For example, (4.26) and (4.27) can be written as

$$\mathbb{P}(P_{g,\min} \le P_g(k) \le P_{g,\max}) \ge \alpha_1 \tag{4.29}$$

$$\mathbb{P}(\omega_{g,\min} \le \omega_g(k) \le \omega_{g,\max}) \ge \alpha_2 \tag{4.30}$$

Then, the first problem with Gaussian noise is given by:

Problem 1: **Find**

$\mathbf{u}(x_0) := arg\ min_{\mathbf{u}}\ \mathbb{E}V_N$

Subject to (4.24), (4.25), (4.29), (4.30), and discretized version of the system (4.19), (4.20).

In the above formulation, $\mathbb{E}$ is the expectation operator.

The second problem formulation considers a noise variable that does not have a known statistics, but a bounded set, e.g., $\mathbb{D}_\gamma = \{\mathbf{d} \,|\, \|\mathbf{d}\|_2 \le \gamma\}$. In this case, the problem is formulated as a min-max problem to find a control input that minimizes the largest value of the cost function throughout the whole bounded set. The problem formulation is given by:

Problem 2: **Find**

$$\mathbf{u}(x_0) := arg\ min_{\mathbf{u}}\ \max_{d \in \mathbb{D}_\gamma} V_N$$

Subject to (4.24), (4.25), (4.29), (4.30), and discretized version of the system (4.19), (4.20).

Note that constraints (4.29) and (4.30) are not convex, thus, they will be simplified in the next section.

4.4 Proposed Control Strategy

In this section, we discuss about the control strategy employed to solve the two problems formulated in the previous section. Unlike MPC method, which is quadratic programming (QP), we further convert the problems to semi-definite programming (SDP) optimization problems. Particularly, we first introduce the concept of SDP briefly, then, we simplify the constraints (4.29) and (4.30) into linear constraints, which help us to formulate the problems as SDP problems that have tractable solutions.

4.4.1 SDP

A semi-definite program has the following form [boyd, convex optimization]:

$$\text{minimize } c^T x$$

Subject to

$$F^i(x) = x_1 F_1^i + ... + x_n F_n^i + G^i \le 0,\ i = 1,..., K$$

$$Gx \le g,\ Ax = b$$

where $G^i,\ F_1^i,\ ...,\ F_n^i \in \mathbb{R}^{n \times n}$, $x \in \mathbb{R}^n$, $G,\ A$ are matrices, and $g,\ b$ are vectors with appropriate dimensions. Note that SDP is subject to constraints such as linear matrix inequalities

(LMI), linear inequalities, and linear equalities.

SDP optimization problems are convex optimization problems that can be solved efficiently.

4.4.2 Approximating Chance Constraints to Linear Constraints

As previously mentioned, two cases regarding wind speed disturbance are considered in this paper:

1) The disturbance to the wind speed, $d(k)$, is known to be Gaussian;

2) The disturbance distribution is unknown but subject to some norm-bounded set.

Since the disturbance ($d(k)$) is random, the state is not exactly known and any constraints on the state could be formulated in a probabilistic sense. Thus, the constraints on the output (P_g, ω_g) can be described by chance constraints which are already given in (4.29) and (4.30).

The above constraints are non-convex and hard to resolve directly. In the first case when the disturbance ($d(k)$) is Gaussian, the chance constrains can be reduced to linear inequalities as shown in [43]. In the second case, if we do not assume any form of the noise, we can approximate the chance constraints by some hard constraints.

For problem 1, where the disturbance ($d(k)$) is Gaussian, e.g., $\mathbf{d} \sim \mathcal{N}(\boldsymbol{\mu}, \boldsymbol{\Sigma})$, (4.29) is taken as an example to demonstrate how to convert it into linear inequality. Starting from (4.29), where

$$
\begin{aligned}
&\mathbb{P}(P_{g,\min} \le P_g(k) \le P_{g,\max}) \\
&= \mathbb{P}(P_{g,\min} \le P_g(k) \bigcap P_g(k) \le P_{g,\max}) \\
&= \mathbb{P}(P_{g,\min} \le P_g(k)) + \mathbb{P}(P_g(k) \le P_{g,\max}) \ - \mathbb{P}(P_{g,\min} \le P_g(k) \bigcup P_g(k) \le P_{g,\max}) \\
&= \mathbb{P}(P_{g,\min} \le P_g(k)) + \mathbb{P}(P_g(k) \le P_{g,\max}) - 1 \\
&\ge \alpha_1
\end{aligned}
$$

Then, we have $\mathbb{P}(P_{g,\min} \le P_g(k)) + \mathbb{P}(P_g(k) \le P_{g,\max}) \ge \alpha_1 + 1$, Thus, to guarantee (29), the above inequality can be separated into two inequalities:

$$\mathbb{P}(P_g(k) \le P_{g,\max}) \ge \frac{1+\alpha_1}{2} \tag{4.31}$$

and

$$\mathbb{P}(P_{g,\min} \le P_g(k)) \ge \frac{1+\alpha_1}{2} \tag{4.32}$$

Note, (31) indicates $\mathbb{P}(P_g(k) > P_{g,\max}) < \frac{1-\alpha_1}{2}$, and $P_g(k) > P_{g,\max}$ can be further written as $G_1 x > g_1$, where $G_1 = [0 \ \ 1] C_d$ and $g_1 = P_{g,\max} - P_{g,rat}$. For $k = 1,...,N$, we have $\mathbf{G}_1 \mathbf{x} > g_1$ for each *k*, where $\mathbf{G}_1 = [0,...,0,\underbrace{G_1}_{kth},0,...,0]$. Thus, for each *k*, (31) can be represented as

$$\mathbb{P}(\mathbf{G}_1 \mathbf{x} > g_1) < \frac{1-\alpha_1}{2} \tag{4.33}$$

Similarly, (4.30) and (4.32) may also be represented in the form of inequalities as (33).

Theorem 4.1 [43]: Consider a discrete-time linear system with the state equation written as

$$\mathbf{x} = \mathbf{A}_S x_0 + \mathbf{B}_S \mathbf{u} + \mathbf{C}_S \mathbf{d} \tag{4.34}$$

where corresponding to (14),

$$\mathbf{A}_s = [A_d^1, \cdots, A_d^k, \cdots, A_d^N]^T$$

$\mathbf{B}_S = [\bar{\mathbf{B}}_0^T, \cdots, \bar{\mathbf{B}}_{N-1}^T]^T$, $\tilde{\mathbf{B}}_{k-1} = [A_d^{k-1}B_u, \cdots, B_u, \mathbf{0}_{5\times 2(N-k)}]$,

$\mathbf{C}_S = [\tilde{\mathbf{C}}_0^T, \cdots, \tilde{\mathbf{C}}_{N-1}^T]^T$, $\tilde{\mathbf{C}}_{k-1} = [A_d^{k-1}B_d, \cdots, B_d, \mathbf{0}_{5\times (N-k)}]$,

Then, the constraint

$$\mathbf{p}^T\mathbf{u} \le q \tag{4.35}$$

where $\mathbf{p} = \mathbf{B}_S^T\mathbf{G}_1$, $q = g_1 - \mathbf{G}_1\mathbf{A}_S x_0 - \mathbf{G}_1\mathbf{C}_S\boldsymbol{\mu} - \boldsymbol{\Sigma}^{\frac{1}{2}}\mathbf{C}_S^T\mathbf{G}_1 \Phi^{-1}(\alpha_1)$ *implies the chance constraint (4.33).* Φ *is the cumulative distribution functions of standard normal variables, and* Φ^{-1} *is its inverse.*

Thus, based on the above theorem, the chance constraints (4.29) and (4.30) can be reduced to linear inequalities.

For Problem 2, (4.29) and (4.30) can't be transformed to a hard constraint as shown above because the distribution of the wind speed disturbance is not known. Thus, a hard constraint can be employed to approximate it.

First recall from (4.33) that we hope $\mathbf{G}_1\mathbf{x} > g_1$ to be satisfied. Then, by (4.34), we have:

$$\mathbf{G}_1\mathbf{A}_S x_0 + \mathbf{G}_1\mathbf{B}_S\mathbf{u} + \mathbf{G}_i\mathbf{B}_S\mathbf{d} > g_1$$

which is further implied by

$$\mathbf{G}_1\mathbf{B}_S\mathbf{u} > g_1 - \mathbf{G}_1\mathbf{A}_S x_0 + \left\|\mathbf{C}_S^T\mathbf{G}_1\right\|_2 \gamma \tag{4.36}$$

as $\|\mathbf{d}\|_2 \le \gamma$.

Note that (4.36) will introduce some conservativeness comparing to the desired constraint, but it is more practical as the distribution of the noise is unknown in the reality. Similarly, (4.30) and (4.32) can also be formulated as linear inequalities as (4.36).

In the previous paragraphs, the chance constraints for both problems are converted

into linear constraints, which are convex. In the discussion below, both problems will be formulated as SDP optimization problems.

4.4.3 SDP Approach for Problem 1

In this section, we applied the technique in [43] to provide a tractable solution of problem 1. When the wind speed disturbance ($d(k)$) is Gaussian, the expectation of the cost function can be computed using the statistics of Gaussian noise. Then, with the linear inequalities derived above, problem 1 becomes a convex optimization problem and here we formulate problem 1 as an SDP problem. However, problem 2 does not seem tractable directly as it is a min-max problem. In the next section, it is shown that problem 2 can be also formulated as an SDP problem as in [43].

An obvious result about the cost function is given in the following proposition.

Proposition 3.1: The cost function (4.28) can be written as:

$$V_N\left(x_0,\mathbf{u},\mathbf{d}\right)=x_0^T\mathbf{A}x_0+2\mathbf{b}^T\mathbf{u}+\mathbf{u}^T\mathbf{B}\mathbf{u}+2\mathbf{c}^T\mathbf{d}+\mathbf{d}^T\mathbf{C}\mathbf{d}+2\mathbf{u}^T\mathbf{D}\mathbf{d} \tag{4.37}$$

For vectors $\mathbf{b, c}$ and matrices $\mathbf{A, B, C, D}$ with appropriate dimensions, and where $\mathbf{B>0}$, $\mathbf{C>0}$.

Proof: The original system can be written in terms of system dynamics, at time k,

$$x_k=\tilde{\mathbf{A}}_{k-1}x_0+\tilde{\mathbf{B}}_{k-1}\mathbf{u}+\tilde{\mathbf{C}}_{k-1}\mathbf{d}$$

where $\bar{\mathbf{A}}_{k-1}=A_d^k$.

Then after some manipulations, we can reach the formula of the cost function stated in (4.37) with

$$\mathbf{A}=\sum_{k=1}^{N}\tilde{\mathbf{A}}_{k-1}^T Q\tilde{\mathbf{A}}_{k-1}$$

$$\mathbf{B} = \mathbf{L}^T \mathbf{diag}(R, \cdots, R)\mathbf{L} + \sum_{k=1}^{N} \tilde{\mathbf{B}}_{k-1}^T Q \tilde{\mathbf{B}}_{k-1}$$

$$\mathbf{L} = \begin{bmatrix} 1 & 0 & -1 & & 0 \\ 0 & 1 & 0 & -1 & \ddots & 0 \\ 0 & \cdots & \ddots & & & -1 \\ 0 & 0 & 0 & \cdots & & 1 \end{bmatrix}, \mathbf{C} = \sum_{k=1}^{N} \tilde{\mathbf{C}}_{k-1}^T Q \tilde{\mathbf{C}}_{k-1}$$

$$\mathbf{D} = \sum_{k=1}^{N} \tilde{\mathbf{B}}_{k-1}^T Q \tilde{\mathbf{C}}_{k-1}, \mathbf{c} = \left(\sum_{k=1}^{N} \tilde{\mathbf{C}}_{k-1}^T Q \tilde{\mathbf{A}}_{k-1} \right) x_0$$

$$\mathbf{b} = \left(\sum_{k=1}^{N} \tilde{\mathbf{B}}_{k-1}^T Q \tilde{\mathbf{A}}_{k-1} \right) x_0 - \mathbf{R}^T \mathbf{U}, \ \mathbf{U} = [0, \cdots, 0, u(-1)^T]^T$$

where, $\mathbf{L}$ comes from the difference of control inputs in the const function (4.28).

Let $\mathbf{h} = \mathbf{c} - \mathbf{D}^T \mathbf{B}^{-1} \mathbf{b}$ and $\mathbf{F} = \mathbf{B}^{-1/2} \mathbf{D}$, then by eliminating the constant terms and taking $\mathbf{u} = \mathbf{B}^{-1/2} \mathbf{y} - \mathbf{B}^{-1} \mathbf{b}$, the cost function above can be further rewritten as:

$$\tilde{V}_N(x_0, \mathbf{y}, \mathbf{d}) = \mathbf{y}^T \mathbf{y} + 2\mathbf{h}^T \mathbf{d} + 2\mathbf{y}^T \mathbf{F} \mathbf{d} + \mathbf{d}^T \mathbf{C} \mathbf{d} \tag{4.38}$$

Taking the expectation of the above cost, we have

$$\hat{V}_N(x_0, \mathbf{y}, \mathbf{d}) = \mathbf{y}^T \mathbf{y} + 2\mathbf{h}^T \boldsymbol{\mu} + 2\mathbf{y}^T \mathbf{F} \boldsymbol{\mu} + trace(\mathbf{C}\boldsymbol{\Sigma}) \tag{4.39}$$

Again, with the constant terms ignored, the cost to be minimized is $\hat{V}_N(x_0, \mathbf{y}, \mathbf{d}) = \mathbf{y}^T \mathbf{y} + 2\mathbf{y}^T \mathbf{F} \boldsymbol{\mu}$. Then, the problem 1 is equivalent to find $\mathbf{u}(x_0) := \arg\min_{\mathbf{u}} \hat{V}_N$.

Theorem 4.2: Problem 2 may be solved by the following semi-definite optimization problem:

Minimize z

Subject to (4.24), (4.25), and (4.35)

$$\begin{bmatrix} \mathbf{I}_N & \mathbf{y} + \mathbf{F}\boldsymbol{\mu} \\ \mathbf{y}^T + \boldsymbol{\mu}^T \mathbf{F}^T & z + (\mathbf{F}\boldsymbol{\mu})^T \mathbf{F}\boldsymbol{\mu} \end{bmatrix} \geq 0 \tag{4.40}$$

in decision variables $\mathbf{y}$ *and* z.

Proof: The proof is given below by following the technique in theorem 3 in [43].

First, the minimization of $\hat{V}_N(e_0, \mathbf{y}, \omega)$ can be written as

Minimize z

Subject to $z - \mathbf{y}^T\mathbf{y} - 2\mathbf{y}^T\mathbf{F}\boldsymbol{\mu} \geq 0$ (4.41)

The constraint (4.31) can be further written as

$z - \mathbf{y}^T\mathbf{y} - 2\mathbf{y}^T\mathbf{F}\boldsymbol{\mu} - (\mathbf{F}\boldsymbol{\mu})^T\mathbf{F}\boldsymbol{\mu} + (\mathbf{F}\boldsymbol{\mu})^T\mathbf{F}\boldsymbol{\mu} \geq 0$

$z + (\mathbf{F}\boldsymbol{\mu})^T\mathbf{F}\boldsymbol{\mu} - (\mathbf{y} + \mathbf{F}\boldsymbol{\mu})^T(\mathbf{y} + \mathbf{F}\boldsymbol{\mu}) \geq 0$ (4.42)

Thus, by Schur complement lemma, (4.42) can be formulated as (4.40). Moreover, note that (4.24), (4.25), and (4.35) are linear constraints on the control input, which can be added without increasing the complexity type. Thus, we obtain the statement.

4.4.4 SDP Approach for Problem 2

In the last section, an exact solution is provided for problem 1 under the assumption that the disturbance is Gaussian. However, as previously mentioned, the distribution statistics may not be known or follow a regular probability distribution in the real world. However, it is not difficult to make a reasonable assumption on the bounds of the wind speed disturbance in a given set (e.g., temperatures will not go unbounded). Thus, the problem was formulated as problem 2.

It can be viewed as finding the optimal control that minimizes the worst cost in searching in the wind speed disturbance bound. The advantage of solving this problem is that it is not necessary to know the distribution of the disturbance, which is used to compute the expected cost. Furthermore, by minimizing the maximum of the cost, it can be guaranteed that the overall cost will be limited in an appropriate range. The solution of

problem 2 can be represented by the following semi-definite optimization problem by directly applying the approach in [43] and stated in the next theorem.

Theorem 4.3: Problem 2 may be solved by:

Minimize z

Subject to (4.24), (4.25), and (4.36)

$$\begin{bmatrix} \mathbf{I}_N & \mathbf{y} & \mathbf{F} \\ \mathbf{y}^T & z-\gamma^2\lambda & -\mathbf{h}^T \\ \mathbf{F}^T & -\mathbf{h} & \lambda\mathbf{I}-\mathbf{C}+\mathbf{F}^T\mathbf{F} \end{bmatrix} \geq 0$$

in decision variables $\mathbf{y}$, z *and* λ.

The optimal control input can be obtained by the transformation $\mathbf{u} = \mathbf{B}^{-1/2}\mathbf{y} - \mathbf{B}^{-1}\mathbf{b}$ after solving the above problem.

4.5 Results and Discussion

The performance of the proposed SDP method based control strategy is demonstrated in this section. The rated wind speed used in this work is 12.5 m/s and the cut out wind speed is 27.5 m/s. Other parameters used can be found at appendix.

The results will be divided into three cases. Case one gives the response when there is a step change to the wind speed; Case 2 gives the results when the assumed disturbance follows Gaussian distribution; and Case 3 describes the performance when the disturbance is norm bounded.

4.5.1 Case One: Step Change to the Wind Speed

As the first step to test the proposed control strategy, the disturbance is set as a step change to the wind speed. The wind speed is chosen as the midrange of the full load

regime, which is 20 m/s. The step change is set to 1 m/s and -1 m/s, which is considered as the maximum variance in the model of wind forecast error. The prediction horizon *N* is set to 2. Two different groups of other relevant parameters, as shown below, are chosen for a comparison of the results.

- Group 1: $q_1 = 1000$, $q_2 = 0.5$, $r_1 = 0$, $r_2 = 0.0002$
- Group 2: $q_1 = 1000$, $q_2 = 0.045$, $r_1 = 0$, $r_2 = 0.002$

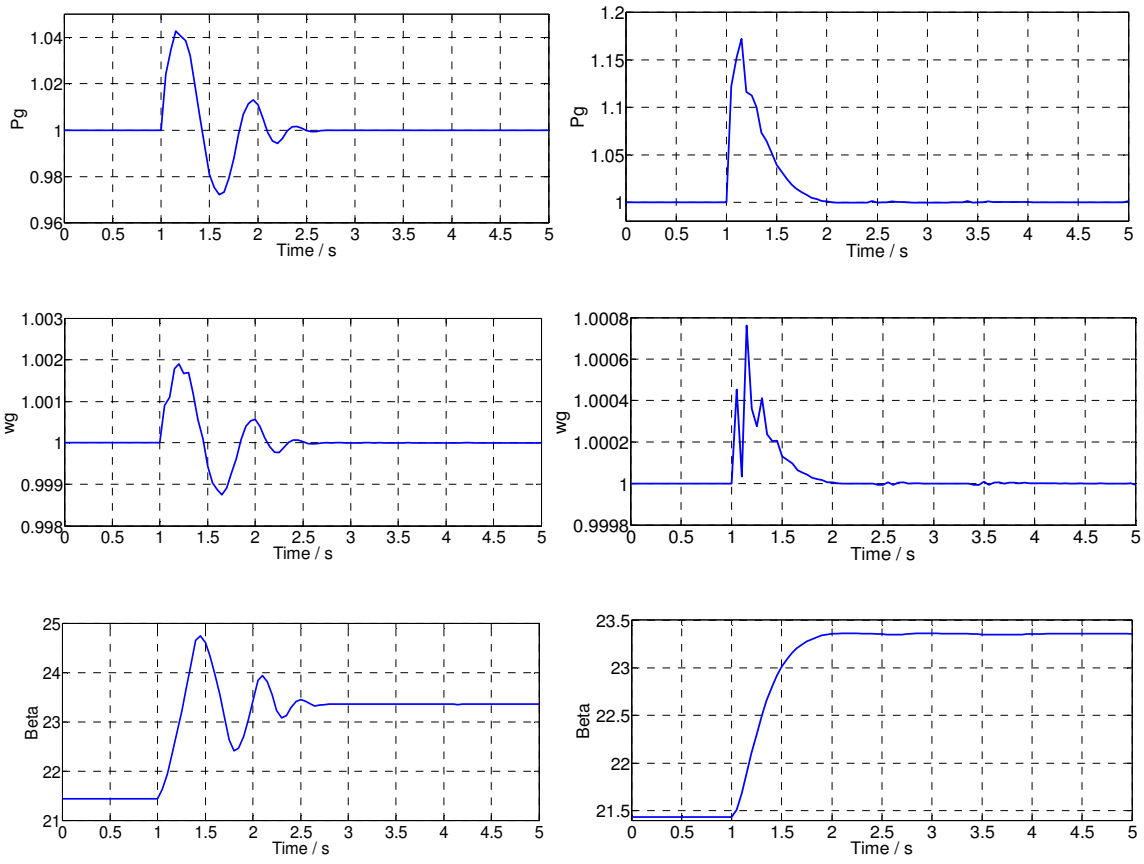

Fig. 4.2 Results when wind speed changes from 20 m/s to 21 m/s. Group 1 on the left side; Group 2 on the right side

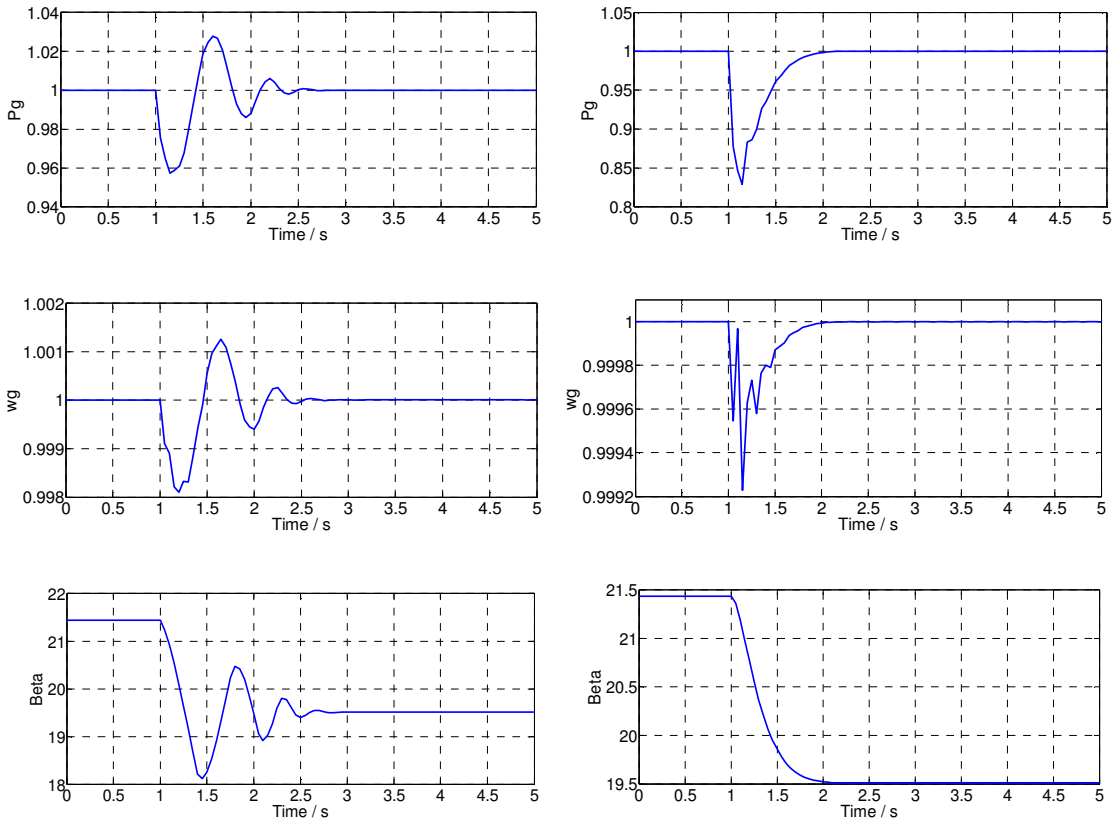

Fig. 4.3 Results when wind speed changes from 20 m/s to 19 m/s. Group 1 on the left side; Group 2 on the right side

Here, the values of q_1 and q_2 are chosen to normalize the per unit values of active power and angular velocity in the cost function. Also, r_1 is set to zero while r_2 is not, because in this study the change of pitch angle is critical while the change of generator torque is not a focal point.

As shown in the above figures, with different parameters, the results are different. The curves of the first group of parameters have smaller amplitudes of dynamics, but with several oscillations in the dynamic process. The curves of the second group of parameters have higher amplitudes, but with no oscillations in the dynamic process. The

reason of these phenomena is due to different parameters giving different weights to different performance characteristics.

The parameters in Group 1 are chosen for the next two case studies because it gives smaller amplitude which is more preferred in power system operation.

4.5.2 Case Two: The Disturbance Distribution is Gaussian

In this case study, the distribution of the high frequency variable part of the wind speed is assumed to be Gaussian. All the other parameters are set the same as those in Group 1. Also, the wind speed is sampled every 0.5 seconds. The chance constraints are set with $\alpha_1 = \alpha_2 = 0.98$. The wind speed, the active power, the angular velocity of the generator and also the beta curves are shown in Fig. 4.4 (a) (b) (c) (d). As we can observe from the curves, the wind speed is around low frequency variable part, which is set to 20 m/s here.

It is perhaps difficult to make direct comparison between the results presented here and the previous works using model predictive control (MPC) in [30, 42], since random noises subject to Gaussian distribution are embedded to the wind speed forecast error. Nevertheless, the results presented in Fig. 4.4 (a) (b) (c) (d) are in the same scale as the results from the previous works using MPC in [30, 42]. For instance, the output wind power (P_g) by the proposed method is within 0.98 and 1.02 per unit of its rated value as shown in Fig. 4.4 (b), while Fig. 7(b) in Reference [30] shows roughly the same range of P_g variation. Furthermore, P_g in Fig. 4.4 (b), as well as Fig. 7(b) in [30], is much better than the original PI control in [30], which gives a much larger P_g variation range between about 0.9 and slightly higher than 1.1 per unit.

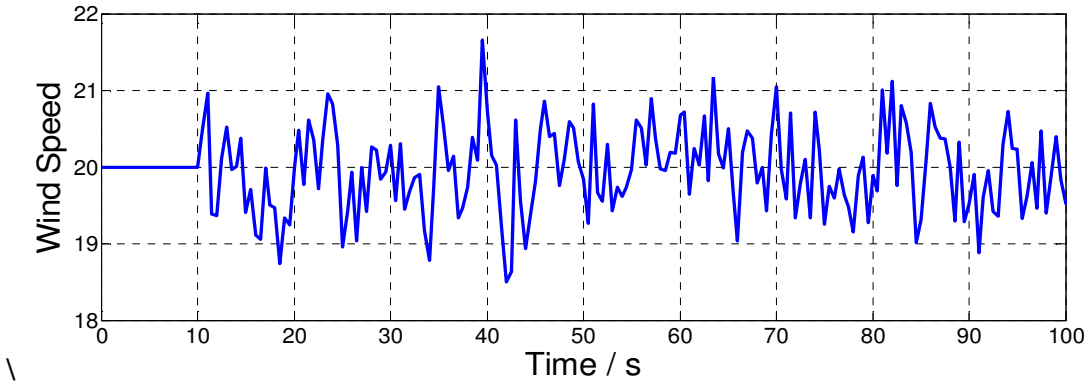

\

Fig. 4.4 (a) Wind speed

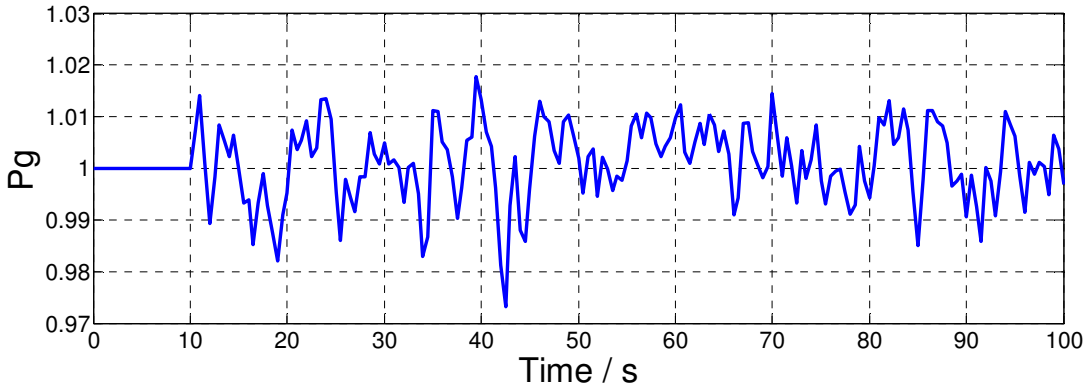

Fig. 4.4 (b) Output power: P_g

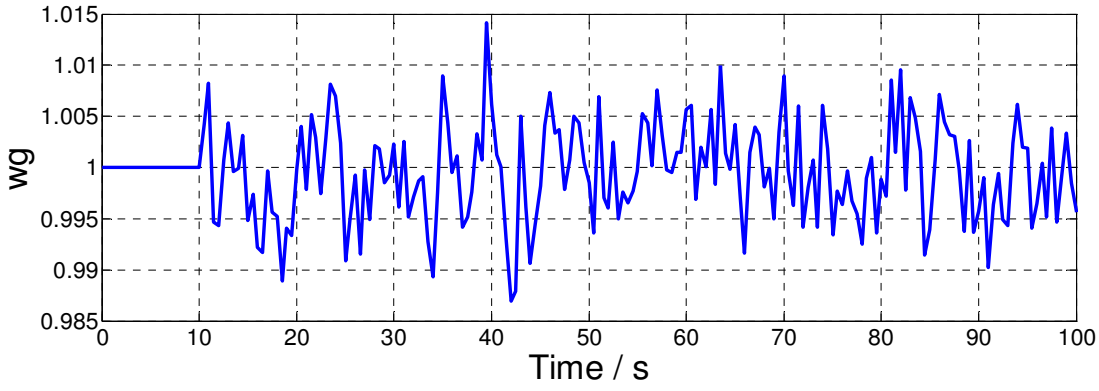

Fig. 4.4 (c) Generator angular velocity: w_g

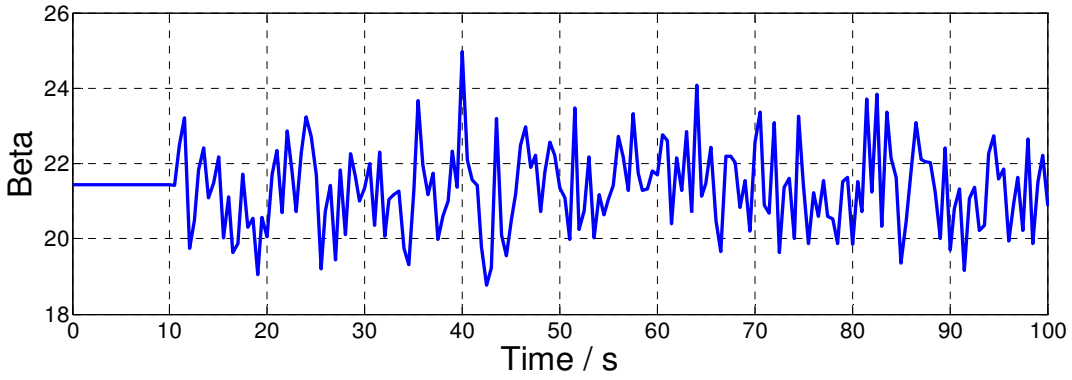

Fig. 4.4 (d) Pitch angle: Beta

Fig. 4.4 Results for case two: disturbance distribution is Gaussian

Note, the proposed method uses stochastic approach to model chance constraints and minimizes the expectation of the cost function, while the MPC method in [1, 13] uses Kalman filter to predict the wind speed disturbance to obtain deterministic constraint, which adds complexity to the model. Both approaches seem to serve its purpose well, as discussed previously.

To verify whether the results from the proposed SDP algorithm meet our intension or not, 10 random simulation runs are carried out under two models: with constraints and without constraints. The output variables P_g and ω_g are examined whether they are within the constraint ranges. The results are shown in Fig. 4.5 and Fig. 4.6.

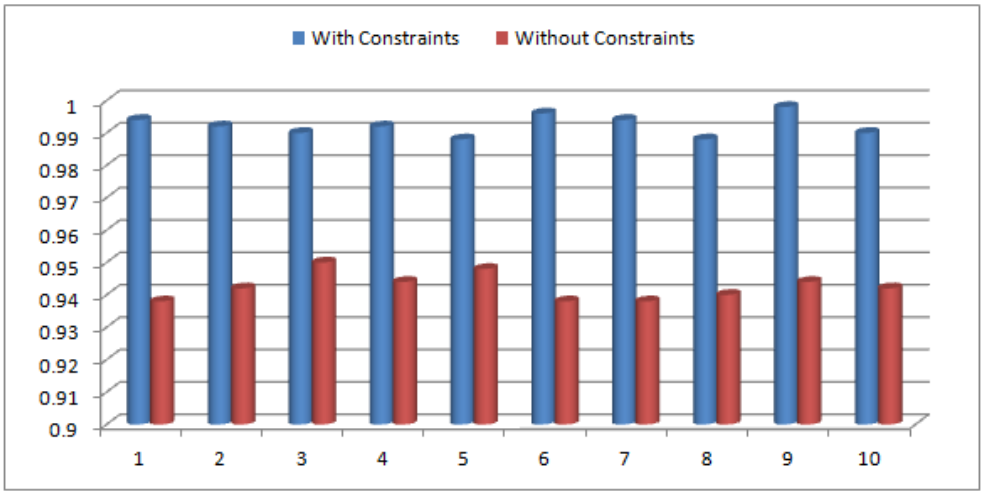

Fig. 4.5 Comparison of the Probability of P_g within bounds under two models: with constraints and without constraints, where the x-coordinate represents 10 different tries, and the y-coordinate represents the probabilities in the range

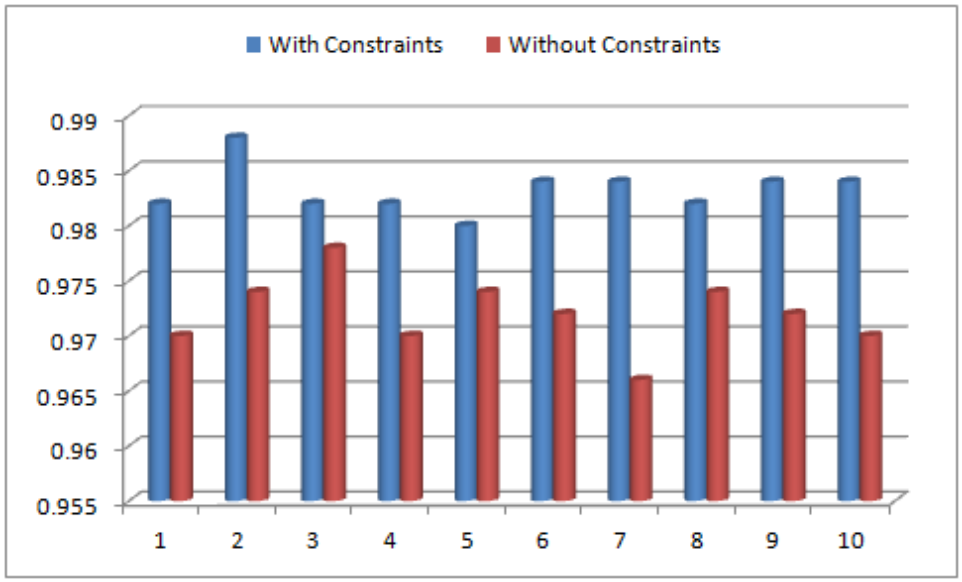

Fig. 4.6 Comparison of the Probability of ω_g within bounds under two models: with constraints and without constraints, where the x-coordinate represents 10 different tries, and the y-coordinate represents the probabilities in the range

Fig. 4.5 shows the probability that P_g falls into the desired range with and without chance constraints (10 random tries, with 1000 sample points for each try). With the constraints modeled, the probability that all the P_g values stay within the range is higher than $\alpha_1 = 98\%$. But when those constraints are removed, such probability drops to around 94%. Similar result for ω_g is shown in Fig. 4.6. These plots demonstrate that the proposed method does meet the expectation very well.

4.5.3 Case Three: The Disturbance is Norm-Bounded

In this case study, the distribution of the wind speed disturbance is unknown, but it is norm bounded. As shown in Fig. 4.7 (a) (b) (c) (d), the high frequency part of the wind speed is set to random values with its norm at 1 m/s. The active power is shown within 0.97 and 1.03 per unit of its rated value. The angular velocity of the generator is even within 0.99 to 1.01 per unit. The results are comparable to the previous results in Case 2. Thus, this is a promising approach to practicing engineers, since it does not require any assumption on the disturbance distribution. This is the unique contribution of the proposed method.

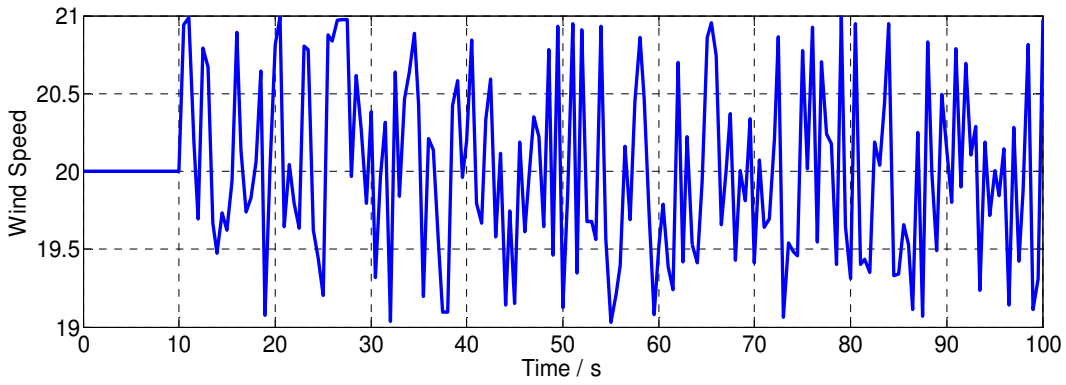

Fig. 4.7 (a) Wind speed

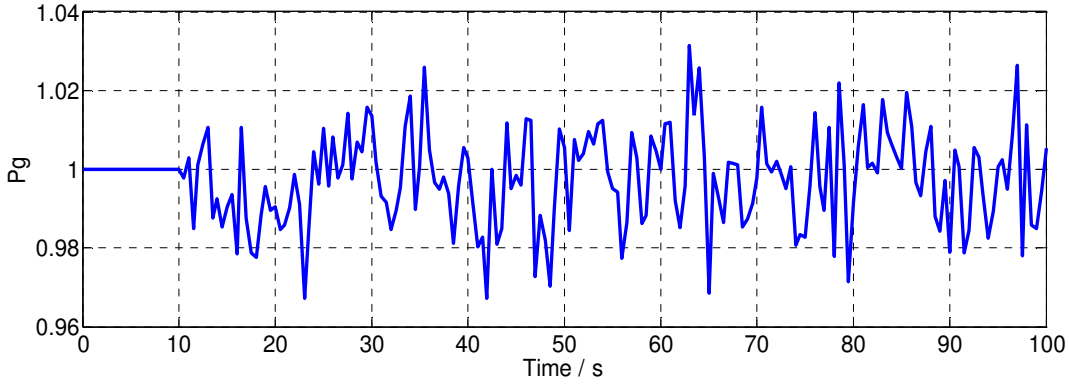

Fig. 4.7 (b) Output power: P_g

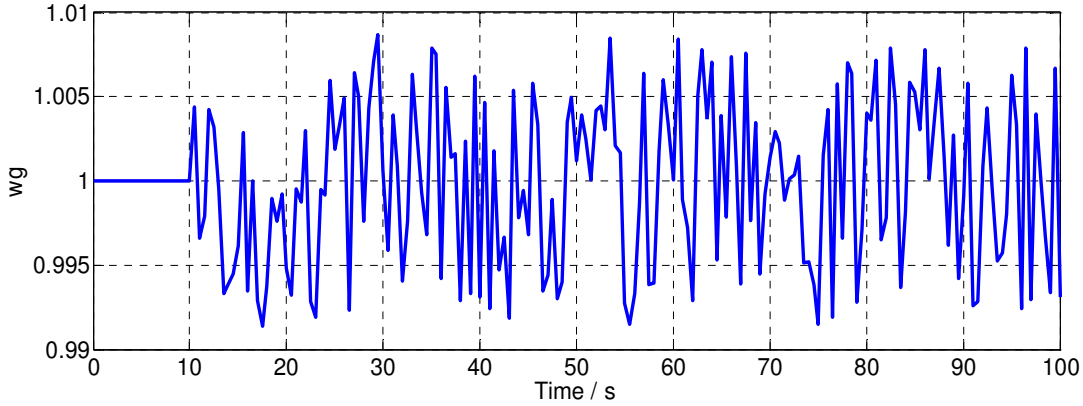

Fig. 4.7 (c) Generator angular velocity: w_g

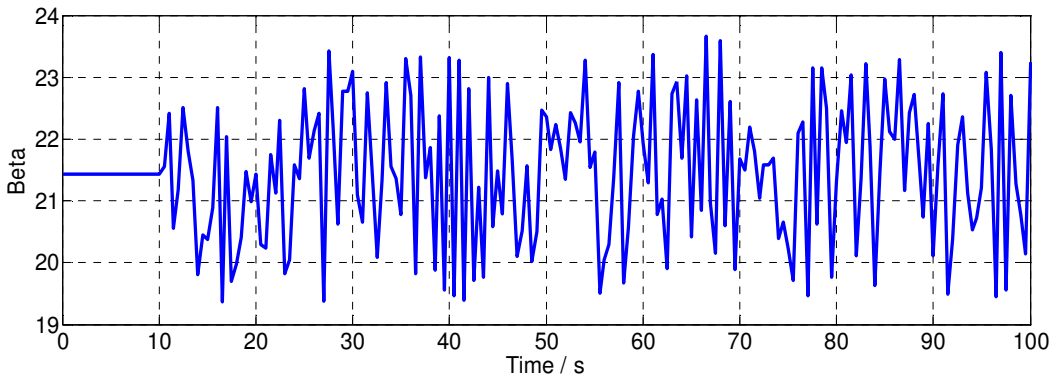

Fig. 4.7 (d) Pitch angle: Beta

Fig. 4.7 Results for case three: disturbance is Norm-bounded

4.6 Discussion and Conclusion

The contribution of this chapter can be summarized as follows:

- In this chapter, a new control strategy based on semi-definite programming (SDP) method is proposed for WECS power control in the full load region. The SDP method solves a stochastic problem by minimizing the expectation of the cost function using the statistics of Gaussian disturbance of wind speed. Also, the chance constraints are employed to capture the stochastic characteristic of the wind speed disturbance which is more practical than deterministic constraints.
- In the proposed approach, the disturbance to wind speed forecast, which represents the high frequency variable component of the wind speed, is modeled as a Gaussian distribution and a norm bounded without a known distribution. Both problems are formulated into SDP models in order to be solved.
- When the disturbance is modeled as Gaussian distribution, SDP gives comparable results to those from the MPC-based method in the literature. Meanwhile, the

proposed SDP method requires less information, i.e., the state space model, which is needed in the MPC model to determine disturbances in the prediction horizon of the deterministic cost function in MPC.

- When the wind speed error is modeled as norm bounded without a known distribution, this likely represents a more realistic assumption in practice and has not been previously reported in wind power control studies. The results are also promising and comparable to the one with Gaussian distribution.

CHAPTER 5 POWER REGULATION FOR WIND ENERGY CONVERSION SYSTEM II

5.1 Chapter Introduction

In this chapter, the semi-definite programming (SDP) control method proposed in Chapter 4 is used to regulate the power output of Wind Energy Conversion System (WECS) in partial load region where wind speed is above the cut-in speed and below rated value, with the consideration of the energy cost and control performance subject to stochastic wind speeds.

5.2 Modeling of Variable Speed Variable Pitch WECS [30, 42]

The Wind Energy Conversion System used here is the same as in chapter 4. For dissertation's convenience and consistency, it is re-described shortly as follows. Fig. 5.1 shows Wind Energy Conversion System.

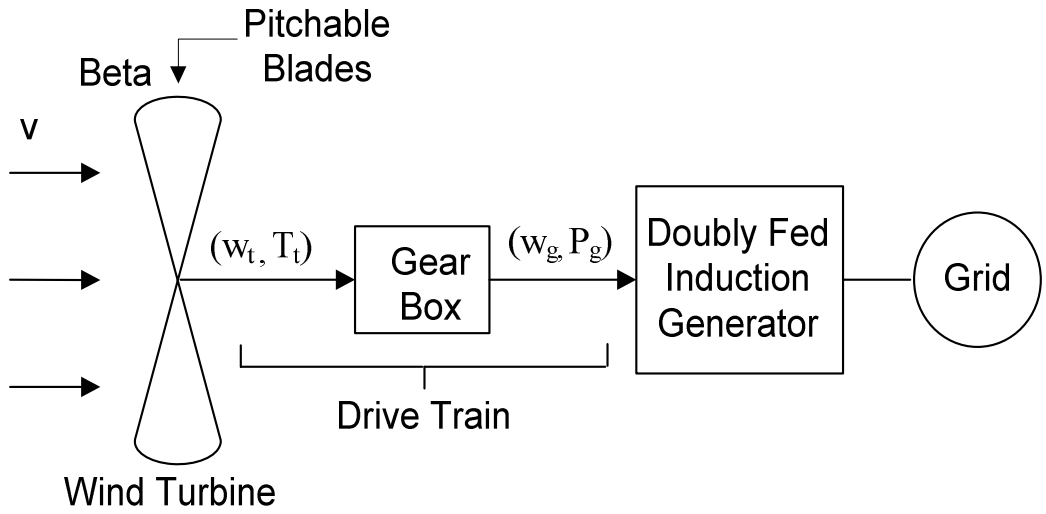

Fig. 5.1 Wind energy conversion system

5.2.1 Wind Speed Model

$$v(t) = v_m(t) + v_t(t) \tag{5.1}$$

where v_m is describing the long-term, low-frequency variable component, and v_t is the turbulence, which describes the high-frequency variable component.

5.2.2 Pitch Actuator Model

$$\dot{\beta} = -\frac{1}{\tau}\beta + \frac{1}{\tau}\beta_d \tag{5.2}$$

where, τ is the time constant of the pitch system, and β is the blade pitch angle.

The constraints of β and its derivative are given by:

$$\beta_{\min} \le \beta \le \beta_{\min} \tag{5.3}$$

$$\dot{\beta}_{\min} \le \dot{\beta} \le \dot{\beta}_{\min} \tag{5.4}$$

5.2.3 Aerodynamic System

The output of the aerodynamic system can be expressed as equation (5.5):

$$P_t = C_p(\lambda, \beta)\frac{\rho\pi R^2}{2}v^3 \tag{5.5}$$

where, P_t is the mechanical output power of the wind turbine; C_p is the performance coefficient of the wind turbine; ρ is the air density; R is the radius of wind turbine blades; v is the wind speed; λ is the tip speed ratio of the rotor blade tip speed to wind speed, $\lambda = \omega_t R / v$ and ω_t is the speed of the low-speed shaft; β is the blade pitch angle.

The turbine torque Γ_t at the low-speed shaft is calculated as follows:

$$\Gamma_t = \frac{P_t}{\omega_t} = \frac{C_p(\lambda, \beta)}{\lambda}\frac{\rho\pi R^3}{2}v^2 \tag{5.6}$$

A generic equation is used to model $C_p(\lambda,\beta)$:

$$C_p(\lambda,\beta)=0.5176\left(\frac{116}{\lambda_i}-0.4\beta-5\right)e^{-21/\lambda_i}+0.0068\lambda \tag{5.7}$$

with

$$\frac{1}{\lambda_i}=\frac{1}{\lambda+0.08\beta}-\frac{0.035}{\beta^3+1} \tag{5.8}$$

5.2.4 Drive Train Model

$$\frac{d\omega_t}{dt}=-\frac{i}{J_t}\Gamma_{tw}+\frac{1}{J_t}\Gamma_t \tag{5.9}$$

$$\frac{d\omega_g}{dt}=\frac{i}{J_g}\Gamma_{tw}-\frac{1}{J_g}\Gamma_g \tag{5.10}$$

$$\frac{d\Gamma_{tw}}{dt}=k_s i\omega_t-k_s\omega_g-\left(\frac{i^2B_s}{J_t}+\frac{B_s}{J_g}\right)\Gamma_{tw}+\frac{iB_s}{J_t}\Gamma_t+\frac{B_s}{J_g}\Gamma_g \tag{5.11}$$

$$\Gamma_{tw}=k_s\theta_{tw}+B_s\left(i\omega_t-\omega_g\right) \tag{5.12}$$

where, i is the gear ratio; Γ_{tw} and Γ_g are the flexible shaft torque and generator torque; ω_g is the generator angular velocity; k_s and B_s are the shaft stiffness and damping coefficients respectively; θ_{tw} is the shaft twist angle.

5.2.5 Generator Model

$$\dot{\Gamma}_g=-\frac{1}{\tau_g}\Gamma_g+\Gamma_g^* \tag{5.13}$$

where, τ_g is the time constant, and Γ_g^* is the generator torque set point.

5.2.6 WECS Linearization

The Wind Energy Conversion System is re-described by previous equations form (5.1) to (5.13). As described in Chapter 4, the linearized WECS is described as follows:

$$\dot{x}(t) = \tilde{A}x(t) + \tilde{B}_u u(t) + \tilde{B}_v \Delta v(t) \tag{5.14}$$

$$y(t) = \tilde{C}x(t) \tag{5.15}$$

with

$$\tilde{A} = \begin{bmatrix} \frac{L_\omega}{J_t} & 0 & -\frac{1}{J_t} & 0 & \frac{L_\beta}{J_t} \\ 0 & 0 & \frac{1}{J_g} & -\frac{1}{J_g} & 0 \\ k_s + \frac{iB_s}{J_t} & -k_s & -\left(\frac{i^2 B_s}{J_t} + \frac{B_s}{J_g}\right) & 0 & \frac{iB_s}{J_t} L_\beta \\ 0 & 0 & 0 & -\frac{1}{\tau_\beta} & 0 \\ 0 & 0 & 0 & 0 & -\frac{1}{\tau} \end{bmatrix}$$

$$\tilde{B}_u = \begin{bmatrix} 0 & 0 \\ 0 & 0 \\ 0 & 0 \\ \frac{1}{\tau_g} & 0 \\ 0 & \frac{1}{\tau} \end{bmatrix} \qquad \tilde{B}_v = \begin{bmatrix} \frac{L_v}{J_t} \\ 0 \\ \frac{iB_s}{J_t} L_v \\ 0 \\ 0 \end{bmatrix}$$

$$\tilde{C} = \begin{bmatrix} 0 & 1 & 0 & 0 & 0 \\ 0 & T_{g,rat} & 0 & \omega_{g,rat} & 0 \end{bmatrix}$$

where, Δ is used for representing variable's deviation from its OP:

$$L_\omega = \frac{\partial f}{\partial \omega_t}\Big|_{op} = \frac{\rho \pi R^2 v^2}{2\omega_t}\left(-C_p(\lambda,\beta)\frac{v}{\omega_t} + R\frac{\partial C_p(\lambda,\beta)}{\partial \lambda}\right) \tag{5.16}$$

$$L_v = \frac{\partial f}{\partial v}\Big|_{op} = \frac{\rho \pi R^2 v}{2}\left(3C_p(\lambda,\beta)\frac{v}{\omega_t} - R\frac{\partial C_p(\lambda,\beta)}{\partial \lambda}\right) \tag{5.17}$$

$$L_\beta = \frac{\partial f}{\partial \beta}\Big|_{op} = \frac{\rho \pi R^2 v^3}{2\omega_t} \frac{\partial C_p(\lambda, \beta)}{\partial \beta} \tag{5.18}$$

$$x = \left[\Delta\omega_t \; \Delta\omega_g \; \Delta\Gamma_{tw} \; \Delta\Gamma_g \; \Delta\beta \right] \tag{5.19}$$

$$u = \left[\Delta\Gamma_g^* \; \Delta\beta_d \right] \tag{5.20}$$

$$y = \left[\Delta\omega_g \; \Delta P_g \right] \tag{5.21}$$

5.3 Proposed Control Strategy

Power output control of variable-speed variable-pitch WECS in partial load region is to regulate the power output from wind energy by modifying the electrical generator speed. In particular, the power control goal is to capture the maximum power available from the wind. For each wind speed in partial load region, there is a certain rotational speed at which the power curve of a given wind turbine has a maximum value.

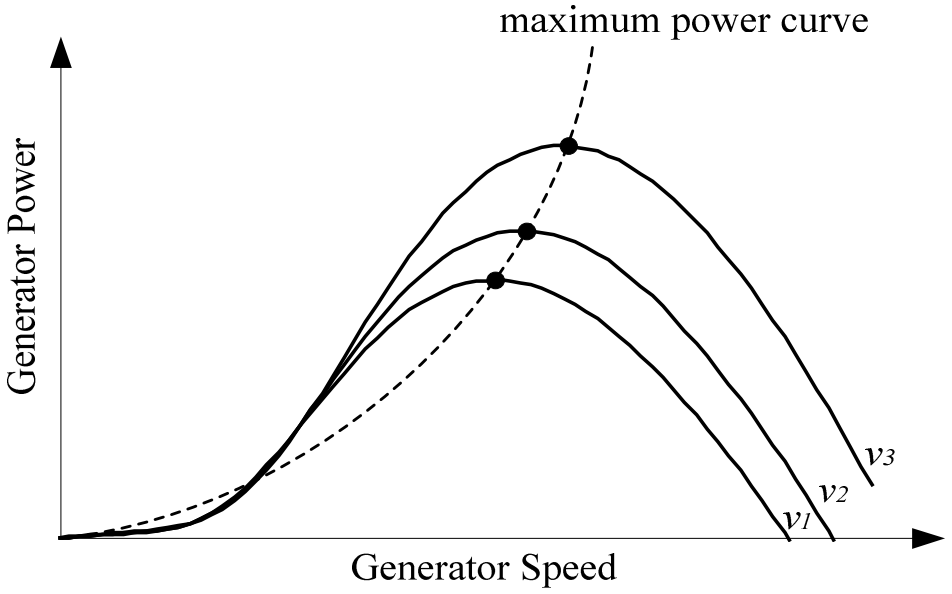

Fig. 5.2. Wind turbine characteristic for maximum power point tracking

According to equation (5.5), the mechanic power output characteristics have different maximum values at different wind speeds, corresponding to the maximum value of C_p. All these maximum values determine the so-called maximum power curve (Fig. 5.2). When the value of λ_{opt} is not known, the control objective is defined on the power characteristics. The most common method used in this case is the so called Maximum Power Point Tracking (MPPT), based on an on-off controller using minimal information from the system.

5.4 Problem Formulation

In this section, the above linearized WECS model is converted into discrete-time format, and then the problem is formulated in a general setting such that the SDP approach can be applied.

5.4.1 Discrete-Time Model

The discrete version of the linearized WECS can be written as follows

$$x(k+1) = A_d x(k) + B_u u(k) + B_d d(k) \tag{5.21}$$

$$y(k) = C_d x(k) \tag{5.22}$$

where, $A_d = e^{\tilde{A}T}$, $d(k)$ is the discrete version of $\Delta v(t)$, and $[B_u, B_d] = \left[\int_0^T e^{\tilde{A}T} dt\right]\left[\tilde{B}_u, \tilde{B}_d\right]$.

To simplify the notation in this paper, we set

$$\mathbf{x} := [x(1)^T, ..., x(N)^T]^T$$

$$\mathbf{u} := [u(0)^T, ..., u(N-1)^T]^T$$

$$\mathbf{d} := [d(0)^T, ..., d(N-1)^T]^T$$

5.4.2 Cost Function

In the partial load region, the power output control of the Wind Energy Conversion System is essentially to maximize the power output by keeping the tip speed ratio constant to its ideal value. With the consideration of the value of the tip speed ratio is relative to generator angular velocity ω_g and pitch angle β, the objective function is to control the outputs (ω_g and β) of the drive train part at optimal values. The pitch angle is normally set to zero aiming at capturing maximum wind energy. Therefore, the cost function is to minimize the deviations of generator angular velocity (ω_g) and electric power (P_g) from the reference values. The change of control vector ($\partial\Gamma_g^*$, where ∂ represents the difference between the value at the current time and the previous time) at each time step is also considered. Thus, the cost function can be written as follows:

$$\min V_N\left(x_0,\mathbf{u},\mathbf{d}\right)=\frac{1}{2}\left[\sum_{k=1}^{N}\left(q_1\left(\omega_{g,\mathrm{ref}}-\omega_g\right)_k^2+q_2\left(P_{g,red}-P_g\right)_k^2\right)+\sum_{k=0}^{N-1}r_1\left(\Delta T_g^*\right)_k^2\right] \tag{5.23}$$

subject to

$$P_{g,\min}\le P_g\left(k\right)\le P_{g,\max} \tag{5.24}$$

$$\omega_{g,\min}\le \omega_g\left(k\right)\le \omega_{g,\max} \tag{5.25}$$

For both of $k=1,...,N$ in (5.23) and $k=0,...,N-1$ in (5.23), x_0 is the initial condition at each time step, and N is the finite prediction horizon.

Since

$$\Delta P_g = P_g - P_{g,rat} = \Delta\omega_g T_{g,rat} + \Delta T_g \omega_{g,rat}$$

$$\Delta\omega_g = \omega_g - \omega_{g,rat}$$

and

$$y(k) = \begin{bmatrix} \Delta\omega_g & \Delta P_g \end{bmatrix}^T = C_d x(k)$$

Then, after some mathematical manipulations, we can rewrite equation (5.23) in the form as follows:

$$V_N\left(x(0), \mathbf{u}, \mathbf{d}\right) = \left[\sum_{k=1}^{N} x(k)^T Q x(k) + \sum_{k=0}^{N-1} \left(u(k) - u(k-1)\right)^T R \left(u(k) - u(k-1)\right) \right] \tag{5.26}$$

with

$$Q = \begin{bmatrix} 0 & 0 & 0 & 0 & 0 \\ 0 & \dfrac{q_1 + q_2}{\omega_{g,rat}^2} & 0 & \dfrac{q_2}{\omega_{g,rat} T_{g,rat}} & 0 \\ 0 & 0 & 0 & 0 & 0 \\ 0 & \dfrac{q_2}{\omega_{g,rat} T_{g,rat}} & 0 & \dfrac{q_2}{T_{g,rat}^2} & 0 \\ 0 & 0 & 0 & 0 & 0 \end{bmatrix}, R = \begin{bmatrix} r_1 & 0 \\ 0 & r_2 \end{bmatrix}$$

where $Q \geq 0$ (i.e., semi-definite positive matrices) and $R > 0$ (i.e., positive definite matrix).

5.4.3 Problem Formulation

As described in Chapter 4, two different sets of control inputs regarding the disturbance of wind speed are considered. The first one assumes that the noise $d(k)$ is Gaussian with known statistics. As such, constraints (5.24) and (5.25) can only be enforced in a probabilistic form. For example, they can be written as:

$$\mathbb{P}(P_{g,\min} \leq P_g\left(k\right) \leq P_{g,\max}) \geq \alpha_1 \tag{5.27}$$

$$\mathbb{P}(\omega_{g,\min} \leq \omega_g\left(k\right) \leq \omega_{g,\max}) \geq \alpha_2 \tag{5.28}$$

Then, the first problem with Gaussian noise is given by:

Problem 1: **Find**

$\mathbf{u}(x_0) \coloneqq arg\ min_{\mathbf{u}}\ \mathbb{E}V_N$

Subject to (5.24), (5.25), (5.27), (5.28), and discretized version of the system (5.21), (5.22).

In the above formulation, $\mathbb{E}$ is the expectation operator.

The second problem formulation considers a noise variable that does not have a known statistics, but a bounded set, e.g., $\mathbb{D}_\gamma = \{\mathbf{d} \mid \|\mathbf{d}\|_2 \leq \gamma\}$. In this case, the problem is formulated as a min-max problem to find a control input that minimizes the largest value of the cost function throughout the whole bounded set. The problem formulation is given by:

Problem 2: **Find**

$$\mathbf{u}(x_0) := arg\ min_{\mathbf{u}}\ \max_{d \in \mathbb{D}_\gamma} V_N$$

Subject to (5.24), (5.25), (5.27), (5.28), and discretized version of the system (5.21), (5.22).

5.5 Results and Discussion

The performance of the proposed SDP method based control strategy in partial load region is demonstrated in this section. The wind speed tested in this chapter is 8 m/s. The weigh factors' values are set as follows:

- $q_1 = 1000$, $q_2 = 0.5$, $r_1 = 0.5$

Other parameters used can be found in the Appendix.

The results will be divided into two cases. Case 1 gives the results when the assumed the wind speed disturbance follows Gaussian distribution; and Case 2 describes the performance when the disturbance is norm bounded.

5.5.1 Case One: The disturbance distribution is Gaussian

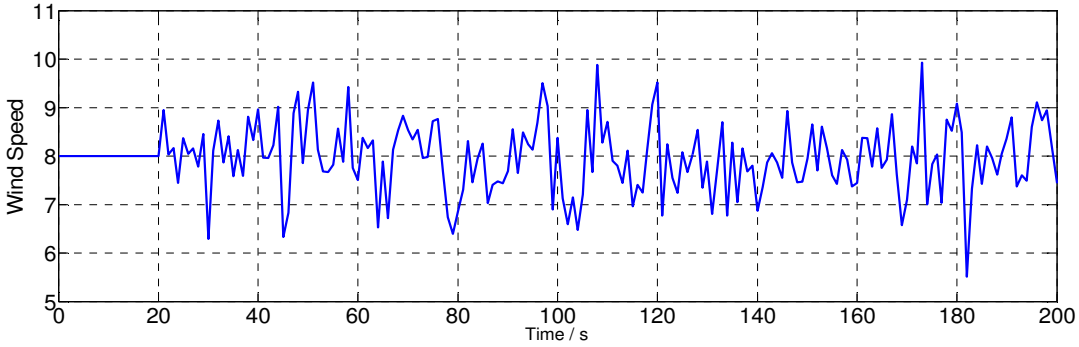

Fig. 5.3 (a) Wind speed

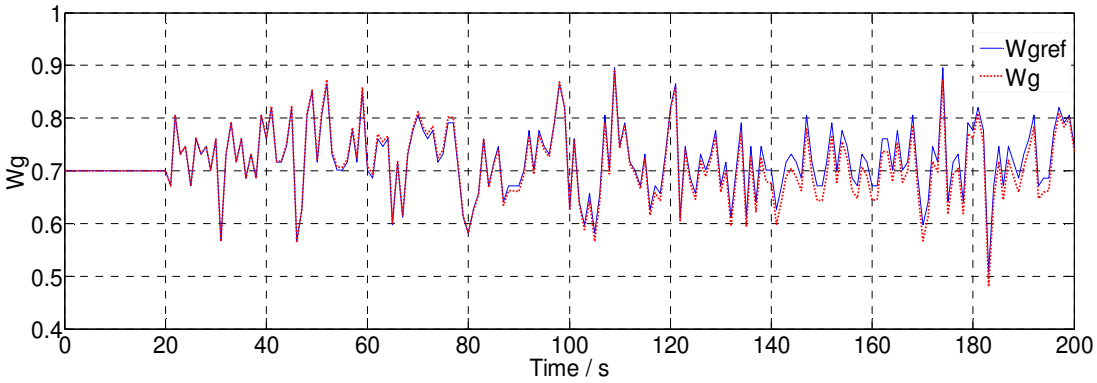

Fig. 5.3 (b) Generator angular velocity: W_g

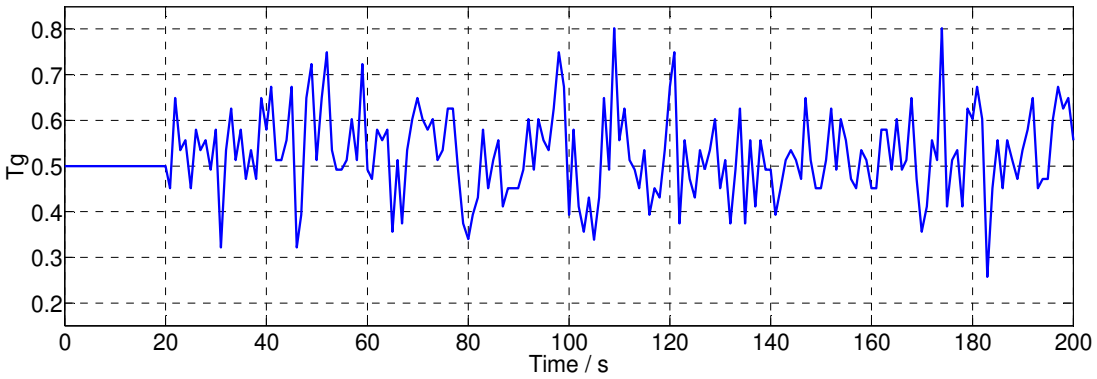

Fig. 5.3 (c) Generator torque: T_g

Fig. 5.3 Results for case one: disturbance is Gaussian

In the partial load region, the pitch angle is set to zero, which contributes to energy maximization and reduction of the drive train torsional torque. The controller tracking performance is measured using the reference w_{gref}. Fig. 5.3 (c) shows the output w_g is close to the reference w_{gref} and the generator torque is proportional to the wind speed.

5.5.2 Case Two: The disturbance is Norm-Bounded

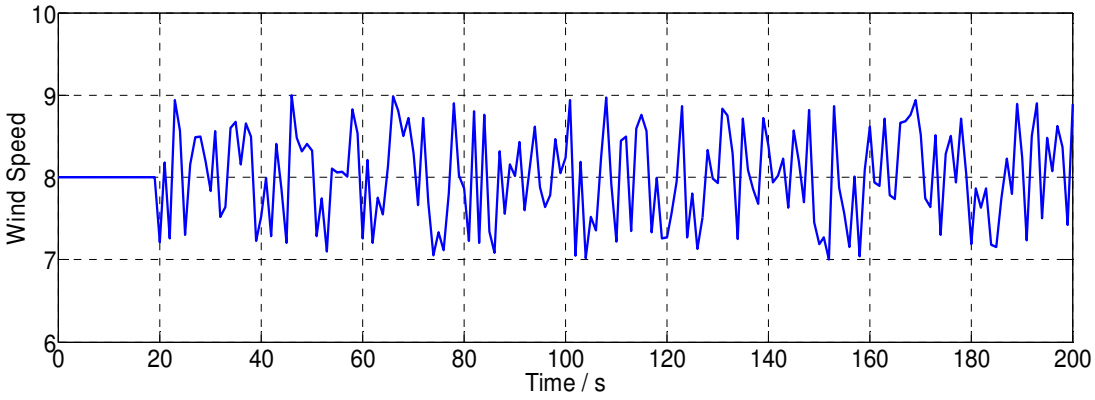

Fig. 5.4 (a) Wind speed

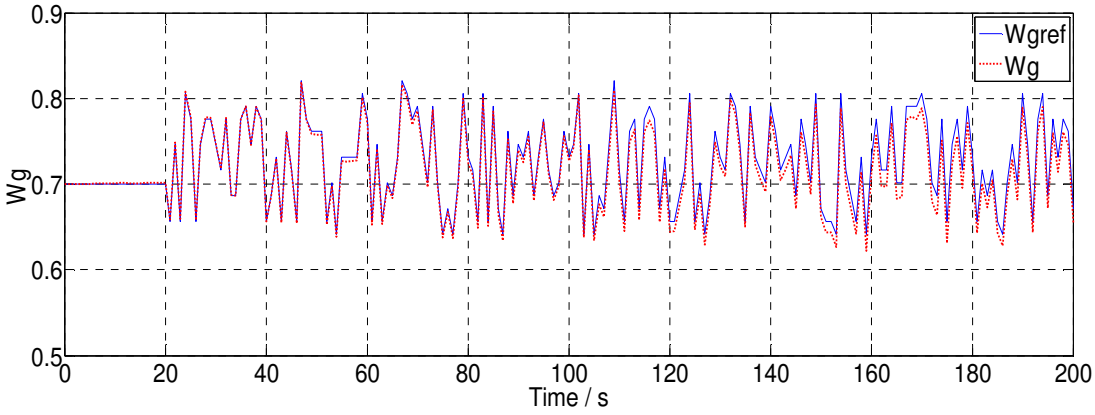

Fig. 5.4 (b) Generator angular velocity: W_g

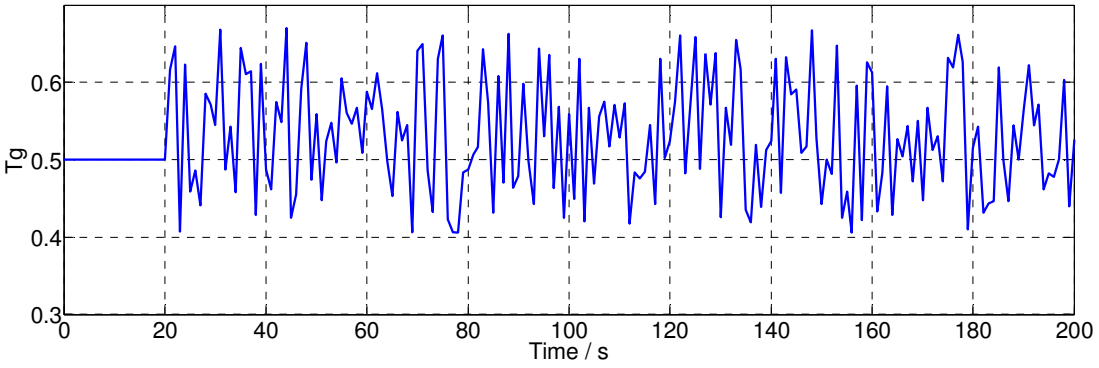

Fig. 5.4 (c) Generator torque: T_g

Fig. 5.4 Results for case two: disturbance is Norm-bounded

In this case, the distribution of the disturbance is unknown. It is set as norm-bounded, which means the high frequency part of the wind speed is set to random values with its norm at 1 m/s.

As we can see from above pictures, wind speed is changing all the time at 8 m/s, without going lower than 7 m/s or higher than 9 m/s. The actual values of w_g are very close to w_{gref}. The results here are very comparable to the results from the literature.

5.6 Discussion and Conclusion

The contribution of this chapter can be summarized as follows:

- In this chapter, a new control strategy based on SDP method, which is proposed in Chapter 4, is used to control power output of variable-speed variable-pitch WECS in the partial operating region. This SDP-based control method is designed to provide the required maximum energy capture from wind energy.

- In the proposed approach, the wind speed disturbance to wind speed forecast, which represents the high frequency variable component of the wind speed, is

modeled in two different ways. The first one is to assume that the wind speed disturbance's distribution is Gaussian and the other one assumes it is norm-bounded with unknown distribution. Both problems are converted into SDP-based optimization problems to be solved.

- When the disturbance is modeled as Gaussian, the results are very comparable to those from the MPC-based method in the literature. However, the proposed method requires less information, i.e., the state space model, which is needed in the MPC model based literature to determine disturbance in the prediction horizon of the deterministic cost function.
- When the wind speed error is modeled as norm-bounded with unknown distribution, it likely represents a more realistic assumption in practice and has not been previously reported in wind power control studies. The results are also promising and comparable to the one with Gaussian distribution.

CHAPTER 6 CONCLUSION AND FUTURE WORK

6.1 Conclusion and Contribution

For voltage regulation of DFIG based power system, PI controllers are usually employed. The parameters of these PI controllers need to be tuned. Many previous works in gain tuning for DFIG are based on some optimization approaches to reach a tradeoff or compromise such that the wind system can achieve good, though not always the most desired, performance under various operating conditions and avoid the worst-case performance under some extreme conditions. Different from these previous approaches for DFIG control, in Chapter 3, a new DFIG voltage control approach based on a philosophy different from the previous works is presented. In the proposed approach, the PI control gains for the DFIG system are dynamically adjusted based on the dynamic, continuous sensitivity which essentially indicates the dynamic relationship between the change of control gains and the desired output voltage. Hence, this control approach does not require any good estimation of fixed control gains because it has the self-learning mechanism via the dynamic sensitivity. This also gives the plug-and-play feature of the proposed DFIG controller to make it promising in utility practices. Simulation results verify that the proposed approach performs as expected under various operating conditions.

For power control of wind energy conversion system, the major challenge is the randomness which may bring fluctuations to output power, as well as undesired dynamic loading of the drive train during high turbulence of wind. Obviously, a sophisticated control strategy plays an important role in wind energy conversion system. In previous

works, Model Predictive Control (MPC), a relatively new control technique, has been used for WECS control. The WECS is modeled as a linear system and the wind speed is modeled as a stochastic process. However, the prediction of disturbances in a finite horizon based on the past estimates during the computation of the control input is needed. In Chapters 4 and 5, a new power output control strategy of wind energy conversion system based on a semi-definite programming (SDP) method is proposed to tackle the difficulty brought by wind speed's randomness. In the proposed approach, the wind speed disturbance, which means wind speed measurement error representing the high frequency variable component of the wind speed, is modeled in two different cases: its distribution is Gaussian and its distribution is unknown, but norm bounded. In both cases, the objective is converted into a SDP-based optimization problem, which can be solved efficiently by existing tools. Simulation results verify that the proposed SDP based control method works as well as the MPC-based control method presented in the literature, however, with less information needed, i.e. no model used for wind speed disturbance prediction.

6.2 Future Work

The following directions may be considered as future works of this dissertation.

6.2.1 Voltage Regulation for wind turbine based power system

- The proposed adaptive control method may be applied to a power system with multiple wind turbines, different load levels, and different transmission networks;
- Adaptive control method as proposed in this research work is a new concept in voltage control of wind plant based power system. More research work can focus on developing a generally used control approach with plug-and-play feature from the proposed method.

6.2.2 Power regulation for wind energy conversion system

- Wind speed's stochasticity brings difficulties to control of wind plant based power system. A better wind speed prediction method will definitely help control the wind plant based power system;
- The proposed control method for power regulation of wind energy conversion system into wind power based power system may be extended from the control of a single or multiple wind plants based power system to the control of power output at a higher level.

LIST OF REFERENCES

[1] P. Kundur, J. Paserba, V. Ajjarapu, G. Andersson, A. Bose, C. Canizares, N. Hatziargyriou, D. Hill, A. Stankovic, C. Taylor, T. Van Cutsem and V. Vittal, "Definition and classification of power system," *IEEE Trans. Power System,* vol. 19, no. 3, pp. 1387-1401, May. 2004.

[2] C. P. Steinmetz, "Power control and stability of electrical generating stations," *AIEE Trans.,* vol. XXXIX, Part II, pp. 1215-1287, Jul. 1920.

[3] AIEE Subcommittee on Interconnection and Stability Factors, "First report of power system stability," *AIEE Trans*., pp. 51-80, 1926.

[4] V. I. Vorotnikov, *Partial Stability and Control*. Cambridge, MA: Birkhauser, 1998.

[5] V. V. Rumyantsev and A. S. Osiraner, *Stability and Stabilization of Motion with Respect to a Part of the Variables*. Moscow, Nauka, Russia, 1987.

[6] N. Rouche, P. Habets, and M. Laloy, *Stability Theory by Liapunov's Direct Method*. New York: Springer, 1977.

[7] P. Kundur, Power System Stability and Control. New York: McGrawhill, 1994.

[8] T. Ackermann, *Wind Power in Power Systems*, England, 2005.

[9] E. H. Camm, M. R. Behnke, O. Bolado, M. Bollen, M. Bradt, C. Brooks, W. Dilling, M. Edds, W. J. Hejdak, D. Houseman, S. Klein, F. Li, J. Li, P. Maibach, T. Nicolai, J. Patino, S. V. Pasupulati, N. Samaan, S. Saylors, T. Siebert, T. Smith, M. Starke and R. Walling, "Characteristics of wind turbine generators for wind power plants," *IEEE Power & Energy Society General Meeting*, PP. 1-5, 2009.

[10] Y. Mishra, S. Mishra, F. Li, Z. Y. Dong, and R. C. Bansal, "Small-signal stability analysis of a DFIG-based wind power system under different modes of operation," *IEEE Trans. Energy Conversion,* vol. 24, no. 4, pp. 972-982, Dec. 2009.

[11] L. Holdsworth, X. Wu, J. B. Ekanayake, and N. Jenkins, "Comparison of fixed speed and doubly-fed induction wind turbines during power system disturbances," *Proc. Inst. Elect. Eng., Gener., Transm., Distrib*., vol. 150, no. 3, pp. 343-352, May. 2005.

[12] F. Mei, and B. C. Pal, "Modelling and small-signal analysis of a grid connected doubly-fed induction generator," *IEEE Power Engineering Society General Meeting*, *2005*.

[13] F. Mei and B. C. Pal, "Modal analysis of grid connected doubly fed induction generator," *IEEE Trans. Energy Conversion*, vol. 22, no. 3, pp. 728-736, Sept. 2007.

[14] Y. Lei, A. Mullane, G. Lightbody, and R. Yacamini, "Modeling of the wind turbine with a doubly fed induction generator for grid integration studies," *IEEE Trans. Energy Conversion*, vol. 21, pp.257-264, Mar. 2006.

[15] F. Wu, X. P. Zhang, K. Godfrey, and P. Ju, "Small signal stability analysis and optimal control of a wind turbine with doubly fed Induction generator," *IET Gener. Transm. Distrib*., vol. 1, no. 5, pp. 751-769, 2007.

[16] R. Cardenas, R. Pena, G. Tobar, P.Wheeler and G. Asher, "Stability analysis of a wind energy conversion system based on a doubly fed induction generator fed by

a matrix converter," *IEEE Trans. Industrial Electronics*, vol. 56, no. 10, pp. 4194-4206, Sept. 2009.

[17] W. Qiao, G. K. Venayagamoorthy, and R. G. Harley, "Design of optimal PI controllers for doubly fed induction generators driven by wind turbines using particle swarm optimization," *Int. Joint Conf. In Neural Networks, Canada,* pp. 1982-1987, Jul. 2009.

[18] F. Wu, X. P. Zhang, K. Godfrey, and P. Ju, "Small signal stability analysis and optimal control of a wind turbine with doubly fed induction generator," *IET Gen. Trans. Dist.,* vol. 1, no. 5, pp. 751-760, 2007.

[19] H. Banakar, C. Luo, B. T. Ooi, "Steady-state stability analysis of doubly-fed induction generators under decoupled P-Q control," *IEE Proceedings on Electric Power Applications,* vol. 153, no. 2, pp. 300-306, Mar. 2006.

[20] Mwinyiwiwa, Y. Z. Zhang, B. Shen, B. T. Ooi, "Rotor position phase-locked loop for decoupled P-Q control of DFIG for wind power generation," *IEEE Trans. Energy Conversion*, vol. 24, no. 3, pp. 758-765, Sept. 2009.

[21] Z. Miao, L. Fan, D. Osborn, and S. Yuvarajan, "Control of DFIG based wind generation to improve inter area oscillation damping," *IEEE PES General Meeting*, Pittsburgh, PA, Jul. 2008, pp. 1-7.

[22] L. Fan, Z. Miao, and D. Osborn, "Impact of doubly fed wind turbine generation on inter-area oscillation damping," *IEEE PES General Meeting*, Pittsburgh, PA, Jul. 2008, pp. 1-8.

[23] F. M. Hughes, O. A. Lara, N. Jenkins, and G. Ancell, "A power system stabilizer for DFIG-based wind generation," *IEEE Trans. Power Systems,* vol. 21, no. 2, pp. 763-772, May. 2006.

[24] S. Mishra, "A hybrid least square-fuzzy bacteria foraging strategy for harmonic estimation," *IEEE Trans. Evolutionary Comput*., vol 9, no. 1, pp. 61-73, Feb. 2005

[25] T.K.A. Brekken, N. Mohan, "Control of a doubly fed induction wind generator under unbalanced grid voltage conditions," *IEEE Trans. Energy Conversion*, vol. 22, no. 1, pp. 129-135, Feb. 2007.

[26] D. Santos-Martin, J.L. Rodriguez-Amenedo, S. Arnalte, "Direct power control applied to doubly fed induction generator under unbalanced grid voltage conditions," *IEEE Trans. Power Electronics*, vol. 23, no. 5, pp. 2328-2336, Sept. 2008.

[27] J. Hu, Y. He, "Reinforced control and operation of DFIG-based wind power generation system under unbalanced grid voltage conditions," *IEEE Trans. Energy Conversion*, vol. 24, no. 4, pp. 905-915, Nov. 2009.

[28] Huijuan Li, Fangxing Li, Yan Xu, D. T. Rizy, and J. D. Kueck, "Adaptive voltage control with distributed energy resources: algorithm, theoretical analysis, simulation, and field test verification," *IEEE Trans. Power Systems,* vol. 25, no. 3, pp. 1638-1647, Aug. 2010.

[29] The MathWorks, "SimPowerSystems for Use with Simulink", User's Guide Version 4.

[30] M. Soliman, O. P. Malik, and D. T. Westwick, "Multiple model multiple-input multiple-output predictive control for variable speed variable pitch wind energy

conversion systems," *IET Renewable Power Generation,* vol. 5, no. 2, pp. 124-136, 2011.

[31] H. Camblong, I. M. de Alegria, M. Rodriguez, and G. Abad, "Experimental evaluation of wind turbines maximum power point tracking controllers," *Energy Convers. Manage*., vol. 47, pp. 2846-2858, 2006.

[32] E. A. Bossanyi, "The design of closed loop controllers for wind turbines," *Wind Energy*, vol. 3, pp. 149-163, 2000.

[33] Y. Mishra, S. Mishra, F. Li, Z. Y. Dong, and R. C. Bansal, "Small-signal stability analysis of a DFIG-based wind power system under different modes of operation," *IEEE Trans. Energy Conversion,* vol. 24, no. 4, pp. 972-982, Dec. 2009.

[34] F. D. Bianchi, R. J. Mantz, and C. F. Christiansen, "Control of variable-speed wind turbines by LPV gain scheduling," *Wind Energy*, vol. 7, pp.1-8, 2004.

[35] I. Munteanu, N. A. Cutululis, A. I. Bratcu, and E. Ceanga, "Optimization of variable speed wind power systems based on a LQG approach," *Control Eng. Pract*., vol. 13, pp.903-912, Jul. 2005.

[36] E. B. Muhando, T. Senjyu, O. Z. Siagi, and T. Funabashi, "Intelligent optimal control of wind power generating system by a complemented linear quadratic Gaussian approach," *IEEE Power Engineering Society Conference and Exposition in Afria*, pp. 1-8, 2007.

[37] E. B. Muhando, T. Senjyu, N. Urasaki, and T. Funabashi, "Online WTG performance and transient stability enhancement by evolutionary LQG," *IEEE Power Engineering Society General Meeting*, pp. 1-8, 2007.

[38] S. Nourdine, H. Camblong, I. Vechiu, and G. Tapia, "Comparison of wind turbine LQG controllers designed to alleviate fatigue loads," *8th IEEE international Conference on Control and Automation (ICCA),* pp. 1502-1507, 2010.

[39] S. Nourdine, H. Camblong, I. Vechiu, and G. Tapia, "Comparison of wind turbine LQG controllers using individual pitch control to alleviate fatigue loads," *18th Mediterranean Conference on Control & Automation (med),* pp. 1591-1596, 2010.

[40] F. D. Bianchi, R. J. Mantz, and C. F. Christiansen, "Power regulation in pitch-controlled variable-speed WECS above rated wind speed," *Renewable Energy*, vol. 29, pp. 1911-1922, 2004.

[41] Y. She, X. She, and M. E. Baran, "Universal tracking control of wind conversion system for purpose of maximum power acquisition under hierarchical control system," *IEEE Trans. on Energy Conversion,* vol. 26, no. 3, pp. 766-775, Sep. 2011.

[42] M. Soliman, O. P. Malik, and D. T. Westwick, "Multiple model predictive control for wind turbines with doubly fed induction generators," *IEEE Trans. Sustainable Energy*, vol. 2, no. 3, pp. 215-225, Jul. 2011.

[43] D. Bertsimas, and D. Brown, "Constrained Stochastic LQC: A Tractable Approach," *IEEE Trans. Automatic Control,* vol. 52, no. 10, pp. 1826 - 1841, 2007.

[44] A. D. Hansen, P. Sorensen, F. Lov and F. Blaabjerg, "Control of variable speed wind turbines with doubly-fed induction generators," *Wind Eng.,* vol. 28, no. 4, pp. 411-432, 2004.

[45] E. B. Muhando, T. Senjyu, A. Yona, H. Kinjo and T. Funabashi, "Disturbance rejection by dual pitch control and self-tuning regulator for wind turbine generator parametric uncertainty compensation," *IET Control Theory Appl.,* vol. 1, no. 5, pp. 1431 - 1440, Sept. 2007.

[46] http://www.windpoweringamerica.gov

APPENDIX

WECS Parameters

Wind Turbine

$P_{t\_rat} = 2MW,\ \omega_{t\_rat} = 3.0408 rad/s,\ R = 33.29m$

Pitch Actuator

$\tau = 0.1s,\ \beta_{\min} = 0^0,\ \beta_{max} = 45^0,$

$\dot{\beta}_{\min} = -10^0/s,\ \dot{\beta}_{max} = 10^0/s$

Drive train

$i = 74.38,\ J_t = 1.86E+06 kgm^2,\ J_g = 56.29 kgm^2$

$k_s = 31.8E+04 Nm/rad,\ B_s = 212.2 Nm.s/rad$

Generator

$\tau_g = 20ms$

Publications during Ph.D. study

Journal

[1] **Zhiqiang Jin**, Fangxing Li, "DFIG voltage control based on dynamically adjusted control gains," submitted to IEEE *Transactions on Energy Conversion*, under revision.

[2] **Zhiqiang Jin**, Fangxing Li and Xiao Ma, "Semi-Definite programming for power output control in wind energy conversion system," second revision submitted to *IEEE Transaction on Sustainable Energy*.

[3] Can Huang, Tao Ding, Fangxing Li and **Zhiqiang Jin**, "Robust optimization for maximum wind power capture with box uncertainty," submitted to *IEEE Transaction on Sustainable Energy*.

[4] Can Huang, **Zhiqiang Jin** and Fangxing Li, "Semi-Definite Programming based optimal control for wind energy conversion system over full operating regions", under preparation.

Conference

[5] Yan Yang, Haoyu Chen, Yao Zhang, **Zhiqiang Jin and** Fangxing Li, "Searching for electricity market equilibrium using co-evolutionary computation approach," *2011 Asia-Pacific Power and Energy Engineering Conference (APPEEC)*, Wuhan, China, March 25-28. 2011.

Vita

Zhiqiang Jin joined The University of Tennessee at Knoxville in January 2009 to pursue a Ph.D. degree in Electrical Engineering. He received his B.S. and M.S. degrees in electric power engineering from Tianjin University (China) in 2005 and 2007, respectively. And he received another M.S. degree from University of Florida in electrical engineering in 2008. His research interests include wind turbine plant voltage regulation, power regulation and wind power integration.